The Development and Characterization of a Novel Instrument for Measuring Vaginal Closing Force: EVE the Elevated-Surface Vaginal Elastometer

By

Mark D. Pacey

Submitted to the graduate degree program in Mechanical Engineering and the Graduate Faculty of the University of Kansas in partial fulfillment of the requirements for the degree of Doctor of Philosophy.

_____

Chairperson Sarah L. Kieweg

_____

Ronald L. Dougherty

_____

Kenneth J. Fischer

_____

Erik S. Van Vleck

_____

Sara E. Wilson

Date Defended: July 7th, 2016

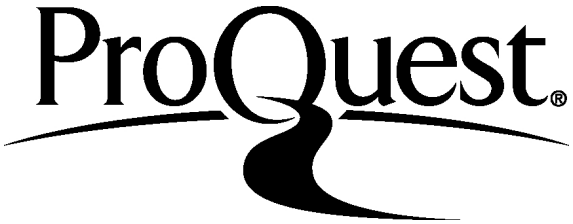

The Dissertation Committee for Mark D. Pacey

certifies that this is the approved version of the following dissertation:

The Development and Characterization of a Novel Instrument for Measuring Vaginal Closing Force: EVE the Elevated-Surface Vaginal Elastometer

_____

Chairperson Sarah L. Kieweg

Date approved: July 7th, 2016

Abstract

In 2012 there were an estimated 35.3 million people living with HIV [1]. Microbicides address an important gap in HIV prevention for vulnerable groups unable to implement other prevention strategies [2]. Models are being developed in our lab to optimize microbicide delivery vehicle properties so that the microbicide will coat the entire vaginal epithelial surface, stay in place for the duration of possible exposure, and coat thick enough to deliver sufficient active ingredient to prevent infection.

A complete model should incorporate vaginal closing force to understand how a delivery vehicle will be distributed and retained in the vagina. However, the physiological magnitudes of vaginal closing forces are not known. Several previous methods have been utilized to determine an appropriate magnitude of one or several components, but they all neglect important features to measure the forces relevant to microbicide delivery vehicle spreading. An ideal measurement device to measure all aspects of vaginal closing force should: be controllable, operate in a variety of modes, have a constant contact area, be able to measure at different places along the vaginal axis and in different directions, be modular, be convenient and easy to operate in a clinical environment, and be safe to operate.

This dissertation describes the design and testing of a new instrument to measure vaginal closing force, its calibration process, and the software to control it. Throughout this document the identified obstacles and the strategies used to mitigate them are discussed. Validation testing was performed on tissue phantoms and by bench testing using the calibration instrument. Validation testing shows that the instrument has the ability to differentiate between phantoms. Future testing on more tissue phantoms will allow further quantification of the instrument and a better determination of the precision of the measurements.

Two alternate approaches have also been developed for the possible refinement of the EVE instrument. Utilizing force sensing within the probe body would violate the initial design constraints, but might be a relatively simple way to address the issues which have disrupted the instrument's development. Alternatively a new probe which completely eliminates the hydraulic system in favor of mechanical linkages, although more drastic of a change, might allow for data generation without compromising the initial design requirements.

The EVE instrument is a successful step forward in properly measuring vaginal tissue closing force. Many of the initial design challenges have been overcome, and a majority of the programming necessary has been completed. Measurements of phantom tissue elasticity are now possible. EVE is nearly ready for *in vivo* testing.

Acknowledgements

I would like to express my deepest appreciation and respect for my committee chair, Dr. Sarah Kieweg, who was a wonderful advisor and constant source of optimism through this long project. Without her guidance this dissertation would have been impossible.

I would also like to thank all of my committee members both current members, Dr. Ron Dougherty, Dr. Ken Fischer, Dr. Sara Wilson, and Dr. Erik Van Vleck, and past members, Dr. Terry Faddis and Dr. Lorin Maletsky, who were all of invaluable assistance during this process.

I would also like to give a special thank you to the departmental and outside help that I received along the way from Dr. Carl Weiner, Doug Kieweg, Charles Gabel, Justin Lohrmeyer, and Matt Gifford. All of your technical support made EVE possible.

Finally, I would like to thank my ever patient wife Eryn Pacey for her love and encouragement throughout this long journey, and my parents David and Carol for instilling in me a love of science and engineering.

This work was supported by NIH R21/R33 AI082697 and the Kansas City Area Life Sciences Institute (KCALSI).

Table of Contents

List of Figures

List of Tables

Nomenclature, Variables, and Abbreviations

AIDS – Acquired Immunodeficiency Syndrome, a condition of progressive failure of the human immune system, caused by HIV.

Barbed Tube Fitting – A tube fitting which holds the tubing in place by force fitting the tubing over one or more barbs on the fitting surface.

Bellows – Metal vessels that can be compressed or extended by pressure or force changes, but return to their original shape.

Daughter Bellows – The bellows housed in the probe end of EVE, synonym of Probe Bellows

Driving Bellows – The bellows housed in the driving end of EVE.

Parent Bellows – The bellows housed in the driving end of EVE, synonym of Driving Bellows.

Probe Bellows – The bellows housed in the probe end of EVE.

C – The concentration of gel within a phantom, in g/L of solution.

$c_{\#}$ - A constant used to calculate probe position.

Compression tube fitting – A tube fitting which holds the tubing in place by deforming a malleable collar over the outside of the tubing and held in place by a nut.

C-T-C – Calibrate-Test-Calibrate, an EVE protocol where the calibrate protocol is run three times sequentially, to calibrate EVE, test an unknown material, and then recalibrate EVE.

$d_{\#}$ - A constant used to calculate probe force.

Driving End Displacement – The displacement measured at the driving end of EVE, with zero displacement being the displacement of the driving end at equilibrium when the probe end is fully collapsed.

Driving End Force – The force measured at the driving end of EVE

Driving End Position – A synonym of driving end displacement.

dP/dt – The velocity of the driving end.

E_{agar} – The Young's modulus of an agar phantom.

E_{cal} – The elasticity of the load applied to the calibration instrument.

$E_{driving}$ – The elasticity of the system measured at the driving end of EVE.

$E_{gelatin}$ – The Young's modulus of a gelatin phantom.

Elasticity – The ratio between force and displacement in linear elastic materials.

Encoder – An optical readhead that converts marks on the encoder scale into a digital signal for measuring displacement.

Encoder Tape - The encoder scale that is affixed to the moving body.

EVE - Elevated-surface Vaginal Elastometer.

F – The force measured at the driving end.

F_P – The force measured or calculated at the probe end.

Fingering – The pattern that emerges from gravity driven flows under the influence of surface tension. Instead of a straight leading edge, the fluid forms a sinusoidal pattern.

FPGA – Field Programmable Gate Array, an integrated circuit which can be reconfigured.

HIV - Human Immunodeficiency Virus, a retrovirus that leads to AIDS.

Least-Squares Fit – The method of fitting an equation to a set of data by minimizing the sum of the squares of the errors.

Load Cell – A sensor which creates and electrical signal proportional to the force applied to it.

Microbicides – A topical drug which destroys or inhibits pathogens before they can infect.

P – The position measured at the driving end.

P_P – The position measured or calculated at the probe end.

Phantom – A specially designed object used as a test material to evaluate, analyze, and tune the performance of devices.

PI controller – Proportional-Integral Controller, a control feedback software element which uses the error and the integral of the error to control input to a process.

PID Controller – Proportional-Integral-Derivative Controller, a control feedback software element which uses the error, the integral of the error, and the derivative of the error to control input to a process.

Probe Control Mode – Controlling the probe force or position of EVE based on calibration equations using the measured force and displacement of the driving end.

Probe Displacement – The displacement of the measuring surface of EVE, with zero displacement being fully collapsed.

Probe Force – The force experienced by the measuring surface of EVE.

Probe Position – A synonym of probe displacement.

PWM – Pulse-Width Modulation, a method of controlling the average current supplied to the motor by switching the power supplied on and off at regular intervals, with longer on periods supplying more current.

R^2 – The coefficient of determination, a measure of the goodness of fit.

Relative Error – The percentage error of a calculation compared with a measurement.

Spring Constant – The ratio between force and displacement of a linear spring.

Standard Deviation – The statistical measure of the variation within a set of data.

Strain – The relative displacement of a material with respect to its original length

Stress – The force experienced over an area of material.

Vaginal Closing Force – The combination of forces from tissue properties, intra-abdominal pressure, voluntary squeezing, and involuntary squeezing, which collapse the vaginal canal.

Viscoelasticity – The properties of materials that have both viscous and elastic traits.

Voice Coil Linear Actuator – A linear motor that uses magnetic force from an electromagnet in order to develop displacement.

Young's Modulus – The ratio between stress and strain in linear elastic materials.

Chapter 1) Significance and Relevant Background

HIV: Statistics, Transmission, and Prevention

In 2012 there were an estimated 35.3 million people living with the Human Immunodeficiency Virus or HIV [1]. There were 2.3 million new HIV infections in 2012, and 1.6 million AIDS deaths in 2012 [1]. 70% of all new infections in 2012 were in sub-Saharan Africa [1]. Heterosexual sex is the primary mode of HIV transmission in sub-Saharan Africa, and female commercial sex workers are a key population for prevention efforts [3]. Women have been shown to be at a higher risk of infection than their male counterparts due to various anatomical, social, and cultural factors [2]. In sub-Saharan Africa, women account for approximately 57% of all people living with HIV [1]. Sub-Saharan women in the 15-20 year old age group have a three to six times higher infection rate and are infected, on average, five to seven years earlier than their male peers [4].

Since women are more susceptible to HIV infection, and heterosexual sex is the most common transmission mode, it is important to understand how a woman may contract HIV through vaginal intercourse. The vagina is a tubular passage that connects the introitus to the cervix. The lateral cross-section is often described as having an "H" or "W" shape, while the sagittal cross-section is "S" shaped along the axis between the introitus and the cervix. The vaginal and ectocervix epithelium is multi-layered and stratified [5], as shown in Figure 1, and is supported by the underlying smooth muscles and surrounding pelvic floor structures [6].

During unprotected intercourse with an HIV-infected man, infected leukocytes and cell-free HIV are introduced into the vagina through semen and pre-ejaculate [7]. The epithelial cells themselves are not likely infection sites because they lack the CD4 receptor that the virus requires to infect a target cell [5, 7].

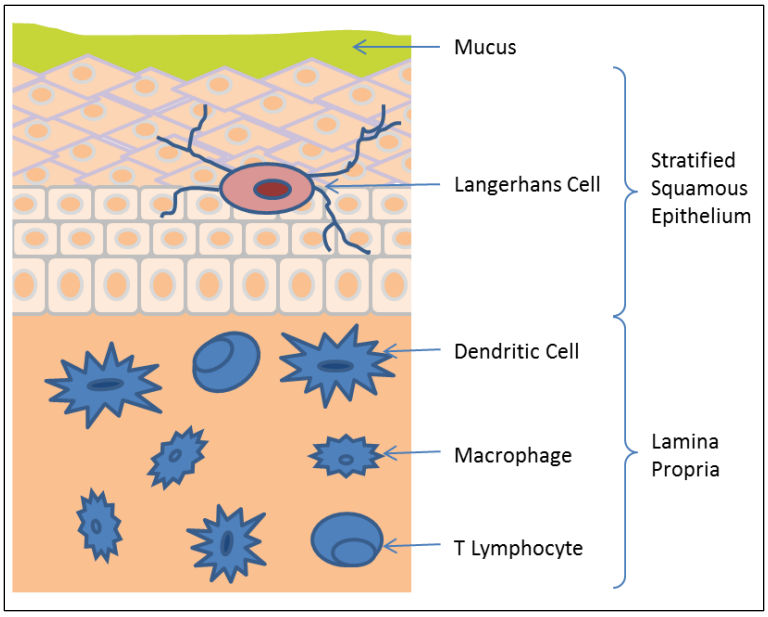

Figure 1: Vaginal epithelium and associated cells pertinent to infection (Adapted from Stone 2002)

Langerhans cells are present in the vaginal epithelium (see Figure 1), and, although they do possess the CD4 receptor, they are unlikely sites for initial infection because they express very little of the co-receptors CCR5 or CXCR4, which are also necessary for infection [5]. The primary infection occurs beneath the epithelium in the lamina propria which contains lymphoid cells, dendritic cells, and macrophages, which all have the necessary receptors and co-receptors for infection [5]. The infection gains access to the lamina propria through disruptions in the epithelial lining caused by traumatic intercourse or pathological conditions like other sexually transmitted infections [7]. It has also been shown that the viron can be transported through the epithelium by Langerhans cells, which have dendrites which reach through the intact epithelial surface [5, 7, 8].

Once infected, treatment for HIV through antiviral medications increases patient life expectancy, and can decrease the chance of passing on the infection by lowering the patient's viral load and thereby reducing the genital secretion of the viron [5]. Nothing has been shown to

reliably cure anyone post-infection, and undiagnosed new hosts are especially likely to spread the infection. In fact, for every two people who are put into antiretroviral therapy, five more become infected [9].

Prevention is the most effective method in combatting the growing HIV pandemic. Ideally a vaccine could be developed that would protect uninfected people from ever acquiring HIV. To be successful, an HIV vaccine will have to deal with a constantly mutating virus and huge viral diversity [10]. A vaccine with only one antigen will not generate effective protection against the broad spectrum of HIV [10]. Vaccines also have additional barriers to overcome in public fears, including fear of vaccine-induced HIV infection, unknown physical side effects, uncertainty about efficacy, and mistrust of government-sponsored medical research [11]. Even without the public fears about vaccination, researchers are not optimistic about developing a human-ready HIV vaccine within the next decade [12].

Comprehensive sex education has been shown to reduce sexual activity and increase protective sexual behaviors [13]. Key to comprehensive sex education is the use of condoms for every sex act. Condoms, when used correctly and consistently, are one of the most efficient technologies to prevent the sexual transmission of HIV [1]. Condom use is not always a viable option, especially in the developing world. Many myths and beliefs have proliferated throughout regions with high infection rates that discourage the use of condoms including: the fear of a condom rupturing and causing infertility, the association with the sex trade and sexually transmitted infections, the concern that condoms have tiny holes that HIV can pass through, and the concern that they limit sexual pleasure [14]. Because of gender inequality and disadvantages in socioeconomic status, women are often subjected to violence and unable to negotiate condom use [1, 8]. When used correctly and consistently, condoms are a great tool to reduce the spread

of HIV; but other less intrusive products, which are under the control of women, are important to increase prevention and slow the spread of HIV.

Microbicides address an important gap in HIV prevention options for vulnerable groups, such as young women, who are at high risk of infection, but are unable to implement other HIV prevention strategies like abstinence, female or male condoms, or monogamy [2]. A microbicide consists of two main parts: the active ingredient and the delivery vehicle. The active ingredient is a drug or chemical that destroys or otherwise inhibits pathogens so that they will not have an opportunity to pass on infection. Delivery vehicles are used to get the active ingredient to the target site. They are often in the form of a gel, foam, or cream, but are sometimes more innovative materials such as rings or films [15]. Ideal delivery vehicles also perform other actions besides transporting the active ingredient. An ideal delivery vehicle also acts as a lubricant, which can help prevent trauma to the vaginal epithelium, preventing the virus from being able to access the lamina propria, where infection occurs. Delivery vehicles can also provide a physical barrier, possibly providing some additional protection from infection.

Relation to Longer-Term Goals

The vehicle's ability to coat the vulnerable surface has been identified as a crucial variable [15]. Otherwise effective active ingredients could easily be rendered ineffective by poor delivery vehicle design which would leave vulnerable tissue unprotected. Mathematical models of delivery vehicle spread due to gravity and squeezing can be used to speed the development of effective vehicles. Models are being developed in our lab to optimize the delivery vehicle properties so that the microbicide will coat the entire vaginal epithelial surface, stay in place for the duration of possible exposure, and have the necessary thickness for the active ingredient to act. Current models include both gravity and squeezing forces, but future models will also

incorporate the effects of shearing forces on the delivery vehicle that are applied during coitus. Once optimal rheological parameters are determined for proper function, a chemical structure can be developed for delivery vehicles with those optimized properties. Relating the delivery vehicle structure, property, and function together enables a rational design process.

Gravity

Previous work done in our lab has focused on the initial spread of non-Newtonian polymer solutions, commonly referred to as gels, under gravity-driven flow conditions. These gels are shear-thinning, meaning that as the rate of shear within the gel increases, the apparent viscosity of the gel decreases. Two rheological models have been incorporated into our group's fluid flow simulations: the Ellis model [16] and the power-law model [17]. Both models utilize a no-slip boundary assumption for contact between the gel and an inclined plane, and a free surface for the gel-air boundary, using the setup diagramed in Figure 2. These models have been validated by experiment, having shown the ability to accurately predict how these gels will spread under gravity-driven conditions [16, 17].

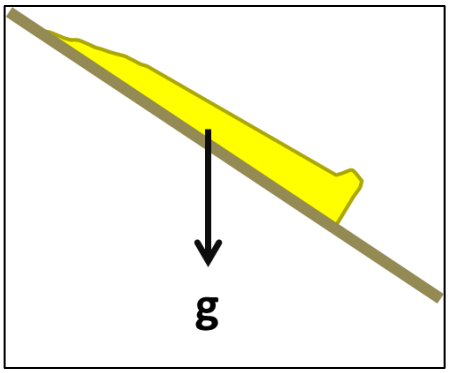

Figure 2: Side view representation of a gel flowing down an inclined plane.

More recently, our group has included surface tension in these gravity-driven models [18, 19]. Surface tension within gels can cause an instability that leads to "fingering" at the front edge of the flow, resulting in an uneven distribution of a gel in a wave pattern instead of a constant even coat [19]. Sheer-thinning fluids have suppressed finger growth and wider fingers [19], so the occurrence and wavelength of the delivery vehicle fingering can be optimized by adjusting a gel's sheer-thinning properties. Unmanaged fingering could have a significant

impact on the initial spread of a microbicide, leaving some of the epithelium unguarded and vulnerable to infection.

Squeezing

The replacement of the free surface boundary condition with an elastic boundary condition to mimic forces applied to the gel by vaginal tissue has made models of initial microbicide spread much more physiological. Numerical modeling, such as the model represented in Figure 3, with both Ellis and power-law rheological properties, has shown that the combined effect of an elastic boundary condition and gravity will greatly influence the final coating of the gel [20-22]. High tissue elasticity has even been shown to dominate the spread of the gel over the force of gravity [20, 22]. Additionally, computational studies have shown that tissue viscoelasticity may also have an impact on gel distribution [23]. Although shown to be important, values of the squeezing forces and the elasticity of the vaginal canal reported in literature are sparse and widely variant. There is a need for measurement of the relevant forces or elasticity that can be applied to the current models.

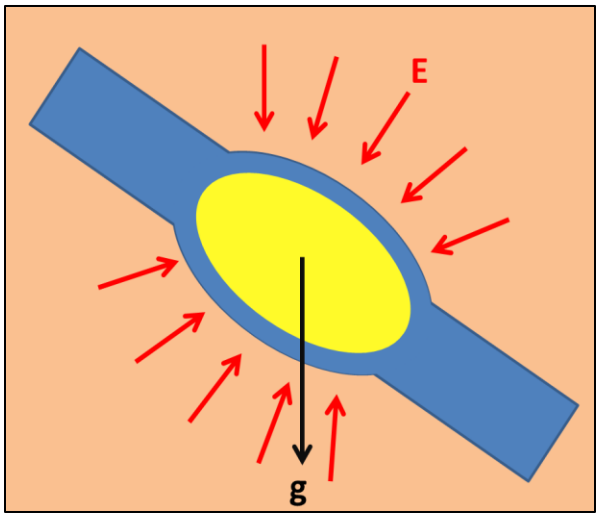

Figure 3: Side view of a representation of a model of gel flowing between two elastic boundaries with squeezing and gravitational forces.

Other Instruments

A complete delivery vehicle spread model should incorporate the vaginal closing force (the combination of forces arising from tissue properties, intra-abdominal pressure, voluntary squeezing, and involuntary squeezing) as a component force or representative pressure acting to

spread the delivery vehicle. Since this varies as a function of the displacement of the vaginal tissue, it is also important to measure the displacement, and to make force measurements at several displacements. The magnitude of the closing force, as it relates to our spreading models, is unclear. Several methods have been utilized to determine magnitudes of one or several of the components, most notably *ex vivo* tissue tensile testing, skin probes, vaginal pressure manometry, dynamometric speculums, force/displacement leaf spring, and vaginal tactile imaging. Although these methods, summarized next in this section, all result in some measure of one or all of the components of closing force, they are all targeted at pelvic organ prolapse. Thus, they all lack, in one way or another, the ability to measure the forces relevant to microbicide delivery vehicle spreading.

An ideal measurement device should have a constant contact area, be able to measure at many discrete sites along the vaginal axis as well as in different directions, evaluate the entire structure *in vivo*, and have controllable and precise displacement control. Constant contact area is important in order to convert measured force into stress in order to interpret vaginal closing force as elasticity. Having a small enough measuring device to be able to measure in different places and in different directions will allow our models to be more precise in the future, as it is highly unlikely that closing force is uniform and independent of direction. Evaluating the structure as a whole in a living human specimen will make the measurements most directly applicable to the current problem. Finally, having precise displacement measurement allows the calculation of strain, which will allow force measurements to be converted into elasticity for use in our models. Making the displacement controllable allows measurements to be converted not just into elasticity, but possibly into a viscoelastic measure for future studies and models.

Ex Vivo Tissue Tensile Testing

In this method a sample of the vaginal epithelium is excised from the vaginal wall during surgery to correct vaginal prolapse [24-27], during a transvaginal hysterectomy [28], from nonformolised cadavers [29], or from ewes sacrificed for other research [30]. The samples are often frozen [25, 26, 29] before being trimmed and affixed to a variety of tensile testing machines, like the one shown in Figure 4. The tissue samples are then subjected to a variety of strains as high as 30% [28], 40% [25, 26] or even to failure [24, 27, 29, 30]. *Ex vivo* tensile testing has produced varied values for the elasticity with a Young's modulus reported as low as 6.65 MPa [28] to as high as 33 MPa [25]. These results are not applicable to our models because they do not account for all components of the vaginal squeezing force, notably the contributions of intra-abdominal pressure, pelvic floor contractions, and contributions from other support structures. Additionally, the available human tissue samples are mostly from prolapsed tissues which often have different properties as compared to those of nonprolapsed samples [29].

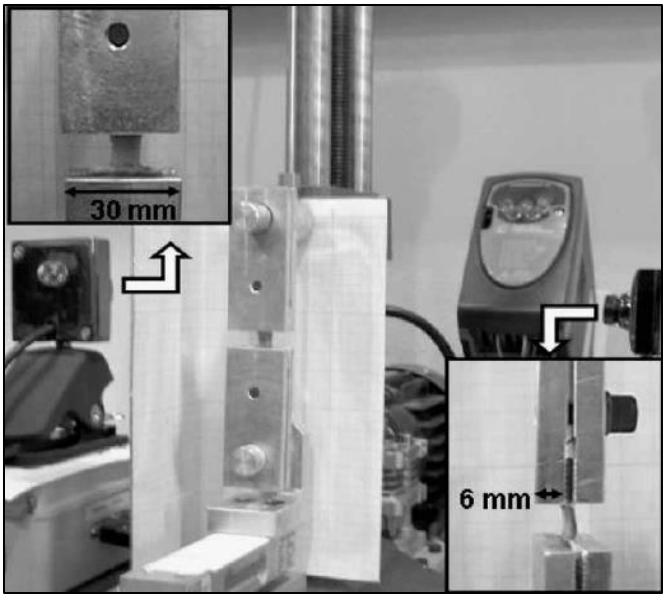

Figure 4: Example of an *ex vivo* tensile test of vaginal tissue copied from Martins *et al.* 2010.

Skin Probe

Probes such as the Cutometer MPA 580 (Courage & Khazaka Electronic) or the DermaLab Skin Probe (Cortex Technology) have also been used to determine vaginal epithelium elasticity [31]. These probes either subject an area of skin to mild suction measuring the

resulting displacement, or measure the amount of suction required to extend the tissue a prescribed amount. These instruments are advantageous for *in vivo* measurements of healthy tissue. They also can be used all along the vaginal axis and in different directions, and they take into account some of the underlying tissue's contribution to the overall vaginal squeezing force. However, they do not measure all of the relevant closing force components, neglecting intra-abdominal pressure, pelvic floor contractions, and most of the underlying structures; and all reported values are in a dimensionless "stiffness index" that cannot be readily adapted to our current models because it is just a comparative method and does not report an elasticity, pressure, or force magnitude.

Newer models, such as the BTC2000™ (SRLI Technologies), incorporate laser altimetry to more precisely measure the tissue uplift [32]. Data from these experiments has been used to fit the vaginal tissue response to a viscoelastic Voigt model yielding Voigt model recovery rates (E/η) between 0.5 and 5.5 sec^{-1} [33]. Although these newer models can provide a much better estimate of tissue viscoelasticity, they still do not take into account the contributions of intra-abdominal pressure, pelvic floor contractions, and most of the underlying structures to the vaginal closing force; and, as can be seen in Figure 5, these models are large and cumbersome enough that they are only used on human subjects who are already under general anesthesia.

Figure 5: The BTC2000™ preforming a suprapubic measurement, similar to the procedure for the vaginal measurement, copied from Mosier *et al.* 2011.

Vaginal Pressure Balloon Manometry

This method uses air filled catheter balloons to measure pelvic floor contractions [34, 35]. A catheter balloon is inserted into the vagina at various depths, and the resting intra-abdominal pressure is used as the zero reference for measurements during voluntary pelvic floor contraction. These instruments are able to be used *in vivo* to measure both a resting vaginal pressure and that due to a pelvic floor contraction. Although some of the balloons are large, smaller balloons can be used to measure at several points along the vaginal axis. Reported values for balloon manometry are as low as 0.49 kPa [34] and as high as 3.1 kPa [35]. These devices measure pressure as a whole and cannot be used to measure force directionally. Since the balloons are flexible silicon rubber, it is never known how far the tissue is being displaced as compared to how much the balloon is elongating under pressure, making it difficult to calculate the proper contact area. These devices come in all different sizes with different technical parameters; so these measurements cannot be compared [6]. Balloon manometry also has no displacement control, and cannot be used to determine viscoelastic properties.

Vaginal Pressure Rigid Manometry

Similar to balloon manometry, vaginal pressure rigid manometry replaces the balloon with a rigid water-infused catheter [36]. These catheters can have from one to several side-holes that can measure pressure in different directions. They have been used to measure the resting and squeezing vaginal pressure profile in four directions with values as low as 0.93 kPa (resting) to as high as 6.67 kPa (squeezing) [36]. Although rigid manometry can be good for measuring absolute pressure and has a constant measurement area, they have a constant displacement; so they cannot be used to generate an elasticity, which our models require.

Dynamometric Speculum

Mounting strain gauges to modified speculums, like the instrument in Figure 6, have also been used to measure the magnitude of vaginal closing force, both resting and during voluntary pelvic floor contractions [37-40]. Strain gauges allow for very high precision measurement of the closing force along the length of the upper and lower measurement arms of the devices. Reported values for these devices also varies widely from a low end of 0.1±0.1 N for incontinent women at the maximum comfortable vaginal opening [41] to the high end of 14.4±3.8 N for healthy women at an unknown opening [38]. This gives a measurement of the summed closing force, but does not offer any spatial resolution. Some dynamometers have no displacement control at all [39], while others have displacement controlled by a hand operated screw [37, 38, 40]. Displacement is measured entirely by eye, and none offer quick and precise displacement control.

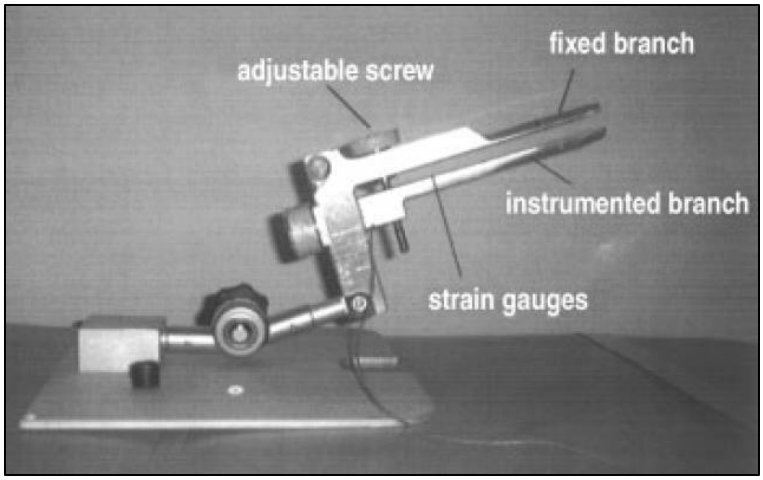

Figure 6: Example dynamometric speculum, copied from Dumoulin *et al.* 2003.

Force/Displacement Leaf Spring

Another approach that can measure along the vaginal axis and has the ability to measure in four directions at once is the force/displacement leaf spring concept developed by Constantinou *et al.* [42-44]. Their device consists of four force sensors mounted to individual leaf springs which, after insertion, are allowed to expand in perpendicular directions as shown in Figure 7. The displacement of each sensor is measured by a Hall Effect transducer. This device

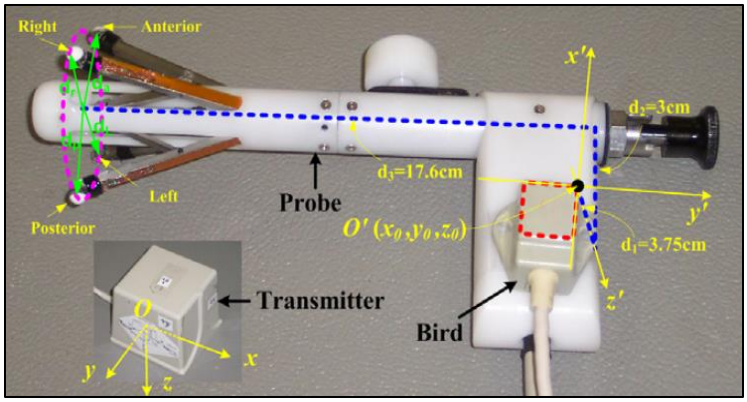

Figure 7: The probe of the Force/Displacement Leaf Spring, copied from Shishido *et al.* 2008.

has been used to measure vaginal closing force: both relaxed and during pelvic floor contractions. Pressure values reported for healthy women are 37.5±4.8 kPa at rest and 48.2±5.0 kPa during pelvic floor contraction [44]. Although displacement is precisely measured by the Hall Effect transducers, it cannot be actively actuated and is only responsive. This makes it impossible to calculate elastic parameters from the data.

Vaginal Tactile Imaging

The most elaborate approach measuring vaginal tissue properties is vaginal tactile imaging. This instrument consists of a vaginal probe equipped with a pressure sensor array and a motion tracking system [45-49]. The hand operated probe, illustrated in Figure 8, measures the 2D pressure pattern on the measuring surface of the probe while the motion tracking system keeps track of the probe position to within 1 mm and 0.25 degree. The only values for vaginal elasticity using Vaginal Tactile Imaging on healthy women reports Young's modulus as 7.4±4.3 kPa [45]. Since the probe is hand operated, it can offer quick position changes, but tissue displacement cannot be precisely controlled. This means that the device could generate elastic properties for vaginal closing force, but would not be able

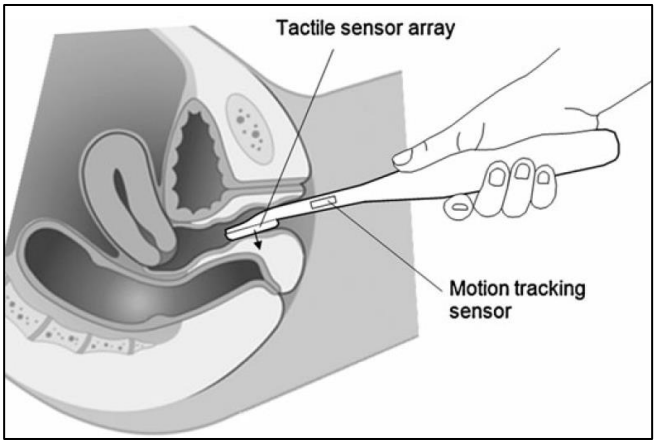

Figure 8: Vaginal Tactile Imaging probe illustration copied from Egorov *et al.* 2012.

to calculate viscoelastic properties in the future. In addition, since the test subject is not also motion-tracked, the system has no way to measure or account for movement other than that of the probe itself, invalidating the measurements if the subject were to move. Additionally, since the probe is only pushing on one side of the vaginal canal, the force could be displacing the entire vagina. If that is the case, the measurement would be measuring forces that are not relevant to squeezing flow models.

Summary

Although there are many devices in the available literature that can provide some measure of one or more component of vaginal closing force, none can provide an appropriate elastic boundary condition for our models to represent vaginal closing force. Table 1 summarizes each method's strengths and weaknesses in the areas of interest for measuring vaginal closing force.

Table 1: Strengths and Weaknesses of Reviewed Devices

Method	Constant Contact Area	Discrete and Directional Measurement	Measures Entire Structure In Vivo	Displacement Measurement	Displacement Control
Ex Vivo Tensile Testing	Y	N	N	Y	Y
Skin Probe	Y	Y	N	Y	N
Balloon Manometry	N	N	Y	N	N
Rigid Manometry	Y	Y	Y	N	N
Dynamometric Speculums	Y	N	Y	Y	N
Force/Displacement Leaf Springs	Y	Y	Y	Y	N
Vaginal Tactile Imaging	Y	Y	Y	Y	N

These instruments do provide data that can inform the design of future instruments. Specifically, the Vaginal Tactile Imaging studies report elasticity arising from vaginal closing force of 7.4 kPa [45]; and the force/displacement leaf springs report pressure measurements of 37.5 kPa [44].

Chapter 2) Instrument Design Process

Design Requirements

There have been many approaches to measuring vaginal closing force. Each of the previously developed instruments investigated gives valuable data, but isn't an ideal instrument for our needs. After reviewing the available literature, I began designing an instrument better suited to our needs and developed the following goals. An ideal measurement device to measure all aspects of vaginal closing force would be controllable, operate in a variety of modes, have a constant contact area, be able to measure at different places along the vaginal axis and in different directions, be modular and upgradable, be convenient and easy to operate in a clinical environment, and, above all else, be safe to operate for both the technician and the test subject.

Measure Force and Displacement

It is important to measure both vaginal closing force and displacement in order to determine appropriate elasticity parameters for our future models.

Controllable

The instrument must have precise and quick displacement control. Precise and quick control will allow the instrument to determine if there is frequency dependence for any component of the vaginal closing force.

Constant Contact Area

Having a constant contact area for the probe will allow the instrument to produce results that can be more easily incorporated into mathematical tissue models.

Discrete and Directional

Having the contact area constant and small will allow the instrument to make measurements along the vaginal axis and in a variety of different orientations. This will allow

the instrument to be used to make a map of the vaginal closing elasticity for more complex 3D models of delivery vehicle spread.

Modular and Upgradable

The device design should be modular to allow the quick upgrade or replacement of individual systems. It should also easily allow for future modifications for viscoelastic measurements and frequency sweeps, and to operate in a controlled force mode, rather than just a controlled displacement mode.

Convenience

The instrument should have an easy user interface so that it can be easily operated by healthcare professionals without engineering training. It is also important to keep the probe size at a minimum and eliminate or conceal the wiring and driving motors to make the device as subject-friendly as possible.

Safety

The safety of the instrument is extremely important. Any leaking hydraulic oil could greatly impact the vaginal flora; so, although not ideal mechanically, any hydraulics should be run with purified water as the fluid. The probe must also be designed with cleaning in mind, using materials and part geometries that can be easily sterilized. Also, there should be no electrical components in the probe.

Mechanical Design

Initial Instrument Design

The initial mechanical design of EVE (Elevated-surface Vaginal Elastometer) consisted of two main parts: the driving end and the probe end. The driving end includes a base, the motor, the encoder, the load cell, the parent bellows, and various support pieces. The driving end is used to drive and monitor the force and displacement of a water filled parent bellows which is hydraulically linked to a daughter bellows on the probe end through tubing. Water forced out of the driving end flows through the tubing and into the bellows housing at the probe end. This influx of water collapses the probe end daughter bellows and extends the measuring surface, as illustrated in Figure 9. Because the two bellows are hydraulically linked, the force and displacement experienced on the probe end should be calculable from the force and displacement measured at the driving end, with proper calibration.

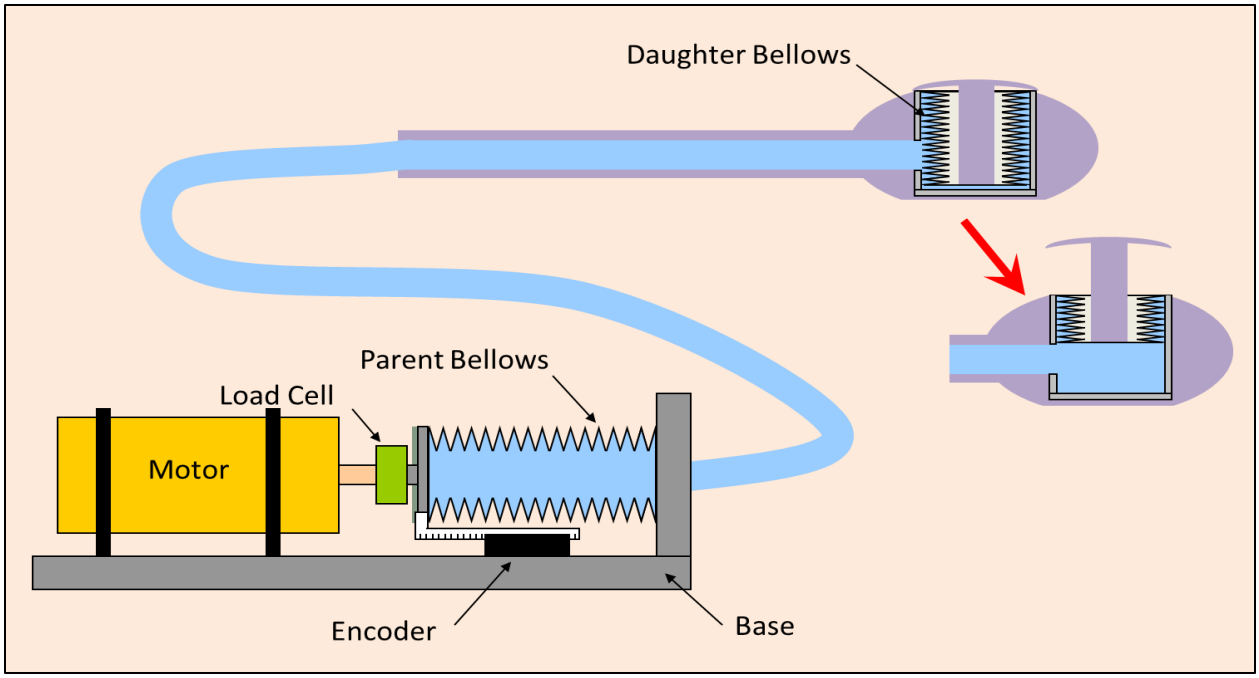

Figure 9: Early schematic of EVE design and actuation.

Driving End

The modular design of the driving end, shown in Figure 10, begins with a 27.5" long aluminum base with three T-slot mounting tracks (1545, 80/20 Inc.). This base provides a solid mounting surface for the individual modules of the driving end. It also allows the modules to be easily changed and ensures that they are aligned when mounting. The custom machined aluminum mounts for each module are allowed to slide back and forth along the base before being tightened into place. This ensures that proper distances between each module can be maintained.

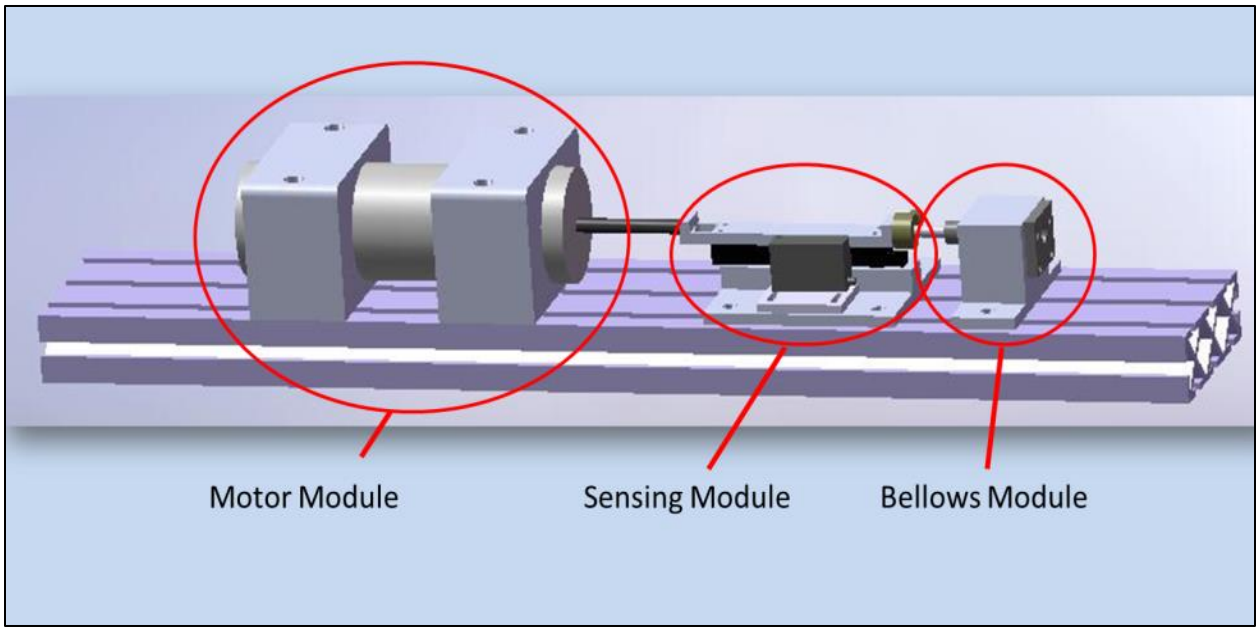

Figure 10: CAD model of the initial driving end design.

To drive the system, a moving magnet DC voice coil linear actuator (NCM30-25-090-2LB, H2W Technologies) was chosen to be the primary component of the motor module. Voice coil actuators have advantages over other linear actuators because they have fewer moving parts while still being quick and controllable. In general mechanical actuators operate at slower speeds, and have screws and threads that can wear and jam. Hydraulic actuators are also more

complex than necessary, and take up much more space due to the required pumps and reservoirs. Pneumatic actuation was not considered because of the bulk of most air compressors, and the loud noise would have been inappropriate in a clinical environment. Voice coil actuators offer a large force-to-size ratio and high accelerations that are required for the application. The selected motor offers a peak continuous force of 40 N and a peak force of 120 N at 10% duty.

The second module of the driving end, the sensing module, incorporates both of the sensors for the device. First, an encoder system (RGH22, Renishaw) measures the displacement of the linear actuator. The RGH22 is an optical encoder that measures displacement with a precision of 50 nm. The system works at high speed without adding any friction to the system, making it ideal for this application. The second sensor, which measures the driving end force, is a sealed load cell (WMC-10, Interface). This was chosen for its small size, because it works in both tension and compression, and, at a capacity of 44 N (10 lbf), matches the peak continuous force of the motor. The load cell and the encoder ribbon are both mounted to a ball slide linear bearing (E-4, Del-Tron Precision), which keeps the travel of the EVE driving end constrained to a precise linear path in order to allow the encoder to operate correctly.

The third module of the initial driving end design houses the water-filled bellows that drives the probe end. The bellows chosen was an edge-welded stainless steel bellows (WB-816, MDC Engineered Process Solutions). This bellows was chosen to match the probe bellows at 0.5” diameter; but, at 1.69” in length, it is much longer. This has the effect of reducing the force required from the motor to displace the bellows by decreasing the bellows spring constant.

Probe End

Connected to the driving end through tube fittings and nylon tubing, the probe end consists of a Delrin body surrounding a stainless steel bellows assembly.

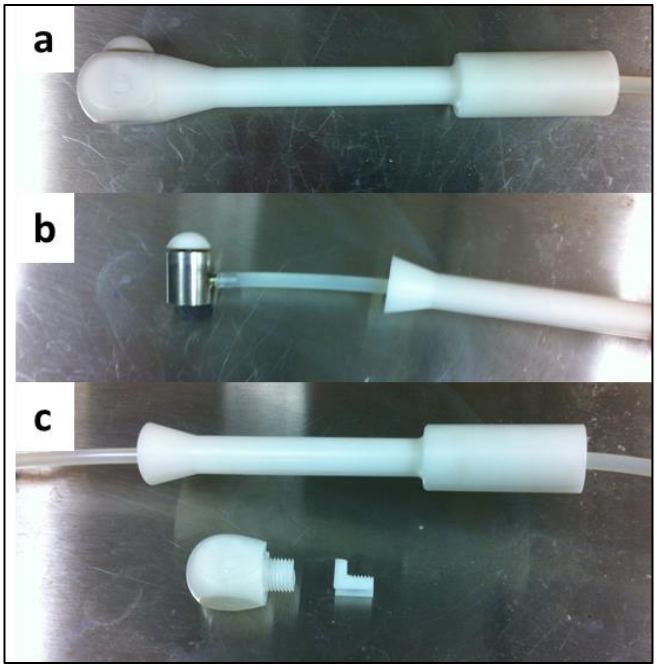

Figure 11: EVE probe end.
a) Assembled probe
b) Bellows casing
c) Disassembled probe end

Delrin was selected for the probe body because of its ease of machining, and ability to be easily sanitized by immersing it in a sterilizing solution (CIDEX OPA, Advanced Sterilization Products). The custom machined body consists of three parts: the two part head and the handle. The head is divided into two parts to allow easy removal of the bellows casing; and the two parts are held together by the handle, which screws over both pieces. The probe body, when assembled, is 19.5 cm long with smooth transitions between the 5 cm long measuring area, 8.75 cm long shaft, and 5.75 cm long handle. The end of the probe containing the bellows casing is 2.5 cm square with rounded corners and a protruding 9.6 mm radius of curvature measuring surface, which tapers down to the 1.5 cm diameter shaft, before becoming the 2.5 cm diameter grip. The maximum collapsed height of the probe is 3.25 cm at the apex of the measuring surface.

The bellows casing consists of several parts which are held together by silver solder (Stay-Brite, Harris Products Group), and biocompatible epoxy (EP21LV, Master Bond). Because bellows are more stable in compression, the housing is designed to have water surround

the bellows. When water is forced into the housing by the driving end, the bellows collapses to accommodate the additional volume. This in turn extends the measuring surface against the material to be measured.

Mechanical Design Revisions

As with any project, unforeseen issues have necessitated some changes in the design. The modular design made many of the changes easier, but significant changes were needed in order to make EVE operational.

Bellows Sealing

The first problem encountered, which necessitated a design change, was difficulty in getting a watertight seal of the probe bellows casing assembly. Initially the assembly was done using only silver solder, which provided a strong bond; but it was difficult to obtain and maintain a watertight seal. Pinhole leaks developed frequently, and the entire assembly would need to be rebuilt. A second solution was attempted with biocompatible epoxy (EP21LV, Master Bond). With the epoxy, it was easy to create and maintain a watertight seal. However, the epoxy lacked the necessary strength and was prone to catastrophic failure, especially in any joint undergoing tensile stress. A solution was found by changing the design to eliminate the joints where tensile stress occurred. The bottom cap was incorporated into the casing wall in order to eliminate one problem joint, and the top cap was modified to incorporate a retaining ring, as shown in Figure 12. These changes removed the tensile stress on the epoxy joints, allowing the epoxy to be only responsible for making the joints watertight.

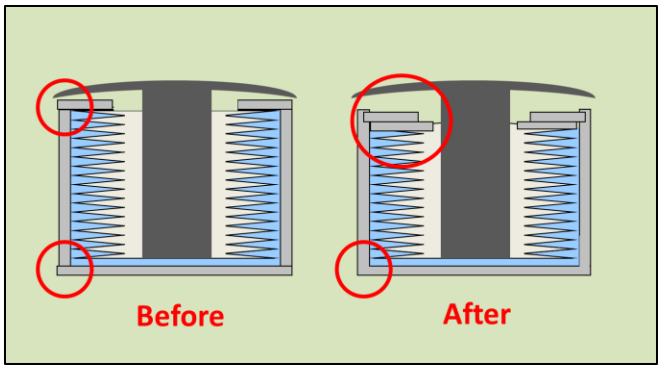

Figure 12: Illustration of the initial and final bellows casing.

Bellows Sizing

Both bellows in the initial bellows set had matching diameters of 0.50". Since water is incompressible at the operational pressures of EVE (under 30 kPa), equal bellows diameters were used with the anticipation that they would have a displacement ratio of 1:1 between the driving and probe ends. Initial testing showed that, not only was the displacement not a 1:1 ratio, the long 1.69" length of the driving bellows combined with the narrow 0.50" diameter caused a significant buckling issue. Slight misalignments would cause the bellows to buckle easily when compressed, which was a problem for two reasons. First, the difference in shape of the unbuckled vs buckled bellows changed the volume of water displaced for the same motor position. Second, the buckled bellows would rub on the support piece adding friction to the force measurements. It was evident very early that a new bellows was necessary. A new bellows was ordered with a 1.07" diameter, and 1.38" free length (WB-801, MDC Engineered Process Solutions). This new bellows, shown in Figure 13, required that some parts, like the bellows mount, be modified, while others, like the bellows mounting plate, were redesigned to fit. Being both wider and shorter than the previous bellows the replacement bellows does not have the buckling issues of the original bellows.

Figure 13: Size comparison of old and new driving bellows.

Motor Sizing

Changing the driving bellows produced consequences beyond eliminating the buckling issues. Increasing the bellows diameter by a factor of two increased the hydraulic area that the motor is now acting on by a factor of four. This increased area means that. in order to develop the same system pressure for extending the measuring surface, the motor must produce four times as much force as previously, assuming no change in bellows stiffness. This necessitated a switch to a much larger voice coil motor (NCM-30-40-350-2LB, H2W Technologies) capable of a maximum continuous force of 156 N, compared to the 40 N maximum of the old motor. This larger motor generates forces well beyond the capacity of the old load cell; so a new matched load cell (WMC-50, Interface force), which has a capacity of 222 N (50 lbf), was also selected and incorporated into the design. The new motor and load cell combination is a scaled up version of the previous pair; so very little adjustment to the programming needed to be done to accommodate the change. The new motor can now easily drive the new bellows system.

Air Within the Hydraulic System

Any air that finds its way into the hydraulic system greatly changes the compressibility of the system, and makes accurately driving the probe bellows more difficult. Air in the system comes primarily from two sources: clinging to crevices during initial assembly and through air-permeable joints when the system is under negative relative pressure. Bleeding air from the system initially involved disassembly of barbed tube fittings underwater to release the air bubbles. This process would deform the tubing and worsen air leakage under negative pressure.

Three design changes were made to the hydraulic system because of air bubbles: two to prevent as much air entry as possible, and the other to enable easier bleeding of the system. The first, and most simple of the changes, was replacing, wherever possible, barbed tube fittings in favor of compression tube fittings. Compression fittings are more airtight, but are larger, so the fitting at the probe end bellows assembly was unable to be changed and remains a barbed fitting. Although the remaining barbed fitting can still let some air into the system, the amount is small enough that regular bleeding is sufficient to maintain reliable operation. The second change was adding a bleed point in the middle of the tubing length. This bleed point is simply a "T" junction with two tube fittings and a male pipe fitting closed with a threaded end cap. Now bleeding consists of removing the end cap under water and allowing the air to escape. This minimizes the damage to the tubing, and simplifies the bleed process.

The third hydraulic system change allows an initial pressure to be applied to the system so that the system is never under negative relative pressure, preventing much of the air from entering the system. A second "T" junction was added, identical to the bleed point junction. The pipe fitting on this junction has a one-way check valve and a modified syringe that can add water to the hydraulic system; this is shown in Figure 14. After assembly and just before testing, up to one additional milliliter of water is added to the system to ensure constant positive pressure. The check valve

Figure 14: The pre-pressure junction, check valve, and syringe.

prevents backflow; and the additional water raises the system pressure to keep air from entering the system from joints that are watertight, but not airtight.

Final Design

The final design, taking the initial design and incorporating the design revisions described previously, can be seen in Figure 15; and technical part drawings for the custom-machined parts are available in Appendix A.

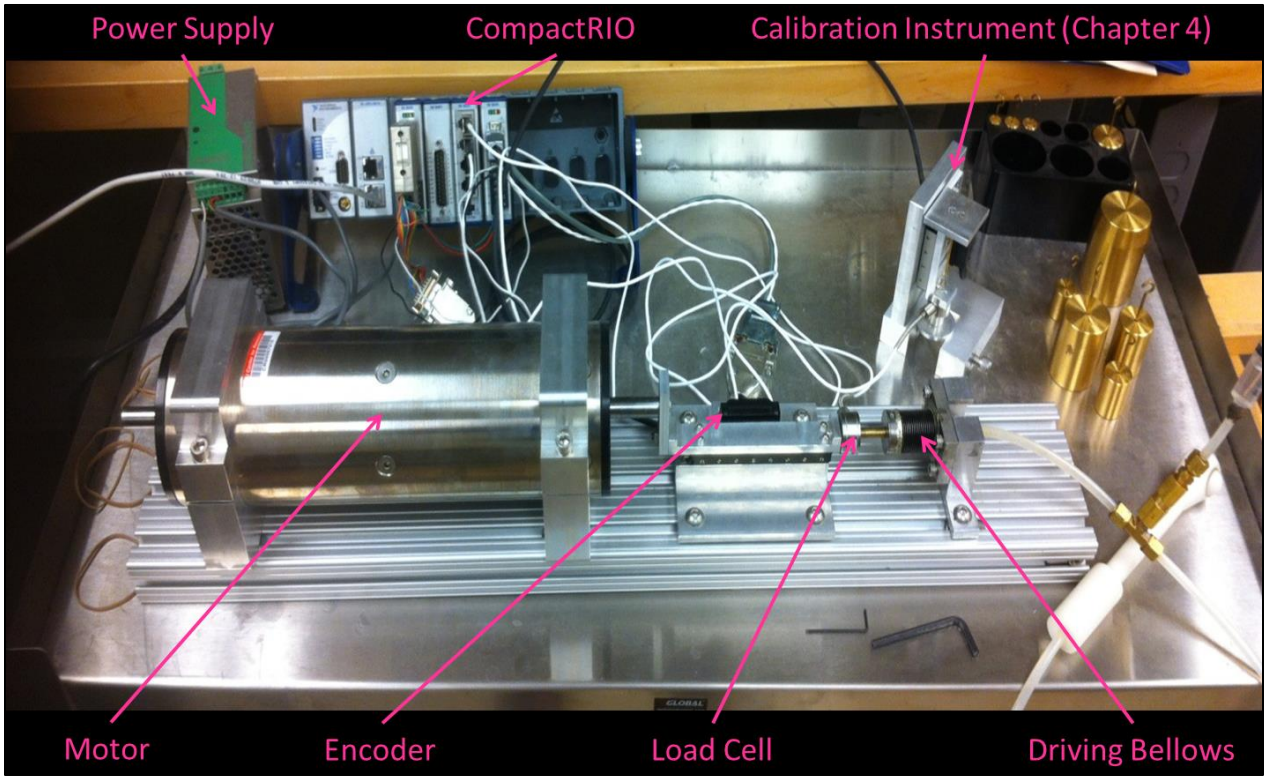

Figure 15: EVE final design and build.

Software Design

The programming for EVE was completed in National Instruments LabVIEW to run on the National Instruments CompactRIO configurable control and monitoring system shown in Figure 16. The CompactRIO allows up to eight swappable modules to customize the platform for a specific application; and EVE utilizes three of these slots. A 9237 module was used to collect load cell data from both the driving end and the calibration instrument. Two 9505 modules were used: one to read the driving end encoder and drive the motor, and the other to read the encoder of the calibration instrument which is discussed in Chapter 4. The code executes on three different computers (FPGA, Real-Time Computer, and Host Computer) simultaneously utilizing each computer's strengths to control the instrument and collect data reliably. The interaction between the computers is summarized in Figure 17.

Figure 16: The National Instruments CompactRIO.

FPGA

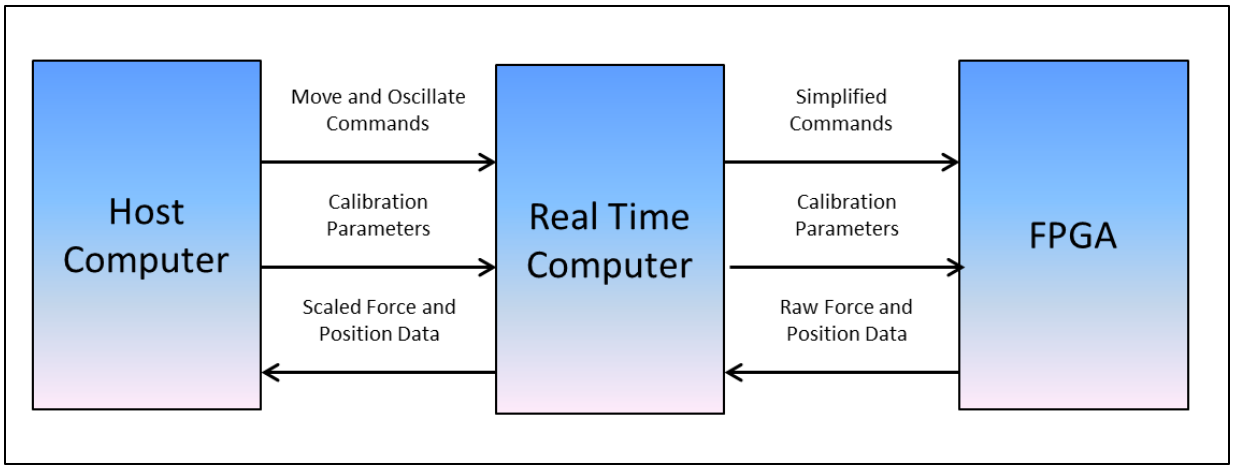

Figure 17: Interactions between the three EVE computers.

The most basic computer is the FPGA, or Field Programmable Gate Array, which is housed on the CompactRIO. The FPGA is the primary processor of signals for EVE. As a programmable gate array the FPGA is essentially an easily customizable logic chip that can process numerous tasks at once in parallel. Currently the FPGA runs 14 loops in parallel, which can all run simultaneously at whatever speed is appropriate for the loop. Several of the loops are in constant communication with each other and the other two computers. Surface level loops communicate with the higher level computers, while several process loops quickly accomplish their continuous lower level tasks.

One of the most important surface level loops is the Position Set Loop; it is the heart of the motor control process diagramed in Figure 18. The Position Set Loop takes commands from the Real-Time Computer and calculates what the driving end encoder position should be. Driving end control is accomplished by sending the Position Set Loop either the velocity and

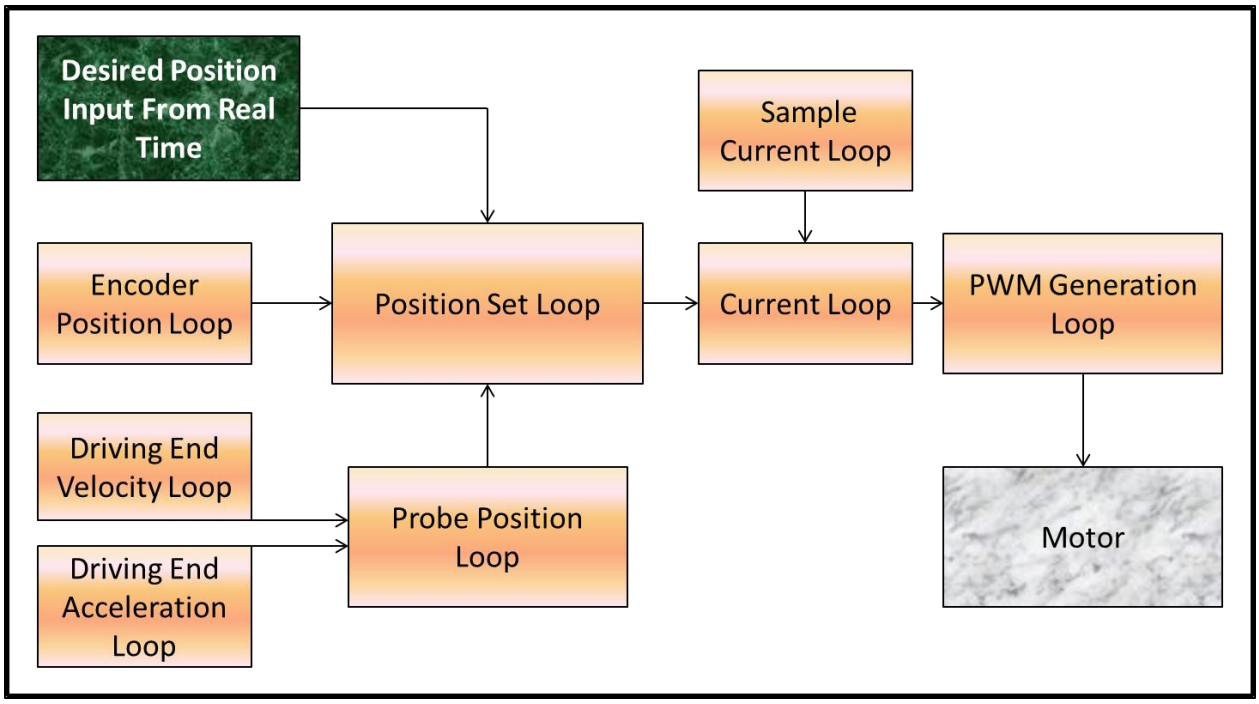

Figure 18: Schematic of FPGA loop interactions for motor control.

desired end position of a move or the frequency, amplitude, and number of cycles of the desired oscillation. The Position Set Loop then calculates the desired position of the driving end encoder and feeds that position, along with the latest driving end position reading, to a PID controller. The PID controller then outputs the value of the electrical current to the motor needed to achieve the desired encoder position. In probe-control mode, a step is added utilizing the Probe Position Loop, a process loop which takes in data from other process loops that calculate the driving end position, velocity, acceleration, and force. Within the Probe Position Loop, the appropriate driving end position is then calculated using the calibration equation determined through the calibration process which is discussed in Chapter 4. This desired driving end position undergoes the same process as driving end control, resulting in the proper probe displacement. The desired electrical current is taken as an input of the Current Loop. The Current Loop is a process loop that evaluates the desired current and makes sure it is safe before comparing it to the current feedback, which is sampled in another process loop (Sample Current Loop), and then sends those values to an internal PI controller. This output is sent to another independent process loop, the PWM Generation Loop, in which a pulse width signal is generated and sent to the motor.

The other main surface level loop is the Data Acquisition Loop. This loop samples important values from other parts of the FPGA program and collects them into an output packet for the Real-Time Computer. This packet is constantly updated to provide the most recent sample of data for the Real-Time Computer.

Real-Time Computer

The second computer is also housed within the CompactRIO, and it operates in real-time. Real-time refers to the deterministic way which this computer processes information. Most computers do not run in real-time. If you tell a standard personal computer to complete a task every 500 cycles it will be completed on average that often, but the task may be completed at

496 clock cycles for one instance of the task and at 504 during another. A real-time computer will accomplish the task at 500 cycles every time. This makes the Real-Time Computer the ideal place to capture the data from the FPGA for saving.

The main tasks of the Real-Time Computer for EVE are to capture the data from the FPGA in a deterministic manner, sending that data to the Host Computer for saving, and coordinating the communication and commands between the Host and FPGA. Since the FPGA does not process higher level mathematical operations, the Real-Time Computer is used to take commands from the Host Computer and reformat them into signals and cues that the FPGA can process. This can be breaking down a velocity for a move into which loop iterations to increment the position set point, or simply getting the commands from the Host Computer to scale correctly from the double precision floating-point structure of the Host Computer to the fixed-point architecture of the FPGA.

Host Computer

The Host Computer is a standard laptop which runs LabVIEW in order to facilitate the human interaction with EVE and to serve as a hard drive to save the relevant data. Data are received from the Real-Time Computer and sent to waveform charts so that the user can monitor the operation of EVE. With the flip of a virtual switch, data can be captured by the user into a .tdms file to be processed later. The HostGUI.vi program uses a user-provided base file name and appends to it the date and time in order to differentiate files and allow the user to capture many files without overwriting the file each time.

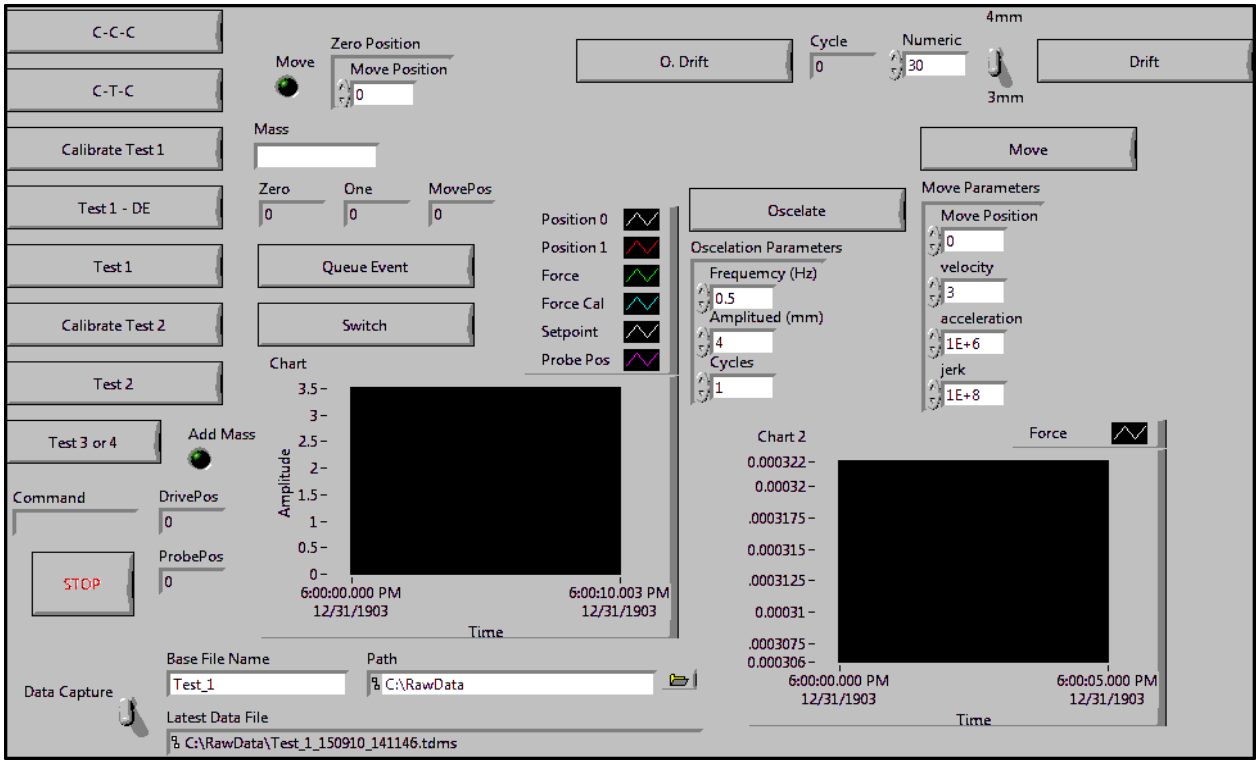

Figure 19: Current host computer user interface, where buttons on the top and right are programmed automatic protocols, data capture is controlled in the bottom left corner, the "Oscillate" and "Move" buttons control the instrument's two basic movements with their respective inputs below, and two charts which display the latest values from the sensors.

In the most basic operation, the user can send EVE to a given position at a given velocity or prescribe an oscillation frequency, amplitude, and number of cycles to complete. The user is also able to designate a base file name and stop or start data capture at any point. I have also programed several custom process buttons, which can be seen in Figure 19, that automatically perform the protocol for a given test, including changing base file names and precisely timed movement commands and data capture periods. Several of these test procedures are described later.

Chapter 3) Tissue Phantom Validation Design Process

Tissue phantoms can be tuned to mimic human tissue elasticity and have been used to validate many methods of measuring elasticity of different tissues [50-53]. Gelatin-based and agar-based phantoms can be used to validate EVE, characterize its operation, finalize the human subject protocol, and ensure its reliable operation before human subject testing begins. Although all of these tests have not been completed, the framework of the test design is still valuable for future validation of EVE.

Selection and Manufacture of Tissue Phantoms

The six phantoms, five gelatin (Ballistic Gelatin Lot#00535, Gelatin Innovations) and one agar (A360-500, Fisher Chemical), shown in Table 2, were selected and produced using a protocol modified from Hall *et al.* [50] described later in this section. The phantoms selected have an expected Young's modulus covering a range from the 7.4 kPa reported from vaginal tactile imaging [45] to higher values that EVE may encounter during contractions or from underlying tissues. The agar phantom is included because it can show nonlinear behavior [50], and data from this study may be used in the future to show that the EVE can detect nonlinearity.

Table 2: Phantom Formulations.

Number	Type	Gel (g)	Water (mL)	Formaldehyde (mL of 37% solution)	Expected E (kPa)
1	Gelatin	40	996	4	7.6
2	Gelatin	60	996	4	17.7
3	Gelatin	80	996	4	32.3
4	Gelatin	100	996	4	51.5
5	Gelatin	120	996	4	75.3
6	Agar	11.4	1000	0	32.2

Formaldehyde is added to the gelatin phantoms as a hardener. The formaldehyde increases crosslinking in the gelatin which increases the stiffness and melting point [54]. The

formaldehyde also continues acting for several weeks after the phantom is manufactured, so it will be important to test each phantom at the same time post-manufacture. Hall *et al.* used n-propanol in order to manage the speed of sound within the phantom [50] because their phantoms were used for ultrasound testing. For these tests, the n-propanol was removed as unnecessary and replaced with an equivalent volume of water.

Hall *et al.* also reported that an expected Young's modulus could be estimated from the concentration of gel by the relationship $E_{gelatin} = 0.0034C^{2.09}$ and $E_{agar} = 0.34C^{1.87}$, where E is the Young's modulus in kPa and C is the concentration of the gel in g/L [50]. These formulas were used to find a set of gelatin phantoms which represented the range of interest. The concentration of the agar phantom was determined in order to match the expected Young's modulus of Phantom 3, the 80 g gelatin phantom.

The phantoms were manufactured using the following procedure adapted from Hall *et al.* [50] and the formulations in Table 2:

1. Heat the water to 80° C and add gel slowly to prevent clumping
2. Stir for 10 minutes using mechanical stirrer to allow gel to dissolve
3. Add formaldehyde (if applicable) and continue stirring for 30 seconds
4. Pour into mold in waiting ice bath and let the solution cool for 3 minutes
5. Remove mold from ice bath, cover and put in refrigerator
6. Remove from mold 8-24 hours later, after hardening
7. Store in airtight bag in refrigerator
8. Let sit for one week from manufacture to allow formaldehyde to crosslink gelatin

Tissue Phantom Mold Design

A special mold, shown in Figure 20, was made for the phantoms to set in, technical drawings of which can be found in Appendix A. The mold creates a cube of phantom which is four inches per side, with a one inch diameter cylindrical cavity through the phantom in the center of two opposing faces. These dimensions were chosen with the cavity matching the approximate size of the probe and the sides to allow the finished phantom to be approximately a cube with a volume of one liter to match the volume of the phantom recipe. The mold was designed to easily disassemble for easy release of the phantom and easy cleaning. Because of this, the mold has several joints which are made temporarily water tight through the use of washable glue. The glue holds a watertight seal long enough for the phantom to set, while still being easy to clean. Soybean oil-based spray is also used on the interior surfaces of the mold to prevent phantom damage by facilitating a clean release of the phantom from the mold.

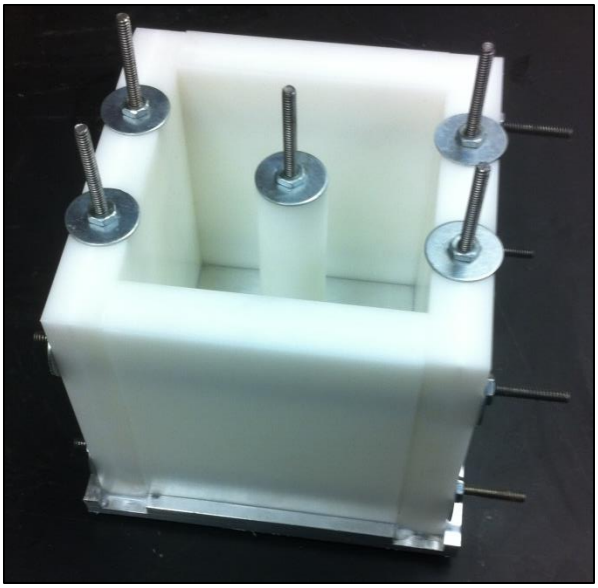

Figure 20: Assembled phantom mold.

Phantom Test Design

Phantom Data Collection Protocol

Prior to testing, the phantom will be removed from the refrigerator and allowed to sit for two hours in order to warm up to room temperature. The phantom will then be placed on its side, and a female condom may be placed into the cavity. After initializing EVE ,the probe will be calibrated following the procedures outlined in Chapter 4 for the target frequency; and then the probe can be inserted approximately six centimeters with the rear supported to keep the probe approximately level, as shown in Figure 21 (support out of frame). Once the probe is inserted, the EVE control software will perform the desired test. At the end of each test the measuring surface will be retracted to zero displacement, and the probe will be removed and recalibrated for the next test.

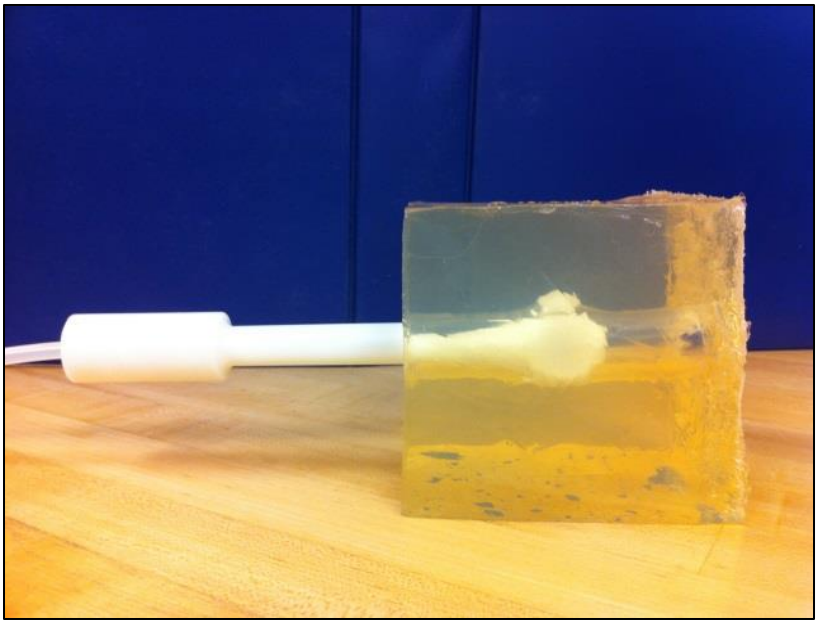

Figure 21: Tissue phantom with probe inserted ready for test procedure.

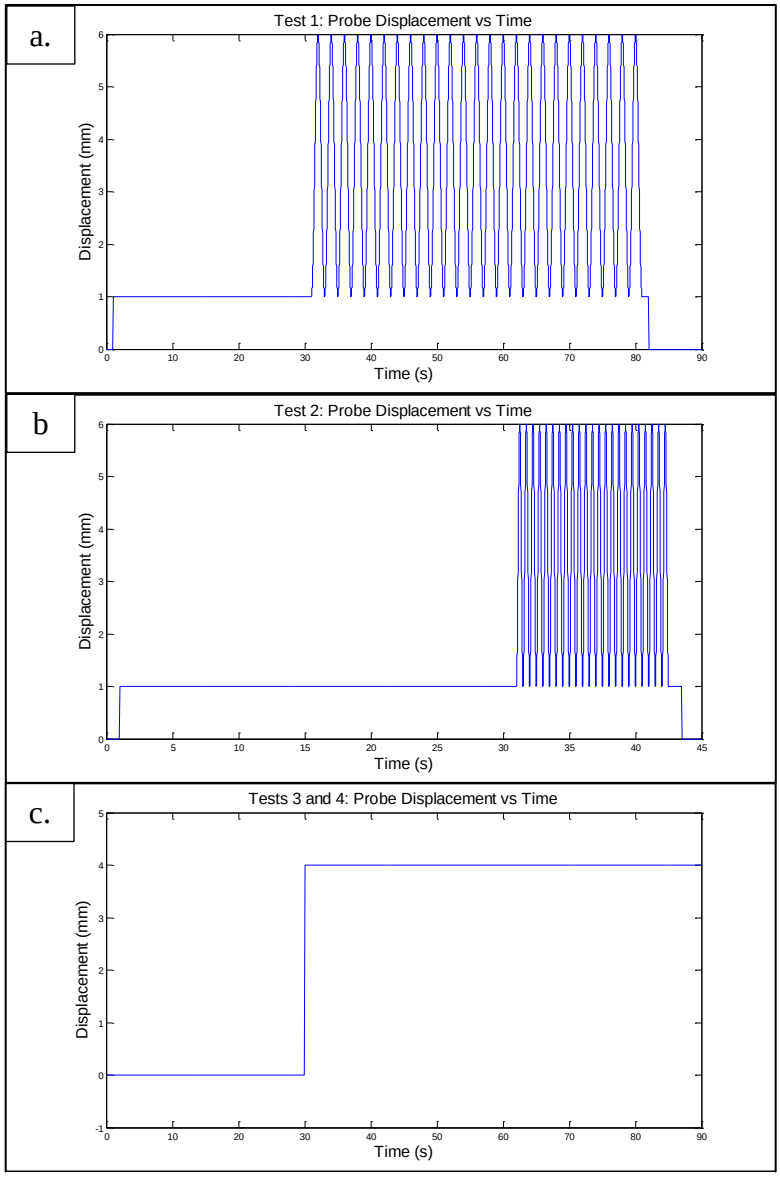

Figure 22: Probe displacement over time for each of the planned tests.

The first test will apply a 1 mm initial displacement which will be held for 30 seconds followed by a 0.5 Hz oscillating displacement with a magnitude of 5 mm for 25 cycles while recording the force and displacement measured at the driving end and the calculated force and position at the measuring surface (Figure 22a). The second test will follow the same procedure as the first, but the frequency of oscillation will be changed to 2 Hz (Figure 22b). For the third test, EVE will apply a step displacement of 4 mm which will then be held for one minute while recording the force and displacement measured at the driving end and the calculated force and position at the measuring surface (Figure 22c). The fourth test will follow the same procedure as the third, but approximately 20 seconds after the step displacement, a 500 mg mass will be gently placed on the top surface of the phantom.

Elasticity will be estimated by looking at the 20th loading cycle of each frequency from Tests 1 and 2. We will estimate stress from the instrument force over the area of the measuring

surface (265 mm^2) and strain from the instrument's displacement over the thickness of the phantom from the cavity edge to the outside edge of the phantom (3.8 cm).

Plans for Pilot Phantom Study 1

The first pilot study was designed to test for phantom damage from the EVE procedure and repeatability of the combined calibration and testing process. Even though tissue damage in human subject testing would be very unlikely, the phantoms were selected in order to match the expected stiffness component of the vaginal closing force and are much more susceptible to damage than the tissue they mimic. It will be important to confirm that testing will not damage the phantoms, and that each phantom can be used for multiple tests.

Phantom 1 will be run through the testing procedure ten times and examined for any damage to the phantom. Special care will be taken to look for tearing of the gelatin and for cracks extending from the measurement site.

In addition to direct observation of phantom damage, a comparison of the elasticity estimates for each frequency will be made over time to check for phantom damage. Additionally, a student t-test will be performed on the elasticity estimates at each frequency to test for repeatability. If the t-test reveals a significant difference among the measurements, steps will need to be taken to ensure that no phantom damage is occurring and to ensure that EVE is operating repeatably.

If damage is found to be more than minimal, the phantom data collection protocol will be modified to decrease total displacement and/or the oscillation frequency. Additionally, this pilot study may be repeated with Phantom 2 Phantom 1 proves to be too delicate for the testing procedure. If Phantom 1 is too fragile to stand up to repeated testing, it may be removed from the future studies, or the number of repeated tests on it may be greatly reduced.

Plans for Pilot Phantom Study 2

The second pilot study was designed to determine the effect of a female condom on the elasticity estimate. Using a female condom will increase patient safety and facilitate easier cleaning of EVE; however, the female condom may affect the elasticity measurement. This study will be used to determine if there is a significant change in the elasticity measurement from using a female condom, and will be used to evaluate the necessity of using female condoms in the main phantom study as well as future *in vivo* studies.

Phantom 3 will be run through the testing procedure ten times, five without a female condom in place and five with the female condom in place alternating between the two cases. The elasticity estimate from the loading portion of the 20^{th} cycle for each condition at each frequency will be compared by using a student t-test. If the t-test reveals a significant difference between the measurements, the use of the female condom may be removed from future *in vivo* studies, and a more thorough probe cleaning process may be required.

Plans for the Main Phantom Study

The main phantom study is designed to demonstrate the reliability and repeatability of EVE. It will involve all six phantoms, and each single phantom will be run through the phantom data collection protocol five times, as shown in Table 3. Data analysis for this study will look at the elasticity estimate at each frequency on the loading portion of the 20^{th} cycle. For each phantom, a standard deviation will be calculated for each frequency to evaluate repeatability. A two factor ANOVA will also be performed on the EVE data, using the two factors of phantom and frequency, in order to verify a significant ability to detect a change in elasticity or a frequency dependence in the phantom or EVE.

Table 3: Data to be Collected in the Phantom Study.

Phantom	Test 1 (0.5 Hz)	Test 2 (2 Hz)
1	E ± SD (n=5)	E ± SD (n=5)
2	E ± SD (n=5)	E ± SD (n=5)
3	E ± SD (n=5)	E ± SD (n=5)
4	E ± SD (n=5)	E ± SD (n=5)
5	E ± SD (n=5)	E ± SD (n=5)
6	E ± SD (n=5)	E ± SD (n=5)

Tests three and four from the protocol will be performed and the data will be archived for possible later use, with no statistical analysis performed at that time. Their inclusion in this procedure is to evaluate possible human subject protocols and monitor the device for proper operation.

Chapter 4) Design Process for Calibration Instrument and Procedure

Calibration Instrument

A second instrument was also developed to be used to calibrate EVE. The calibration instrument, shown in Figure 23, measures the force and displacement of the measuring surface of the EVE probe. These measurements are then used to make the calibration equations, which relate force and displacement at the driving end to the force and displacement of the measuring surface. To simplify programming, the calibration instrument uses the same initial load cell (WMC-10, Interface) and encoder (RGH22, Renishaw) as the driving end of EVE. The calibration instrument features a set screw to keep the probe head in position during the calibration process, as well as a platform for calibration masses. The ability to add elastic bands gives the operator the option to vary the load during the calibration process to calibrate the instrument under more physiologically relevant loads.

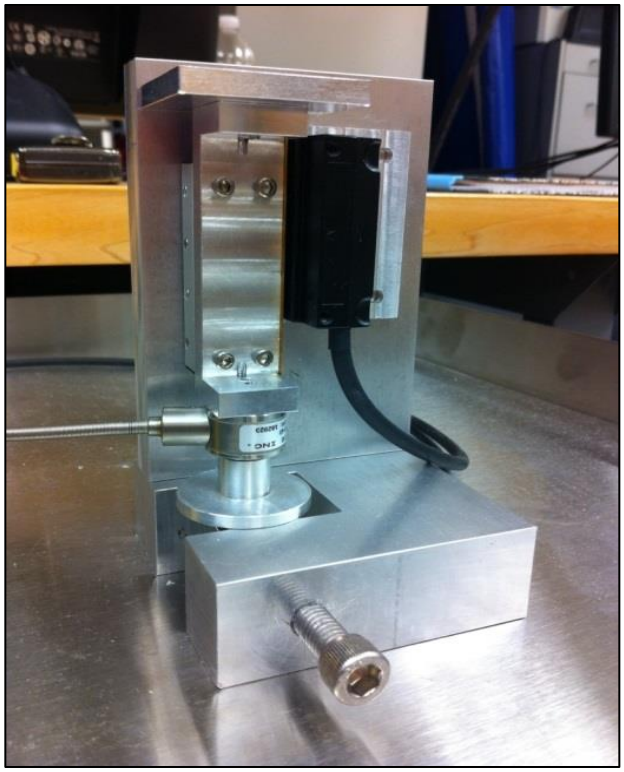

Figure 23: The calibration instrument.

Technical drawings of the calibration instrument machined parts are available in Appendix A.

Force and Position Calibration Process

In the initial design, with both bellows of matching diameter, the expectation was that the displacement at the probe end would be identical to the displacement at the driving end. Even

when the driving bellows had to be replaced; it was hoped, due to the incompressibility of water, that the probe end position would still be a simple ratio of the driving end position.

Similarly, because the two bellows are linearly elastic, determining the force at the probe end was initially thought to be easily calculated through a linear function of the driving end force and position such as: $F_P = c_1F + c_2P$, where F_P is probe end force, F is the driving end force, P is the driving end position and c_1 and c_2 are the two constants to be determined through calibration. The c_1F term represents the relationship between the force at the probe end and the force at the driving end and the c_2P term acting to account for the effect of the elastic bellows.

These models, however, were extremely optimistic as illustrated by Figure 24, which shows that calculating the probe end position requires at least the inclusion of the driving end force, and not simply a ratio of the bellows' dimensions. This began a search for a new calibration equation, with the goal of finding an equation that would allow accurate calculating

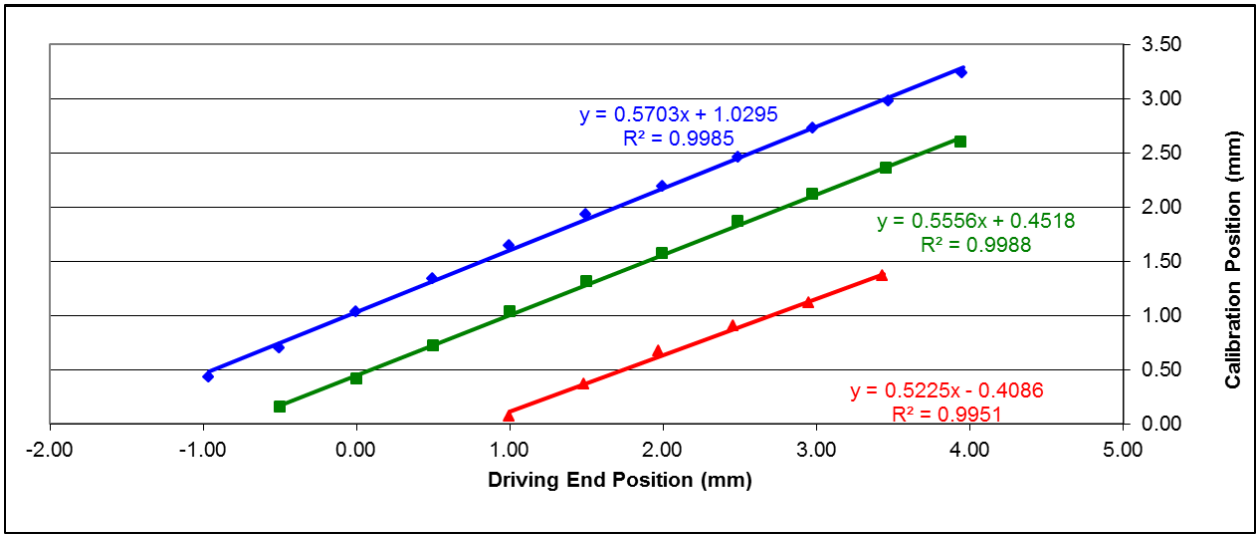

Figure 24: Early position calibration data. Each line represents a different calibration mass. the probe end position and force from the displacement and force measured at the driving end.

Eight Parameter Calibration Process

Several factors may contribute to the necessity for a more complex model, including non-rigid tubing, and air clinging to internal bellows folds. To identify relevant variables for this more complex calibration process, additional parameters were tested by stepwise regression. Stepwise regression showed that eight calibration parameters were important to include in the calibration equation. Probe force and position were determined to be best calculated with the following calibration equations:

$$F_P = c_0 + c_1F + c_2P + c_3F^2 + c_4P^2 + c_5FP + c_6\frac{dP}{dt} + c_7F\frac{dP}{dt}$$

$$P_P = d_0 + d_1F + d_2P + d_3F^2 + d_4P^2 + d_5FP + d_6\frac{dP}{dt} + d_7F\frac{dP}{dt}$$

Probe force (F_p) and position (P_p) are both calculated as functions of the measured driving end force (F) and position (P), squared terms of both force and position (F^2 and P^2) to account for the nonlinear compliance of the system, a term for system work (FP), the driving end velocity ($\frac{dP}{dt}$), and a power term ($F\frac{dP}{dt}$).

When the probe position was calculated as a simple function of the driving end position, moving the probe end to a specified position could be done easily on the Host Computer without monitoring any sensor values. Because the probe position is now also a function of the driving end force and velocity, sensors must be actively monitored and calibration variables calculated in order to control the probe displacement. Calculating probe position and updating the appropriate driving end position to attain the desired probe position would be too slow and cause significant delay if it was still done on the Host Computer. So it became necessary to calculate the probe end displacement using the FPGA in order to have accurate probe position control.

The eight parameter calibration process was designed to match the oscillatory tests run by EVE. The procedure is as follows:

1. Insert the probe into calibration instrument with rubber band in place, as shown in Figure 25
2. Check initial system pressure, and add up to 1 mL of water to the system if necessary to maintain a positive system pressure

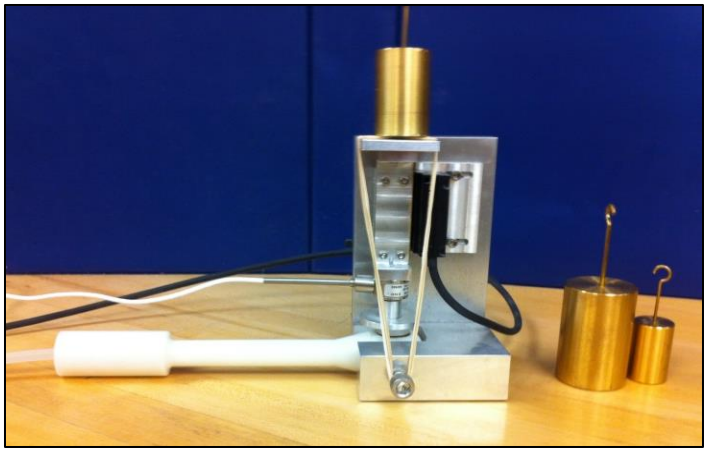

Figure 25: The calibration instrument in use.

3. Add 1 kg mass to the calibration instrument platform to push the probe down to zero displacement for encoder initialization
4. Slightly disturb driving end by manually moving the motor approximately 3 mm and releasing to ensure that the system begins in equilibrium
5. Start program to initialize zero position and begin motor control
6. Remove the 1 kg mass from calibration instrument
7. Start data collection
8. Oscillate from 0 to 4 mm at the target frequency for 40 seconds, changing masses every 10 seconds through the sequence of unloaded, 100 g, 200 g, and 500 g
9. Stop data collection
10. Fit to eight parameter model using a least-squared fit to obtain calibration constants
11. Switch the instrument to probe control mode

Figures 26 and 27 show sample data from the eight parameter calibration process, which consistently yields R^2 values greater than 0.95 for both force and position fits.

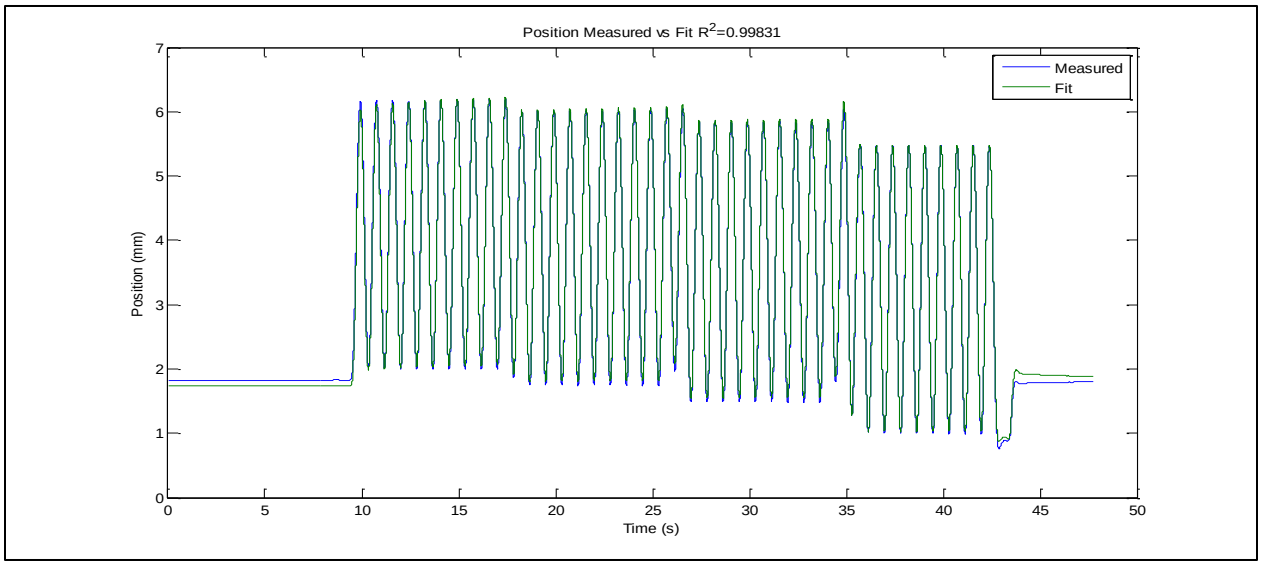

Figure 26: Eight parameter position calibration data. With the measured data vs fit has an R^2=0.998.

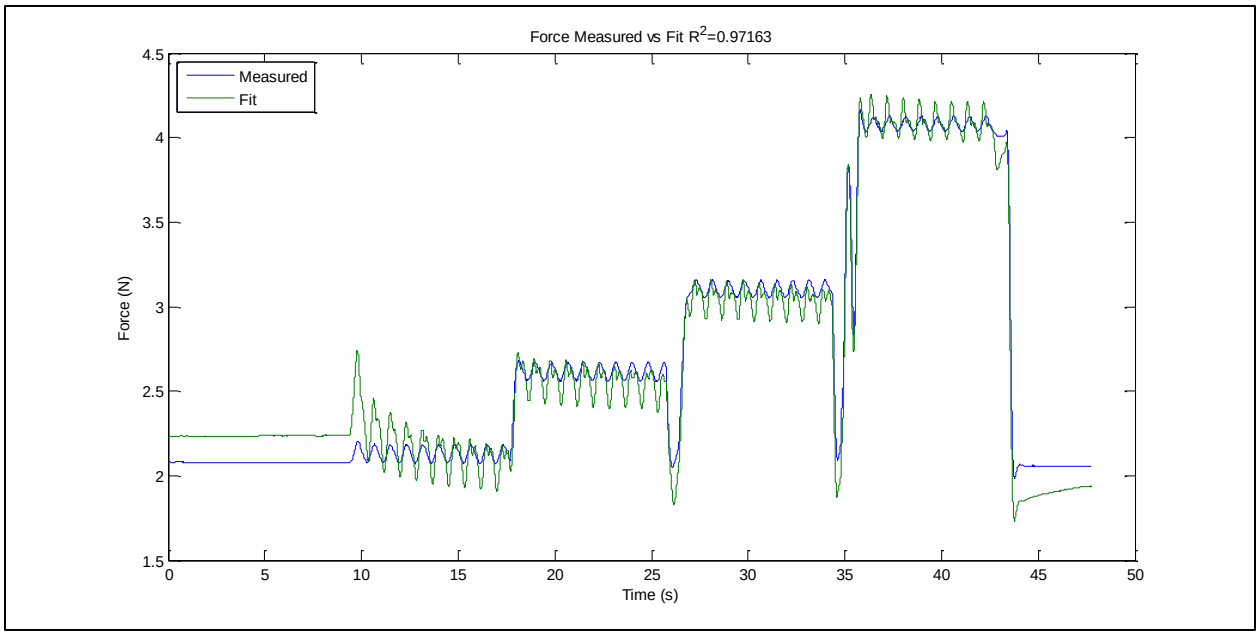

Figure 27: Eight parameter force calibration data. With the measured data vs fit has an R^2=0.972.

The eight parameter model breaks down when actually used for probe control. Although there are good R^2 values matching the measured calibration data to the estimate; it is still not good enough for accurate control. This is especially evident when taking a closer look at the force data in Figure 27. Although the calculated force does follow the bulk moves of the measured force, the actual fit is not close enough to the data to make an accurate elasticity measurement. Looking at the oscillation at 20 seconds in Figure 27, one can see that, although the measured force is only oscillating with a magnitude of approximately 0.1 N, the calculated force is oscillating with a magnitude of approximately double that. This will give elasticity estimates that could be double the actual even though the R^2 value for the fit is very good.

Comparative Elasticity Calibration Process

The previous section shows that finding a fit which can precisely match the displacement and resultant force at the probe end from the values measured at the driving end have proven to be very difficult to find through a calibration equation. Ultimately, since we are interested in finding an approximation of Young's modulus for the tissue, it was determined that it might be possible to get an estimate from measuring the elasticity for the entire system at the driving end and correlating that with a measured calibration Young's modulus.

With that in mind, a new calibration process was created that would rely entirely on calibrating the instrument against varying elastic loads. The new process is as follows:

1. Insert the probe into the calibration instrument making sure that the set screw is tight on the probe head
2. Check initial system pressure, and add up to 1mL of water to the system if necessary to maintain a positive system pressure
3. Add seven elastic resistance bands to the calibration instrument

4. Add 1 kg mass to the calibration instrument platform to push the probe down to zero displacement for encoder initialization
5. Slightly disturb the driving end by manually moving the motor approximately 3 mm and releasing to ensure that the system begins in equilibrium
6. Start program to initialize zero position and begin motor control
7. Remove 1 kg mass from calibration instrument
8. Start data collection
9. Move the driving end from a zero position to a 1 mm displacement
10. Oscillate from 1 mm to 2 mm driving end displacement at a frequency of 0.5 Hz for 3 cycles
11. Hold position at 1 mm driving end displacement for 4 seconds while an elastic resistance band is removed from the calibration instrument
12. Repeat steps 9-11 seven times
13. Move the driving end back to a zero position
14. Stop data collection

A graph of the driving end position over time for this new calibration process can be seen in Figure 28.

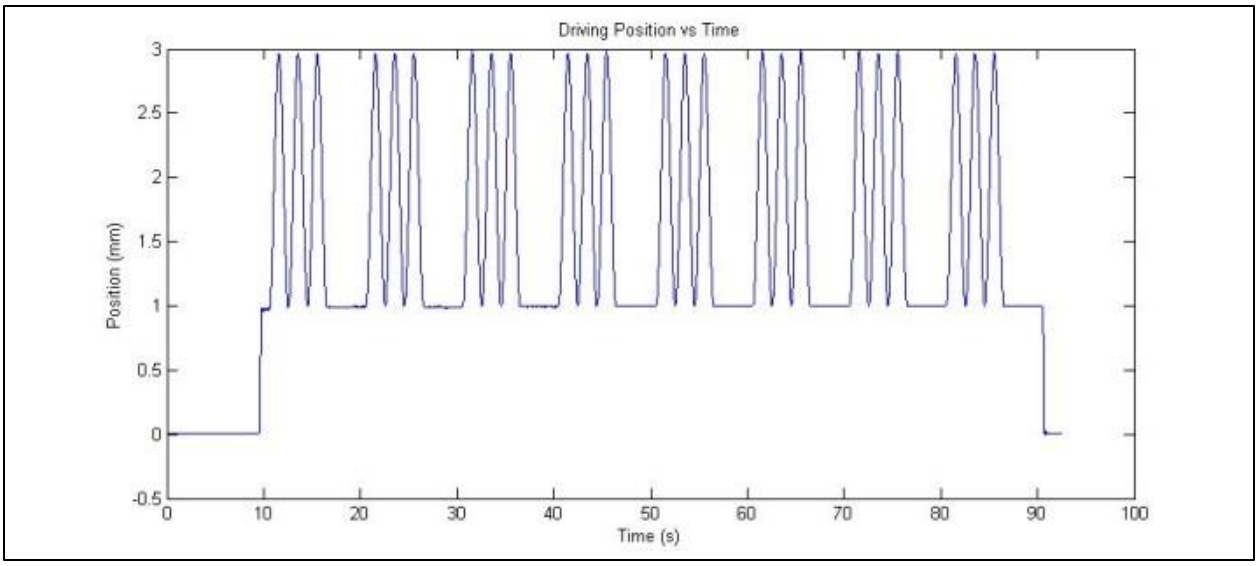

Figure 28: Driving Position vs Time for the comparative elasticity calibration process.

This new calibration process is not sufficient to enable the instrument to enter probe end control. In fact, probe force and position are never calculated. The ability to detect nonlinearity is also sacrificed. However, since we are looking at the change in the whole system's response to varied calibration loads, we are only interested in moving the driving end reliably, which EVE does very well. Looking at the whole system response might negatively affect the instrument's ability to measure viscoelasticity, but allowing for estimation of Young's modulus is a significant beginning.

After the calibration process is complete, the data is processed in the Slopes2.vi data processing program which can be found in Appendix B. The Slopes2.vi code automatically imports the saved data from the trial and plots the driving and calibration positions and forces to allow for a visual inspection of the data to ensure it was taken correctly. Next, the program searches for the second loading phase for each elastic resistance. The indexes of these phases are then used to generate plots of force vs position for both the driving end and the calibration instrument for each of these ranges, examples of which can be seen in Figures 29 and 30. With each loading segment isolated, the slope of each line can be used to calculate elasticity for the entire system ($E_{driving}$) at each load and the Young's modulus of each calibration load (E_{cal}). Then a plot is generated of E_{cal} vs $E_{driving}$ as seen in Figure 31. Using a least-squares fit equation

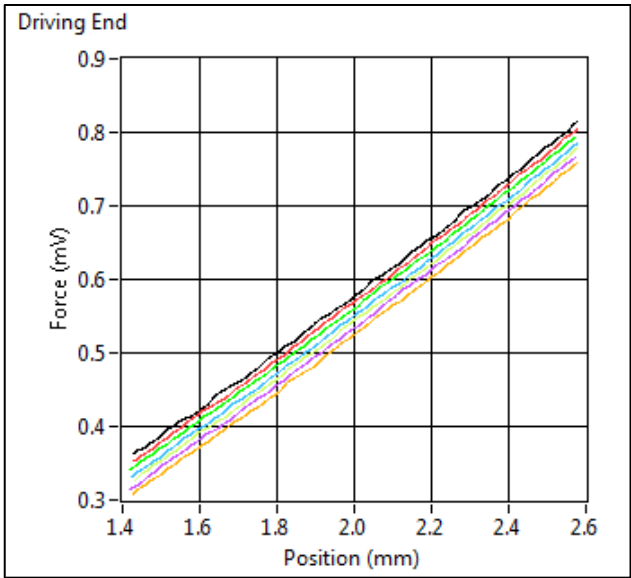

Figure 30: Force vs Position for the comparative elasticity calibration process measured at the driving end. Each line represents one loading segment from low elastic load (orange) to high elastic load (black). The slopes of linear least-squares fits of these lines are used as the elasticity

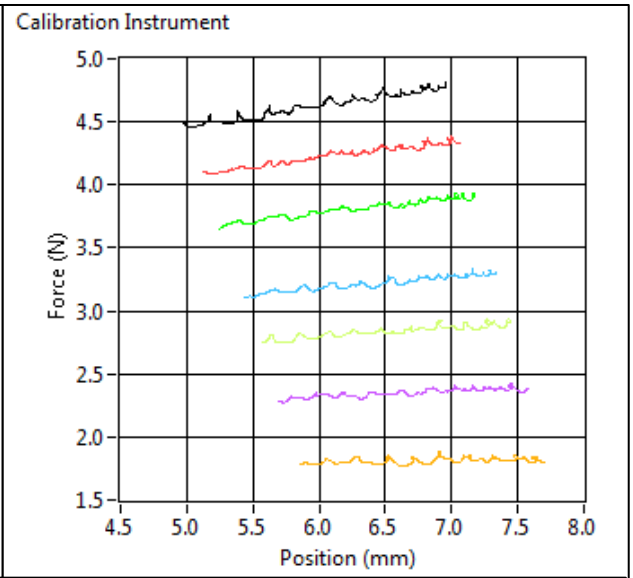

Figure 30: Force vs Position for the comparative elasticity calibration process measured at the calibration instrument. Each line corresponds to the matching color line in Figure 29. The slopes of linear least-squares fits of these lines are used as elasticity estimates of the calibration load.

with these eight data points, an estimate of the calibration instrument's measured elasticity can be made from the system elasticity measured at the driving end.

After calibration, the entire calibration procedure can be repeated as a test procedure with the probe in the tissue phantom. This can generate the desired elasticity estimate for the tissue phantoms based on the measured system elasticity using the calibration curve generated in the comparative elasticity calibration process.

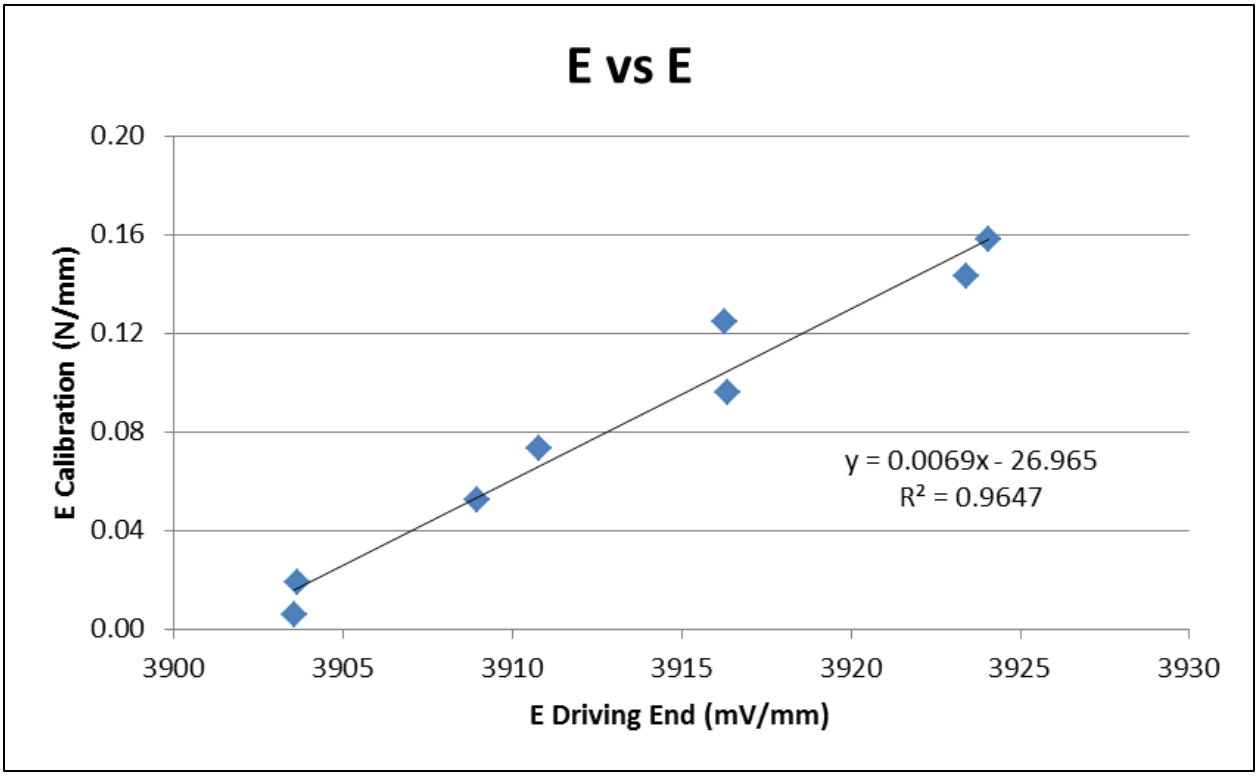

Figure 31: Example E_{cal} vs $E_{driving}$ plot and fit from the comparative elasticity calibration method.

Chapter 5) Design Evaluation

As an instrument, EVE is designed to accurately capture a very small signal embedded within a much larger signal. Looking at the measured driving end force from a sample calibration process in Figure 32, it can be seen how little the peak force transducer reading (in mV) reacts to the addition of a significant load on the probe end. Throughout the entire process,

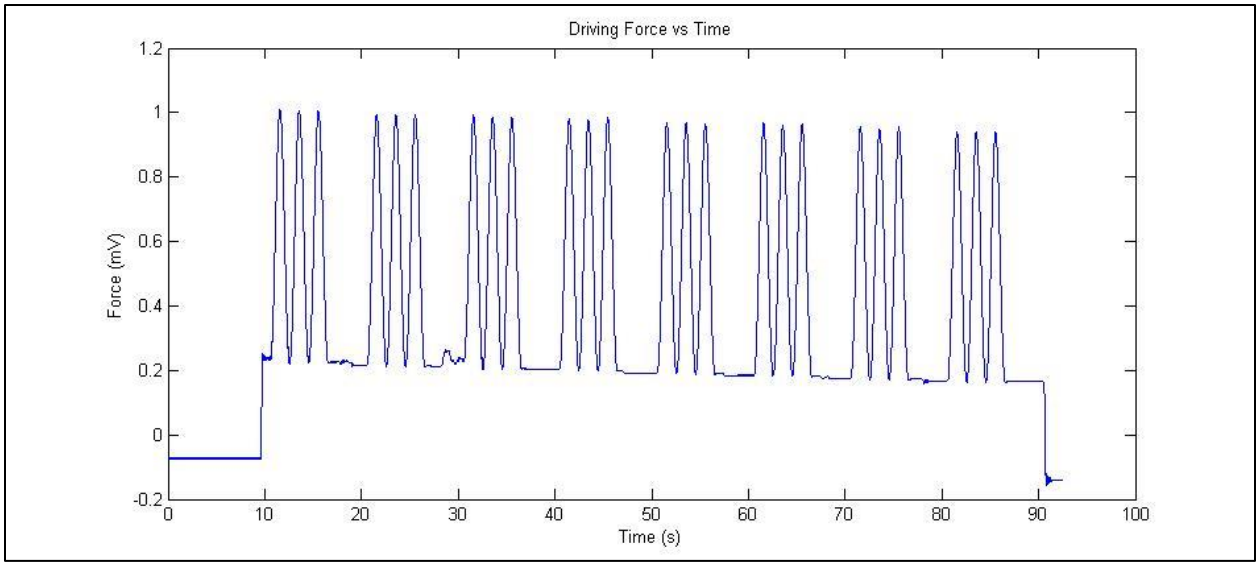

Figure 32: Example driving force transducer reading (in mV) over time for a calibration

from the maximum load during the calibration to a negligible load at the probe end, the peak force measured at the driving end only decreases by approximately 5%. This is also just the change in maximum force; the difference in slope of the force-displacement curve is much more subtle. Up until this point, we have been confident that, whatever happened during the process, we would be able to mathematically determine what was happening at the probe end. Since we are looking for such a small part of a comparatively large signal, any small disruption of the system can have disastrous consequences for our ability to make meaningful measurements. Obvious sealing issues, buckling of bellows, and air within the system all caused major problems with the calibration of EVE, but were readily apparent and have been addressed. This new issue,

although more subtle in its detection, has nonetheless had a major effect on the viability of EVE as a clinical instrument.

Drift

During initial testing, it soon became apparent that there was another issue with the calibration process. Bench tests, with the probe still within the calibration instrument, were performed. Young's modulus values that were measured within calibration range by the calibration instrument were calculated to be well outside of range from the comparative elasticity calibration equation. This can be seen in Figure 33, where the calculated elasticity of the test measurement of the red triangle would have a non-physical negative Young's modulus according to the comparative elasticity calibration equation, despite having a measured Young's modulus that is well within the calibration range. Bench tests were consistently underestimating the calibration force; so it seemed that there was an unaccounted for drift tending toward lower system elasticity.

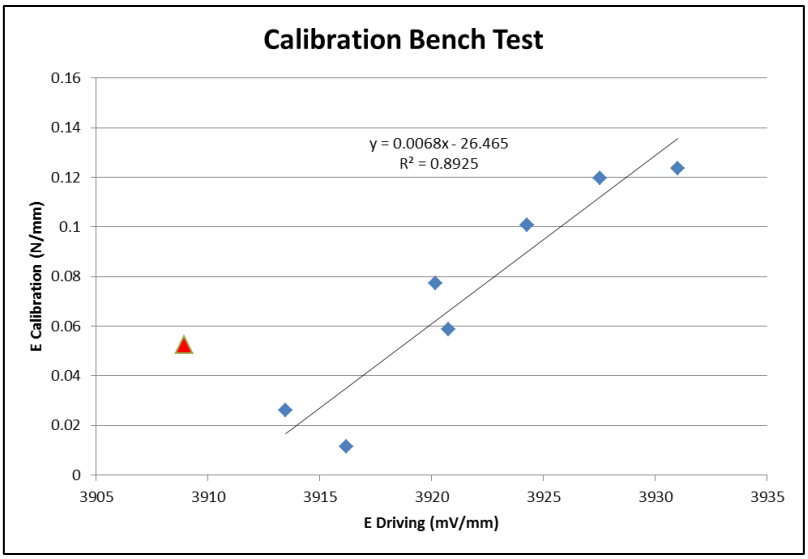

Figure 33: Example bench test of calibration process.

Drift Tests

Test Procedure

In order to quantify this drift and to try to identify the source of the issue, a simple protocol was developed to view the system change over time. A new protocol, called Drift, was

programmed into the HostGUI.vi program. This protocol monitored the system through an approximately thirty-minute ramp and hold test displacement. If necessary, before the test, the system was prepped with a preload of up to 1 mL of water as in the calibration protocol. The 1 kg calibration mass was then placed on the calibration instrument to ensure the calibration encoder was initialized properly. The system was then initialized, after which the 1 kg mass was removed, and the 200 mg test mass was put in place before beginning the Drift Protocol. The Drift Protocol first began collecting data. The next command quickly stepped the driving end to the desired displacement, either three or four millimeters, which was determined by a user input switch. The displacement was held for thirty minutes before the driving end was moved back to zero displacement at the end of the test.

Because of the file size required to constantly record data at 2000 samples per second in six channels of double precision data for half an hour, the host computer would have had trouble processing the data from these tests if the data were collected in that way. To get around this limitation, the drift protocol on the HostGUI.vi was programmed to only collect data for thirty seconds at a time, after which, data was not recorded for thirty seconds before recording again. , Instead of one unmanageable file, this process yielded thirty smaller files that could be sequentially processed more easily by the host computer.

The host processing of the data analysis program (DriftAnalysis.vi shown in Appendix B) opened each file, then took an average of the measured driving end forces, driving end positions, calibration forces, and calibration positions over one second of the collected data. This average point was used as representative data for that file's time point, reducing over 21 million points to the representative 30 used to examine system drift.

Test Results

In order to quantify and look for the source of the system drift, several drift tests were conducted. Each test was run in triplicate to test for repeatability of the situation. First, to ensure that the load cells and encoders were functioning properly, the drift protocol was run with the load cells removed and isolated under static loads, and with the encoders fixed. This test, as expected, showed no drift. A plot of the change in driving force over time can be seen in Figure 34, where the magnitude of force change always remained under 0.15%.

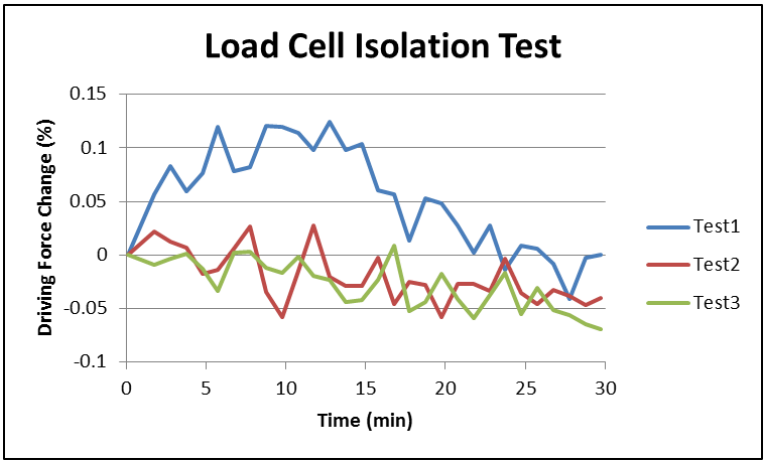

Figure 34: Isolated driving load cell percent force change with a constant load

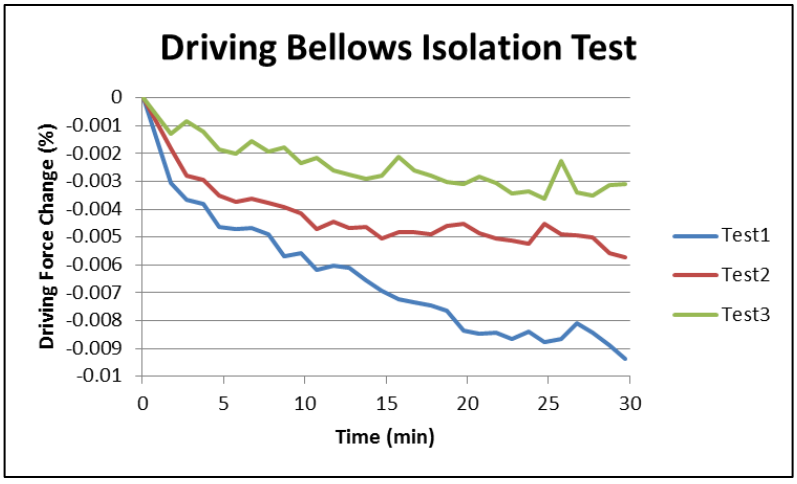

Figure 35: Isolated driving bellows force change with a constant displacement.

After confirming that the sensors were working properly, an additional variable was added to search for the source of the drift. The second drift test was conducted with the hydraulic components removed from the system, with the driving end ramping and holding against the elastic resistance of a drained driving bellows. The driving

bellows was displaced by 4 mm and the resulting driving end force was tracked. This test was to determine if the bellows were showing signs of creep. The results of this test, presented in Figure 35, show that there is a slight relaxation of the bellows, but the force transducer measurement changes are very low, with the maximum change being less than 0.01%.

With this knowledge, the next area of investigation for the third set of tests was the tubing. EVE utilizes 0.25" outer diameter nylon tubing as the hydraulic link between the driving and probe bellows. It was thought that, given that there was no creep in the bellows, the additive creep of all elements of the hydraulic system could be causing the system to drift. If this was the case, then greatly lengthening the tubing would greatly increase the drift, and replacing the nylon tubing with rigid copper tubing, although unsuitable for human trials, would greatly decrease the drift. Three setups were selected for testing: the original short nylon tubing (approximately 0.7 meter of tubing) used in all previous measurements, long nylon tubing (approximately 2.6 meters of tubing), and copper tubing (approximately 0.5 meter of tubing). These tests were once again run in triplicate, and Figure 36 shows the average driving force change for each tubing setup. Interestingly, the force change was the greatest for the short nylon tubing. This could have been because the long nylon tubing setup used all new tubing, while the short nylon tubing setup was using tubing that had

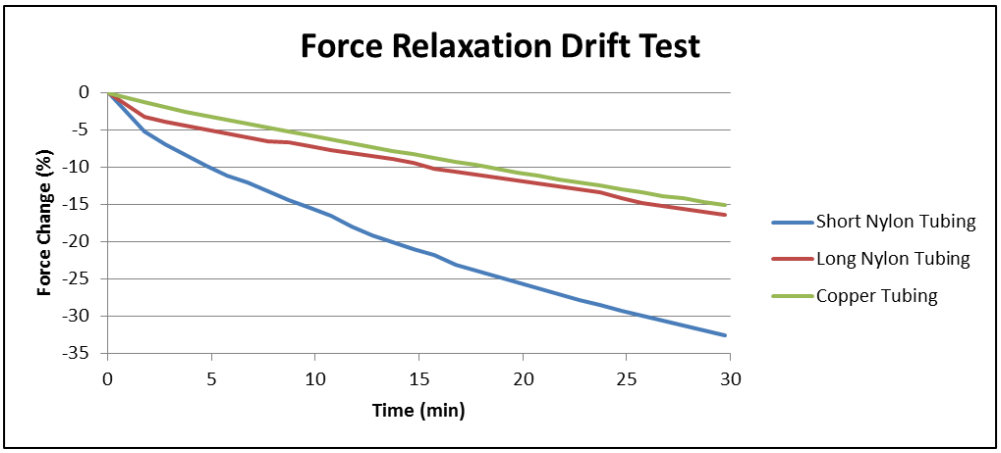

Figure 36: Average driving force reduction over time for three different tubing setups with a driving end displacement of 4 mm.

been used on the instrument for several years. As predicted, the copper tubing showed the least force relaxation of the three. However, it still showed an unacceptable average drift of over 15% of the force reading in the 30 minute test. Thus, there is still a significant source of drift unrelated to the choice of tubing.

To attempt to isolate the effect of the system pressure on the drift issue, drift tests were conducted holding at 3 mm and 4 mm with both the long nylon tubing and copper tubing. Changing the system displacement is the easiest way to increase system pressure. Since the instrument force is of a much greater magnitude than that generated by a load, increasing the displacement of the system increases the system pressure far more than an additional load at the probe end would generate. If the system pressure was an important variable in determining the magnitude of drift, we could expect to see the drift decrease for the lower displacement. As can be seen in Figure 37, these tests had mixed results. For the nylon tubing, it was indeed the case that the drift was smaller for the lower displacement (3 mm compared to 4 mm displacement data). However, the average force change was lower in the 4 mm displacement copper tubing tests than in the 3 mm displacement tests. For both types of tubing, the averages for each displacement fall well within the measured range for the other displacement.

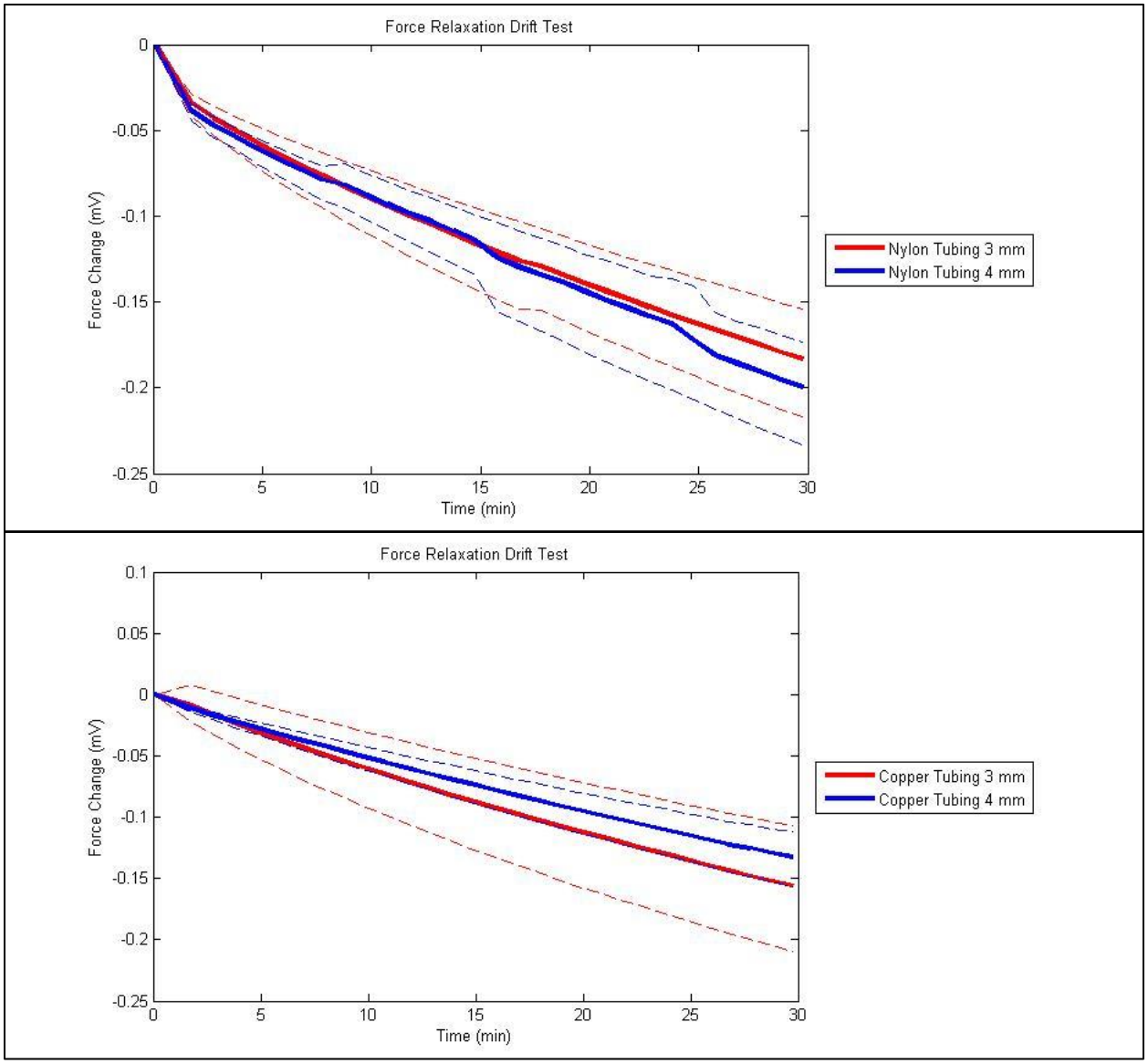

Figure 37: Average driving force reduction over time (solid line) with minimum and maximum measured (dashed lines) values, comparing 3 and 4 mm displacements in two types of tubing.

I believe that system pressure is still an important variable for the amount of drift in the system. However, there is another source of system pressure that was not controlled in these tests, the preload to ensure positive system pressure. The varying amount of preload from adding water to the system before the tests could have changed the system pressure enough to

explain the range of results seen here. In order to control this, a pressure gauge should be incorporated into the instrument in the future in order to ensure a consistent preload.

Although it is not apparent from our testing I believe that there are most likely one or several small leaks causing the drift issue. All of the readily accessible sites for possible leakage have been tested, but there are a few other sites which would be possible for undetected leakage to occur. Any internal joint within the probe bellows assembly is a likely site for concealed leakage. Water leaking from the hydraulic system into the interior of the bellows might evaporate before it could be detected. In addition, the check valve used in the system pre-pressure system may be allowing backflow into the syringe if it is not properly seating. Water leaking in this manner would also not be readily detectable. Although drift testing did not show a definitive link between system pressure and drift, which would strongly indicate a leak, the lack of proper control of the system pressure still leaves this a likely scenario for the origin of the drift issue.

Load-Order

Drift testing yielded no greater insight into what is causing the system drift, so options to minimize or account for the system drift were considered important. In order to be sure that our calibration is valid, and not just measuring the drift within the system, the calibration process needed to be tested to see if the load-order for the calibration instrument mattered. To test this, the comparative elasticity calibration procedure was modified to calibrate against increasing resistance rather than the decreasing resistance of the calibration process. The results, illustrated in Figures 38 and 39, show that changing the calibration process to an increasing load, although it still maintains a positive slope, changes the fit of the data dramatically. The decreasing elastic load test masks the drift

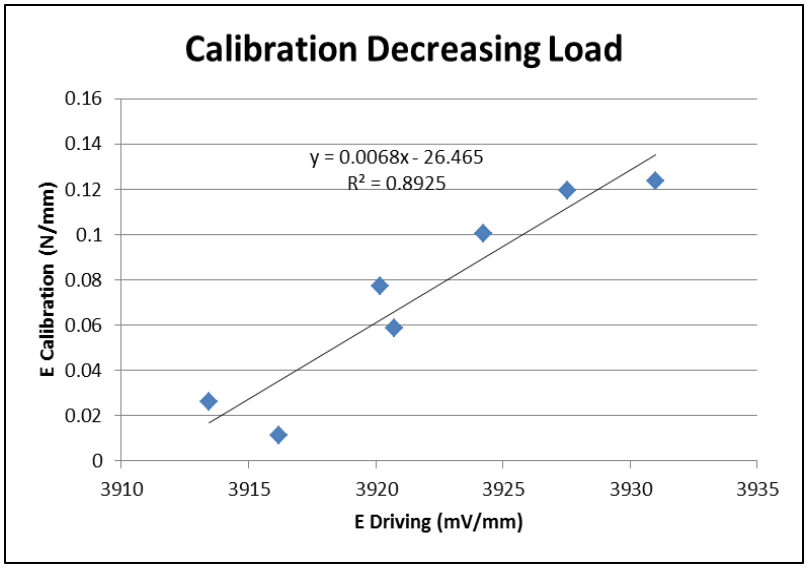

Figure 39: A sample calibration plot generated using a decreasing elastic load (uppermost first, with the drift tending to take points to the left).

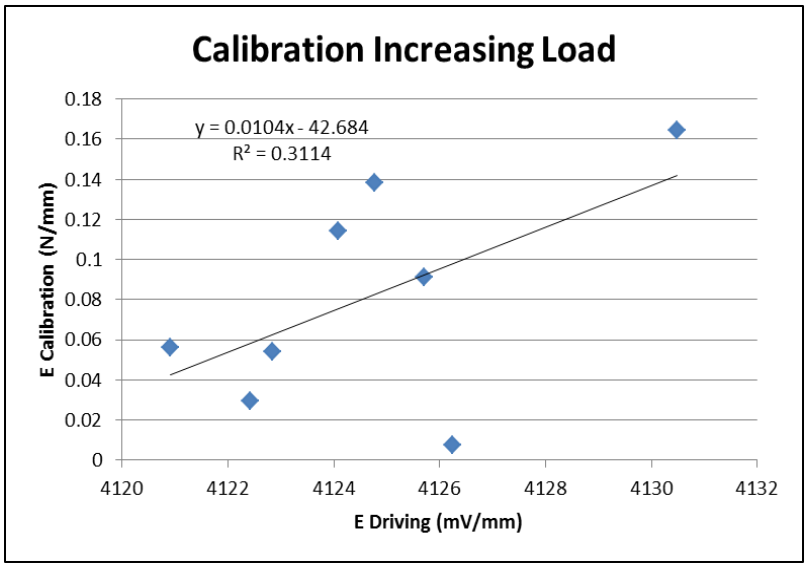

Figure 38: A sample calibration plot generated using an increasing elastic load (bottommost first, with the drift still taking points to the left).

within the expected results. Because the calibration elasticity decreased the driving end elasticity was also expected to decrease. We expect the new point to be to the left of the previous, higher elasticity, point; but this is also the direction that the drift takes the point. By switching to an increasing load calibration process, the next point should be to the right of the previous point, opposite to the drift. Large drift values can cause the next point to end up to the left of the previous point even though it should occur to the right of the previous point. This new loading order highlights the drift rather than masking it in the results. The results of these tests caused reevaluation of the comparative elasticity calibration process and change the procedure to one of increasing elastic loads to ensure that we are taking drift into account as much as possible when we are testing.

Calibrate-Test-Calibrate (C-T-C) Testing

In order to attempt to account for drift in the measurements, it was hoped that performing the calibration process as quickly as possible, both before and after a test, would allow us to average the calibration curves and data collected in between in order to get an estimate of elasticity. To accomplish this, another custom protocol button was added to the HostGUI.vi program that would run the calibration procedure three times sequentially with a standardized short delay between the three protocols

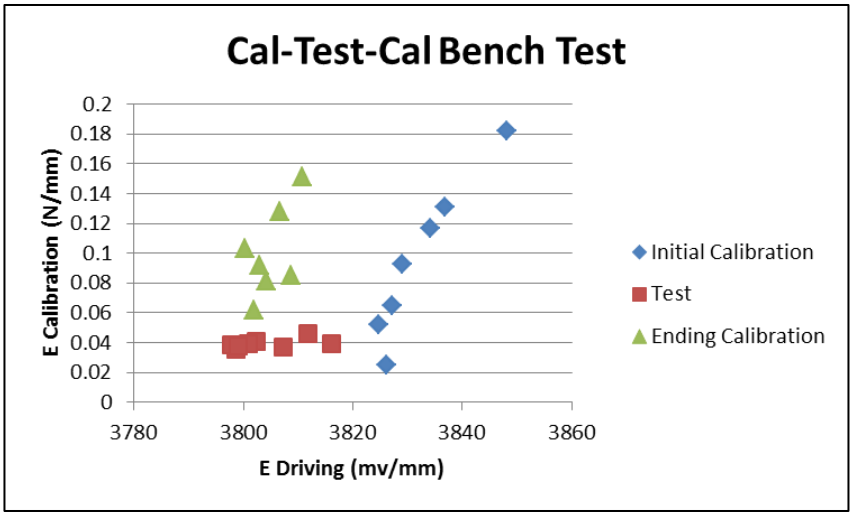

Figure 40: Sample Calibrate-Test-Calibrate bench test against a known elastic resistance.

to allow the probe to be moved into a waiting phantom. This allows performing calibrations both before and after the middle test on a phantom. In order to test this process, bench tests were performed against a measured elastic resistance within the calibration instrument for the test known to be within the calibration range. The results, sample data from which are shown in Figure 40, only prove to illustrate the magnitude of effect that the drift issue has on generating meaningful results. The calibration curves, shown in blue and green, look serviceable enough, and appear to have a slight positive correlation between the elasticity at the driving end and elasticity at the calibration instrument, as hoped. However the test results, shown in red, illustrate how bad the drift is, with the span of the measured driving end elasticity covering almost the entire area between the two calibration curves. If not for them being plotted with the measured elasticity at the calibration instrument, it would be impossible to recognize what the probe end elasticity might be.

Repeated Calibration

To assess the calibration process, tests were run where the calibration process was completed ten times sequentially. Figure 41 shows sample data from the first of three repeated calibration tests. The drift between the individual calibration curves is observed by the calibration curves shifting to the left with

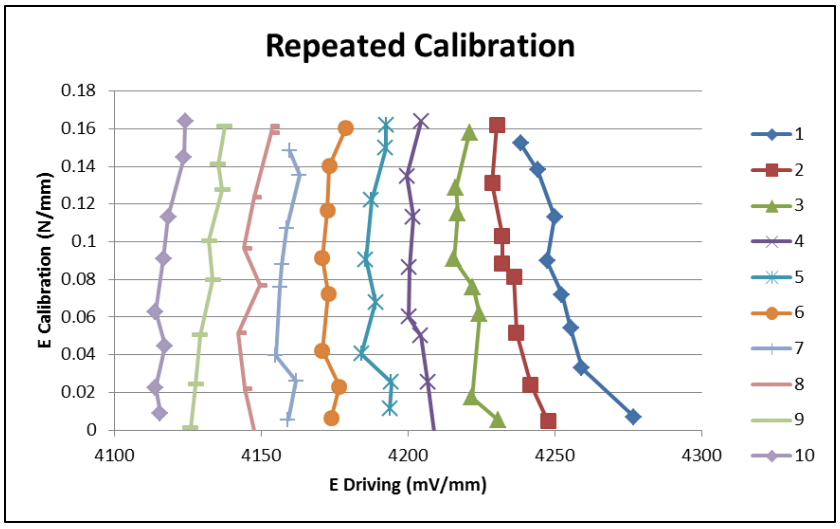

Figure 41: Sample repeated calibration plot.

sequential calibrations. The drift effect did not decrease over time as was initially hoped. It is the comparative shapes of the calibration curves which are of greater interest. Beyond the variance from the drift that the switch to increasing resistance highlights, some of the calibration curves now exhibit negative correlation between the driving end elasticity and the measured calibration elasticity. This is highly nonphysical and very worrisome for the future prospects of the calibration method. This illustrates that the drift in these calibration sets can completely dominate the change in elasticity at the probe end.

Calibrate-Test-Calibrate Testing on Tissue Phantoms

The final evaluation test was conducted to ascertain if any useful information can be obtained from comparative elasticity testing, or if a new calibration process or a complete overhaul of the EVE instrument is necessary. This final test utilized phantoms and was designed to see if Calibrate-Test-Calibrate testing could be used to differentiate among the various phantoms. This utilized the same Calibrate-Test-Calibrate procedure described in the last section, but now the test was performed on a tissue phantom, rather than using a measured load within the calibration instrument. For this test, Phantoms 1 and 5 were chosen because they offer the widest variance in expected elasticity. If the instrument in this state could

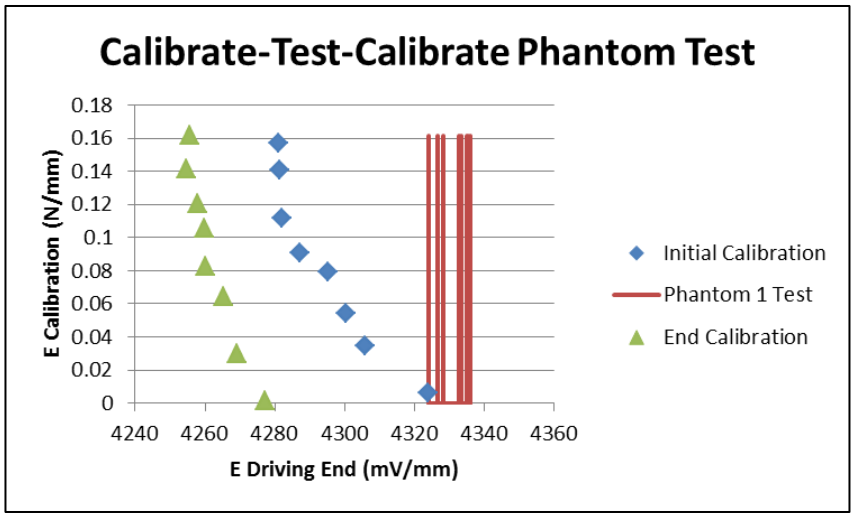

Figure 42: Sample Calibrate-Test-Calibrate test on Phantom 1. The blue and green data points represent the initial and end calibration data points, while the red lines are the driving end elasticity measured during the phantom test

not discern a difference between these two phantoms, then a new calibration process or a major re-design of the instrument would be necessary. However, the results from these tests, sample data of which can be found in Figure 42 for Phantom 1 and Figure 43 for Phantom 5, are very intriguing.

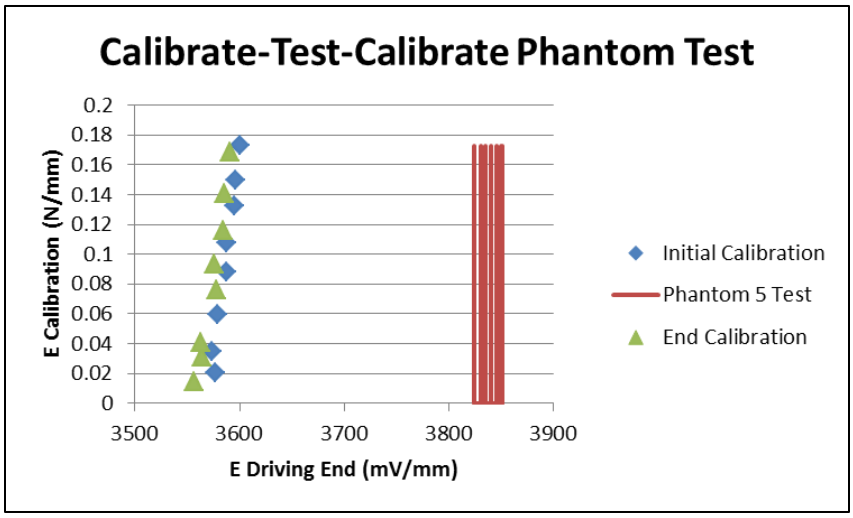

Figure 43: Sample Calibrate-Test-Calibrate test on Phantom 5. The blue and green data points represent the initial and end calibration data points, while the red lines are the driving end elasticity measured during the phantom test.

The results show that, even though the calibration curves are often drifting too badly to be useful, the difference between Phantom 1 and Phantom 5 can be discerned from their distance away from the calibration curves. The much stiffer phantom's (5) driving end elasticity estimate is over 200 mV/mm away from the calibration curves, while Phantom 1's driving end elasticity estimate intersects the initial calibration curve.

This ability to discern between the two phantoms exposed an error in the design of the comparative elasticity calibration process. In choosing the elastic resistance elements for the calibration process, the maximum load was the main consideration. It was assumed that calibrating from a zero load to the maximum load of the calibration instrument would be sufficient to cover the elasticity of all proposed phantoms. However, because of the attachment methods for the elastic resistance elements, the elements were placed on the instrument already under great strain. Because of this, the maximum force of the calibration instrument was reached

before an appropriate range of elasticity was covered. The calibration range used was lower than the measurements we are expecting to make on phantoms and eventually *in vivo*. If a modification to the calibration instrument to accept resistance elements that are not already under such high strains could be made, then retesting with an appropriate elasticity calibration range might increase the signal that we are trying to measure within the much larger measurement of the system elasticity.

Chapter 6) Instrument Validation

The design evaluation of EVE exposed a weakness in the calibration process. Even though the calibration was performed over a large range of elastic loads, because each elastic element was already experiencing a high strain, the process was not done over as large a range of elasticities as possible. If the elastic elements were under lower initial strains the calibration process could utilize higher elasticity elements and still stay under the maximum instrument load.

Calibration Instrument Modification

In order to accept resistance elements that are not already under high strain, a slight modification to the calibration instrument was made. An ordinary hardware store corner brace was cut to fit under the calibration load platform. It is held in place by the same bolts that hold the platform in place. The other arm of the corner brace has a long bolt attached to it with two nuts. This modification, shown in Figure 44, allows the elastic elements to be attached 3.75 cm lower than before, and over a much narrower surface. Instead of being already highly strained at zero probe displacement, the

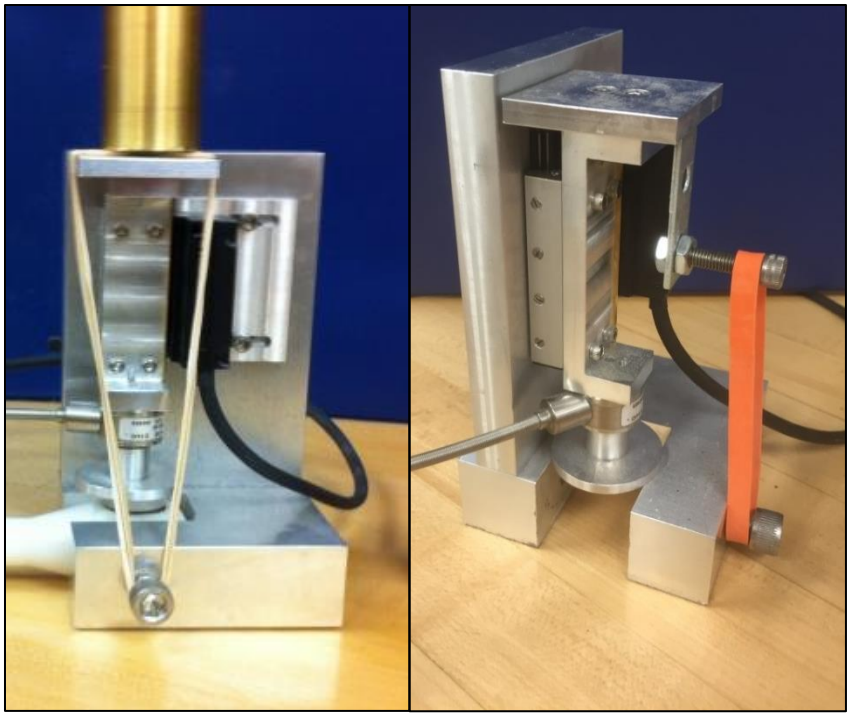

Figure 44: The calibration instrument, pre-modification (left) and modified to accept higher resistance elastic elements (right).

elements are now lightly strained, just enough to ensure that they are taut at zero probe displacement so as to ensure that they never go slack.

The new resistance elements are stiffer, and have a spring constant of 0.097 N/mm, while the old elements were only 0.011 N/mm. This calibration instrument modification allows us to use resistance elements with about nine times the elastic resistance as before and still stay under the instrument's maximum load, and enables us to do testing over a much larger elastic range.

Higher Elasticity Calibrate-Test-Calibrate Bench Testing

The modification of the calibration instrument and new elastic elements should have an effect on the calibration curves generated in the calibration process. In order to evaluate these effects the Calibrate-Test-Calibrate procedure was repeated. The instrument was calibrated using the comparative elasticity calibration procedure detailed in Chapter 4 with the low to high elasticity loading order and from one to eight elastic elements. Then, the test segment of the C-T-C process was performed in the calibration instrument against measured elasticity, either the 2-band or 5-band load of the same elements used during the calibration. Last, it was calibrated again using the same procedure as the initial calibration. This was all done in quick succession (using the same C-T-C computer protocol described in Chapter 5). The process was completed three times for each test load (2-band and 5-band), with each test generating eight data points. Sample results, shown in Figure 45 for two bands and Figure 46 for five bands, show a great improvement over the tests with the old bands. The drift, although still present, is no longer the dominant signal the system. Now the test results lie on the calibration curve. The points from the before and after calibrations of an individual C-T-C test can now be used as one data set and generate a least-squares fit. This new fit uses data from both before and after the test, so the fit

equation is an average fit over the whole time. Because of this the drift issue is further mitigated, and we can relate the driving end elasticity to the calibration instrument measurements.

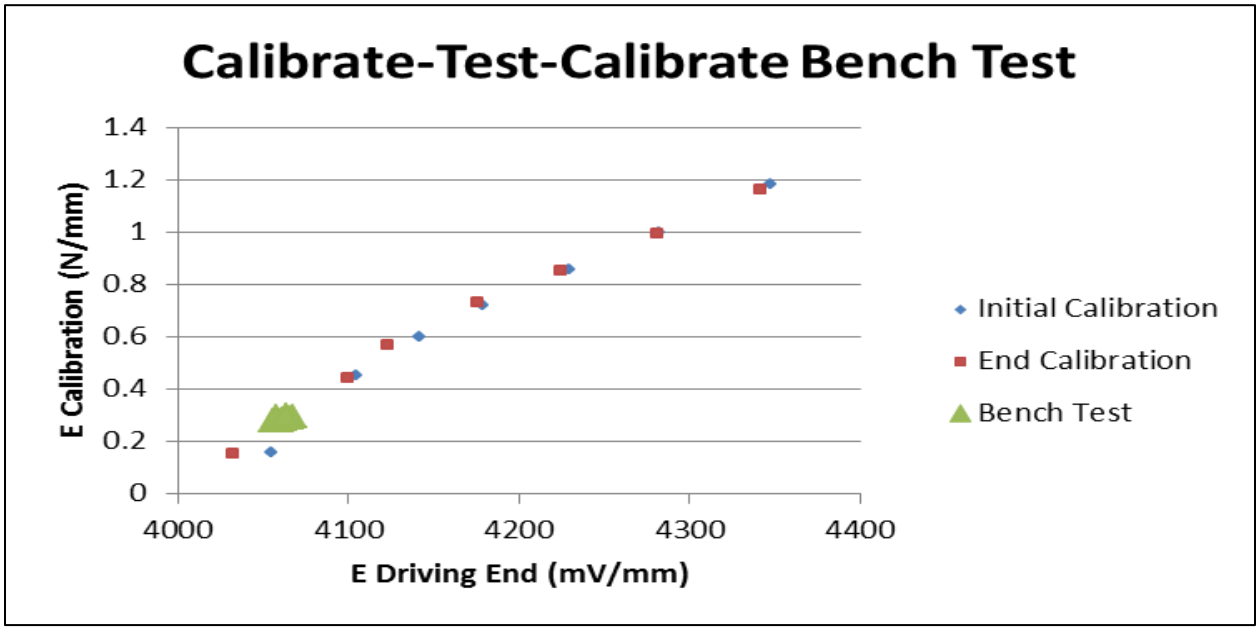

Figure 45: Sample Test-Calibrate-Test bench test data with two elastic resistance elements. The initial and final calibrations are represented by the small red and blue dots, while the bench test performed between the two is represented by larger green triangles.

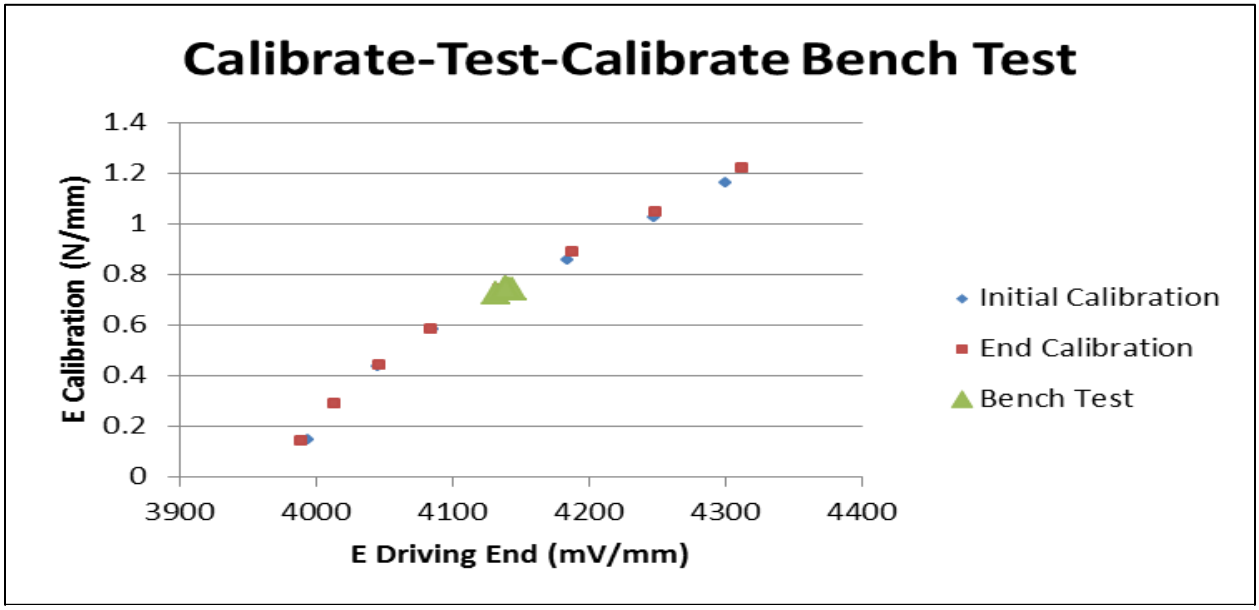

Figure 46: Sample Test-Calibrate-Test bench test data with five elastic resistance elements. The initial and final calibrations are represented by the small red and blue dots, while the bench test performed between the two is represented by larger green triangles.

Results from the tests are shown in Table 4. The results from these tests show that the instrument is now measuring elasticity quite well. For each of the three tests, the total elasticity of the test elements was measured at the calibration instrument eight times and reported as a mean and a standard deviation. The mean calculated elasticity, using the calibration equation, are also reported for those same loading segments with the corresponding standard deviations. As can be seen in Table 4, EVE is calculating elasticity very consistently, with standard deviations within an order of magnitude of the calibration instrument elasticity measurements.

Table 4: C-T-C Bench Testing Results

2-Band	Measured Elasticity (N/mm)	Standard Deviation (N/mm)	Calculated Elasticity (N/mm)	Standard Deviation (N/mm)	Relative Error
1	0.2891	0.0075	0.2941	0.0130	1.72%
2	0.3008	0.0066	0.2988	0.0128	0.67%
3	0.2981	0.0057	0.2973	0.0082	0.26%
5-Band					
1	0.7424	0.0074	0.7000	0.0116	5.72%
2	0.7485	0.0038	0.7312	0.0075	2.30%
3	0.7546	0.0062	0.7286	0.0108	3.45%

Relative error is also small, always under 6%, but as low as 0.26% for one test. The relative error for the 5-band test is slightly higher. This is likely caused by the linear least-squares fit. Each of the comparative elasticity calibration curves has a slight parabolic curve to it, as can be seen in Figures 45 and 46. The linear fit of these curves, although still very good, is less accurate in the middle and calibration range, where the 5-band test operates. Switching to a higher order least-squares fit would reduce this error; but for these initial proof of concept trials, a linear fit is sufficient. With bench testing successful, we can move forward into phantom testing, confident that we will generate meaningful results.

Phantom Calibrate-Test-Calibrate Testing

The new calibration process, which calibrates over a wider range of elasticities, allows us to test phantoms with the likelihood that their elasticities are encompassed within the calibration range. To show this, and validate the instrument's ability to measure phantom elasticity, Calibrate-Test-Calibrate testing was performed on all five test phantoms discussed in Chapter 3. With the new elastic bands, measurements could be made of the phantom elasticity. Sample data for Phantom 1 can be seen in Figure 47, while sample data for Phantom 5 is presented in Figure 48. Each figure shows a single C-T-C test, but the C-T-C protocol was run on each of the test phantoms three times. For each C-T-C, test the protocol collects eight measures of driving elasticity that are averaged before being put into the calibration equation to give a measurement of phantom elasticity.

As in the bench testing that was detailed in the previous section, for each test a calibration equation was determined using the a linear least-squares fit on the calibration data together as a single set. The driving end elasticity was then found for the second loading segment for each of the eight sets of oscillations performed during the test phase. The mean of these measurements was then put in to the calibration equation to determine one measurement of elasticity for the C-T-C test.

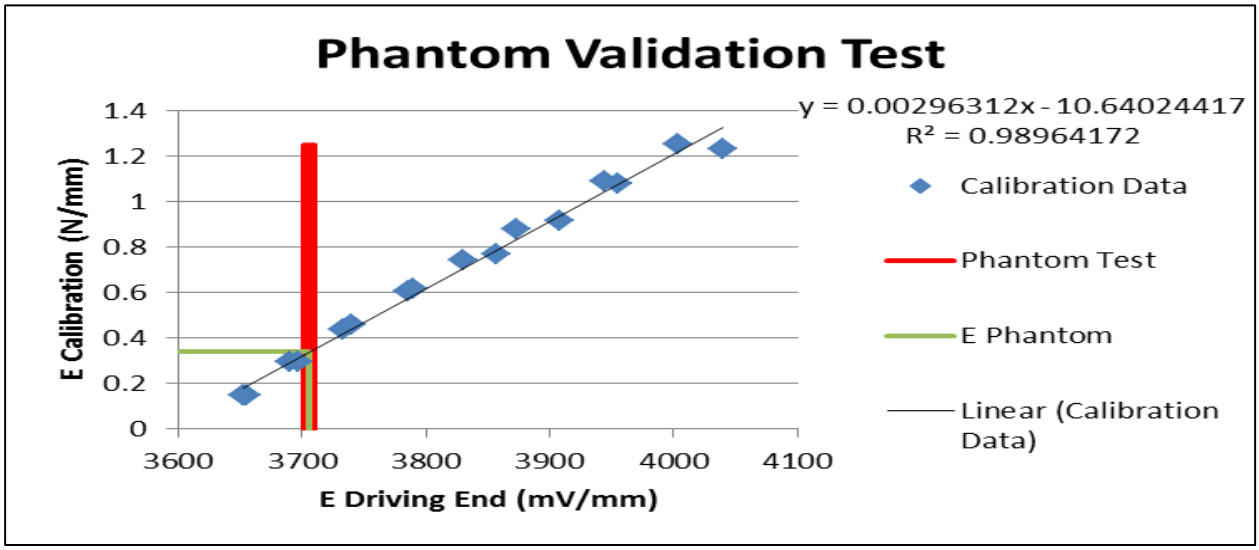

Figure 48: Sample Calibrate-Test-Calibrate phantom test data from Phantom 1. The initial and final calibrations are represented together by the blue dots, with a black least squares fit line. The equation for the fit line is shown on the top right. The red lines are the driving end elasticity values from the phantom test. The green line vertical segment is located at the average driving end elasticity for the eight phantom tests, while the horizontal segment is the calculated phantom elasticity from the least squares fit equation of the calibration data and the average driving end elasticity from the phantom tests.

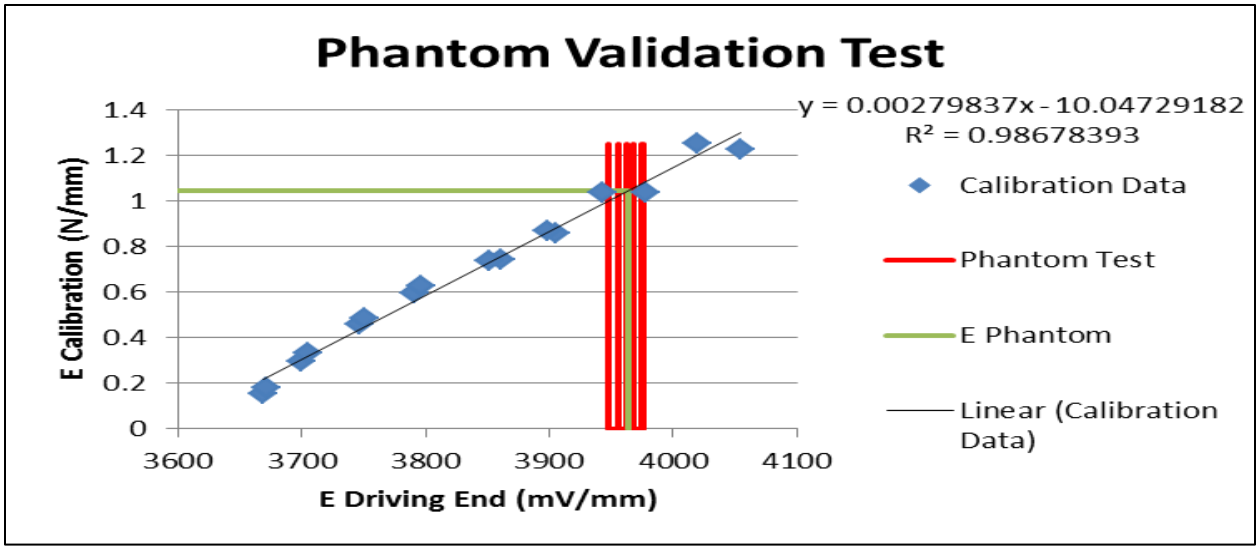

Figure 47: Sample Calibrate-Test-Calibrate phantom test data from Phantom 5. The initial and final calibrations are represented together by the blue dots, with a black least squares fit line. The equation for the fit line is shown on the top right. The red lines are the driving end elasticity values from the phantom test. The green line vertical segment is located at the average driving end elasticity for the eight phantom tests, while the horizontal segment is the calculated phantom elasticity from the least squares fit equation of the calibration data and the average driving end elasticity from the phantom tests.

These tests show that EVE has the ability to distinguish between the each of the test phantoms. Based on these tests, the average measured elasticity of Phantom 1 is 0.3376 N/mm, and the average measured elasticity of Phantom 5 is 1.0923 N/mm. To convert this to a Young's modulus, we estimate the stress by assuming that the force is acting over the area of the measuring surface (265 mm^2). We estimate the strain by assuming that the original length of the phantom is the distance from the central cavity to the edge of the phantom (3.8 cm). This gives an average Young's modulus of 33.03±0.61 kPa for Phantom 1 and 156.63±9.15 kPa for Phantom 5. Calculated Young's modulus for each trial can be seen in Table 5.

Table 5: C-T-C Phantom Validation Elasticities

Test	E Phantom 1 (kPa)	E Phantom 2 (kPa)	E Phantom 3 (kPa)	E Phantom 4 (kPa)	E Phantom 5 (kPa)
1	33.73	45.56	69.30	81.56	149.68
2	32.68	43.79	67.43	84.33	166.99
3	32.66	46.65	70.17	77.20	153.22
Average	33.03	45.33	68.97	81.03	156.63
St Dev	0.61	1.44	1.40	3.60	9.15
Expected	7.6	17.7	32.3	51.5	75.3

These values can be compared to the expected Young's modulus obtained through the equation from Hall *et al.* [50] presented in Chapter 3. Although our values are higher than the estimated values, we did not expect to precisely match and our values are still within reason. This quick estimate of elasticity neglects much of the geometry of the phantom.

Converting the elasticity estimate from the measured N/mm into a Young's modulus in kPa makes several massive approximations to simplify the

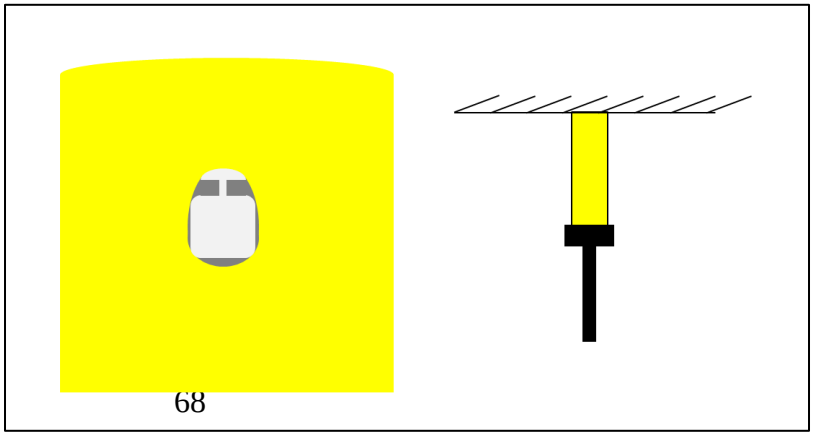

Figure 49: Illustration of the actual (left) vs assumed (right) geometry of phantom tests for translating calculated stiffness into Young's modulus.

geometry. First, for area we assume that the area being compressed is the same as the area of the measurement surface, but there is much more phantom volume around the measurement surface that is being affected by the displacement. Second, the original length being used to calculate strain is just the length from the cavity of the phantom to the surface and the change in length is the displacement of the instrument. These are also not the best measures, because the phantom is not constrained on its outer edges. The displacement of the instrument can move the entire phantom surface up without straining the interior very much. To determine Young's modulus, we have essentially assumed that the probe is acting on a column of phantom the diameter of the measuring surface and height of the length between the phantom cavity and the edge of the phantom which is constrained on the other side. This can be seen in the Figure 49, illustrating the difference between the actual geometry and the geometry assumed in our calculations. Other work, already under way in our lab, to use three-dimensional finite element models to process the data from EVE [55] can be used to refine the Young's modulus obtained by using more physical geometric assumptions.

Additional differences in the measurement may also arise from the changes in manufacturing processes between our procedure and the Hall *et al.* process. For the tests used to generate the equation for expected Young's modulus Hall *et al.* held the gelatin solution at high temperatures for one to two hours. This can cause the gelatin to degrade and may result in up to a 20% loss in stiffness [50]. Additionally, Hall *et al.* did not report how long after manufacture their phantoms were tested, and within the first week of manufacture Young's modulus can increase by 10% due to increased crosslinking over time [50].

More relevant to the current validation of EVE is ensuring that we can statistically show that we are differentiating between these phantoms of different elasticities. A student t-test

confirms that these measures of phantom Young's modulus are statistically different with a 95% confidence interval. All of the phantoms measured did order in their expected rank, increasing in measured stiffness when gelatin concentration increased. Future studies paired with DMA measurements on other gelatin phantoms will be able to determine the ability of the instrument to discern between more similar elasticities.

Chapter 7) Alternate Approaches and Conclusions

Although EVE is currently working in its present configuration to estimate elasticity, it is not working as was hoped at the beginning of the project. Most notably, any measure of viscoelasticity will require an overhaul of the EVE system. Currently we can get a simple elasticity measurement, and discern between some physiologically relevant tissue phantoms, while meeting all of the original design requirements outlined in Chapter 2. We cannot, however, use the current setup and calibration process to measure viscoelasticity, switch to probe displacement control, or easily adapt to probe force control. The comparative elasticity calibration procedure works very well in order to measure elasticity, however, since it skips the intermediate step of finding the probe force and displacement, we cannot use it to switch EVE into probe control.

The lessons learned so far in the creation of EVE can be used to inform a next iteration in a major overhaul of the device. One of two main areas of approach should be chosen in order to advance the design: incorporating a force sensor in the probe end, or the replacement of the hydraulic driving system with a mechanical linkage system. Either of these two improvements might allow us to obtain full force and displacement measurements at the probe end. These measurements could be useful in refining our elasticity estimate, as well as for investigating other avenues, such as viscoelasticity, or allow for other modes of testing, such as ramp-and-hold testing.

Force Sensing at the Probe End

Integrating a force sensor in the probe end would be counter to one of the initial design requirements. However, it would still allow the device to be safe and could greatly increase the accuracy of the force measurement and permit using a calibration process similar to the eight

parameter calibration model again which enables viscoelastic measurements and probe control. A submersible miniature compression load button might be placed under the bellows casing, between it and the probe body. The button's output cable could be run through the handle along with the hydraulic tubing and be read by the 9237 CompactRIO module which is currently only using two of its four inputs. This modification would allow a much more accurate and precise measurement of force at the probe end. This force could also be combined with the parameters from the eight parameter model in order to increase the accuracy of the calculation of the probe end displacement.

Replacing the Hydraulic System

Alternatively the entire hydraulic driving system could be replaced. The hydraulic system adds significant complexity to the instrument and the data processing. Switching to a mechanical linkage would eliminate the problems of air within the system, pre-pressurization variation, and system sealing. A mechanical linkage would also replace the complex bellows spring constant and tubing elasticity with a much more linear spring constant. Switching to a mechanical linkage, however, would require a complete redesign of the probe end, but, unlike implementing a force sensor within the probe, this would allow us to meet all of the initial design requirements. In this proposed design, an illustration of which is shown in Figure 50, the driving end would remain relatively unchanged; but, instead of applying compressive force to the driving bellows, the motor would be used to keep tension on the inner cable of a Bowden cable. Bowden cables, which are used frequently in bicycles brakes, are flexible cables which transmit displacement over a distance by moving an inner cable relative to the outer cable housing. The flexibility of the driving end setup would allow this change to minimally affect the driving end

because all of the sensing and driving components are made to drive and sense in either tension or compression.

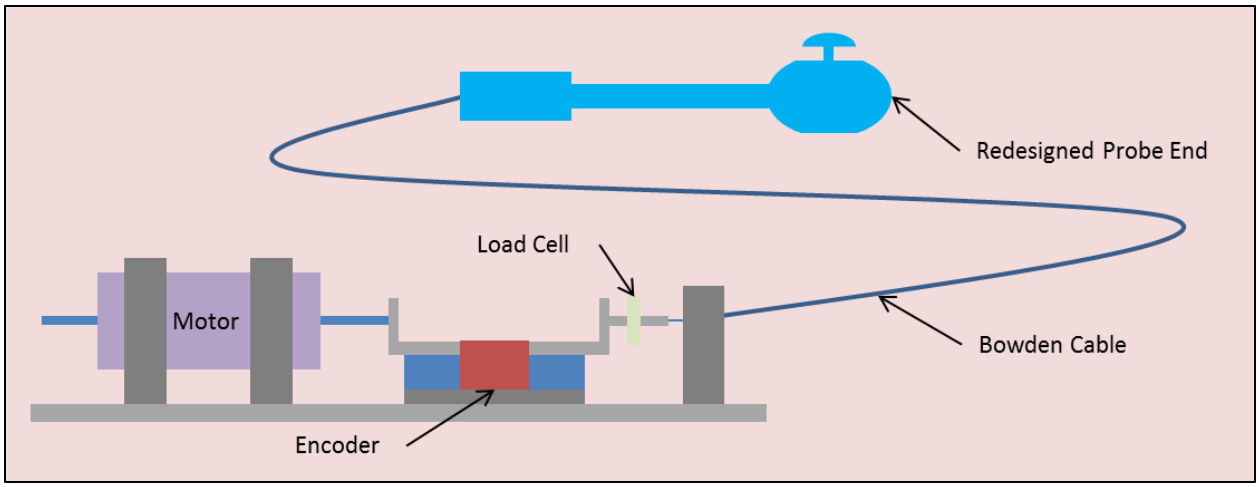

Figure 50: Design exterior schematic of a redesigned EVE utilizing mechanical linkages instead of hydraulics.

The redesigned probe end would need to be entirely remade. In the proposed schematic cutaway, seen in Figure 51, a proposed mechanical linkage would transmit the displacement from the Bowden cable to the measurement surface. Within the probe head would be a mechanical linkage, similar to a car jack or a scissor lift. Tension within the Bowden cable would pull on the forward linkage arm joint. This motion would cause the linkage to become smaller in the lateral direction and expand in the vertical direction, extending the measuring surface. Although we could rely on the tissue to return the measuring surface to rest, a low stiffness spring would ensure that the measuring surface retracts when tension is relaxed in the Bowen cable. The spring constant of the return spring could be removed from the measurement through calibration.

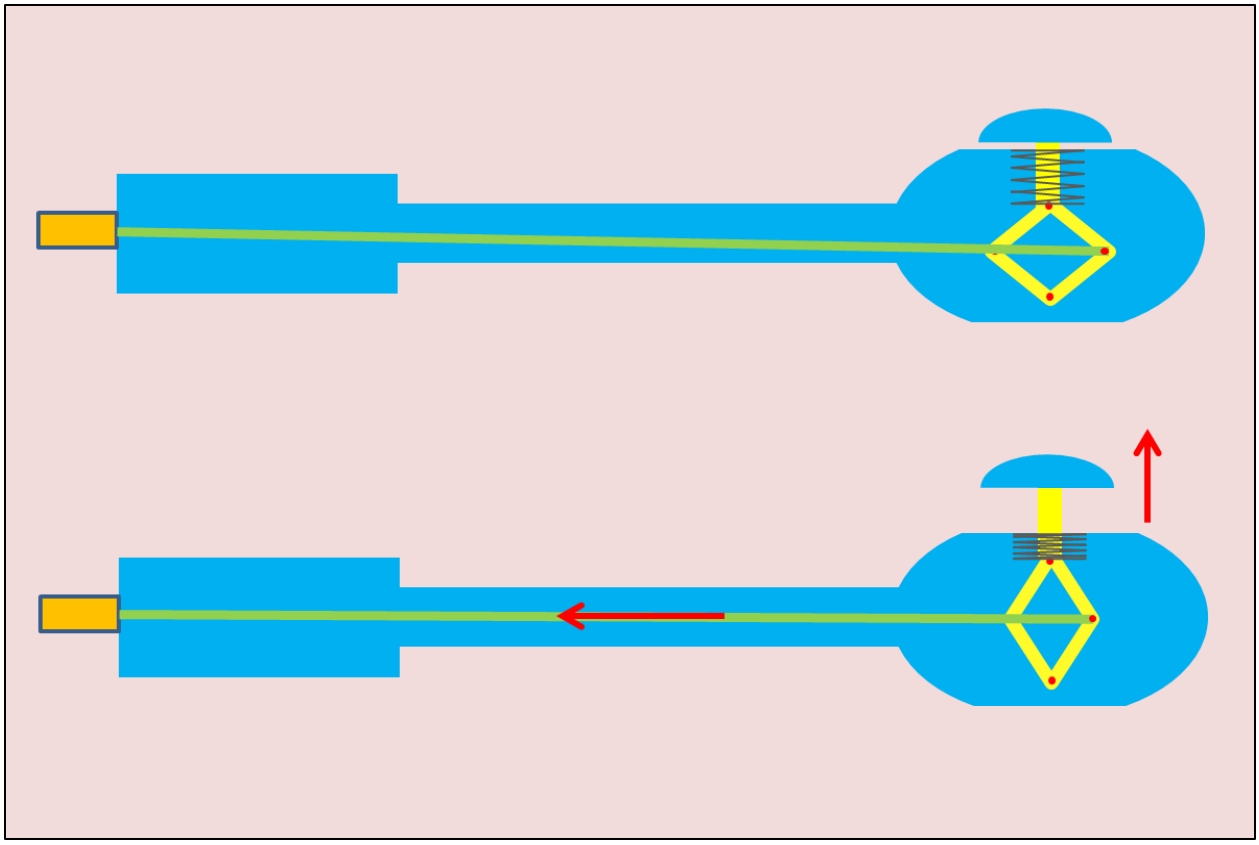

Figure 51: Schematic of a proposed probe design utilizing mechanical linkages. Tension within the Bowden cable pulls on the forward linkage arm joint. This motion causes the linkage to become smaller in the lateral direction and expand in the vertical direction, which extends the measuring surface. A low stiffness spring ensures that the measuring surface retracts when tension is relaxed in the Bowen cable.

This design would have several advantages over the hydraulic system, but come with a few drawbacks as well. Advantages of this system over hydraulics include an expected simplification of the calibration equations that would be needed in order to calculate force and displacement at the probe end. The stainless steel inner cable of the Bowden cable should behave much less elastically than the water with nylon tubing of the current setup. Additionally, all of the complications involving system pressure and air within the system would be gone. This setup also eliminates the variable of the initial system pressure. This might even allow us to calibrate the system much less frequently than the hydraulic setup currently requires. Some

disadvantages might also present themselves. Friction might play a much more significant role in this setup which will have frictional losses along the Bowden cable as well as at all of the proposed linkage joints. Hopefully these friction losses would be on the scale of their hydraulic counterparts, such as head loss, which have been negligible in the current iteration of EVE. Additionally, the probe body for this design might require significantly more pieces, which would increase the difficulty of machining a new probe and have more joints where clinical sterilization might become more difficult.

Future Work

Even without a new design, more work is needed to get EVE ready for *in vivo* studies. In order to fully validate EVE, more phantoms which are closer in elasticity should be measured in order to determine the precision of the elasticity estimates. These tests should also be compared to an independent measure, such as DMA testing, of the phantom elasticities to see if we can discern differences as well as standard measurement devices. With these tests complete, EVE could be ready for *in vivo* testing in the near future.

In tandem with *in vivo* testing, additional 3-D finite element analysis of phantom and vaginal geometry should be run in order to refine our Young's modulus measurement. Decreasing the number of geometric assumptions will greatly enhance the accuracy of our measurements for future applications.

After *in vivo* studies, or in tandem with them, the alternate approaches described earlier in this chapter can be investigated. These instrument refinements have the potential to improve the EVE measurements, as well enable other modes of operation that have had to be sacrificed in the present configuration such as probe control and viscoelastic measurement.

Conclusions

As a whole the EVE instrument is a successful step forward in the ability to properly measure vaginal tissue closing force for the application of mathematical models of delivery vehicle spread. Many of the initial design challenges have been overcome, and a majority of the necessary programming has been completed. Tissue phantoms have been selected and manufactured which will allow for full validation of the instrument. Measurement of phantom tissue elasticity is now possible; and the drift problem has been investigated and mitigated. EVE is nearly ready for *in vivo* testing. During this process, it was necessary to abandon the measurement of viscoelastic properties; however, a redesign of some of the components could allow for their reimplementation into the data collection process. Although EVE is not currently working up to our initial ambitions, we are now able to collect valuable data; and there is a path forward for refining the instrument to collect all of the data envisioned at the start of this project.

References Cited

1. UNAIDS, *Global Report: Unaids Report on the Global Aids Epidemic 2013*. 2013, Joint United Nations Programme on HIV/AIDS (UNAIDS): WHO Library Cataloguing-in-Publication Data.
2. Karim, Q.A., C. Baxter, and S.A. Karim, *Topical Microbicides-What's New?* JAIDS-Journal of Acquired Immune Deficiency Syndromes, 2013. **63**: p. S144-S149.
3. Lewis, D.A., *HIV/Sexually Transmitted Infection Epidemiology, Management and Control in the Iusti Africa Region: Focus on Sub-Saharan Africa.* Sexually Transmitted Infections, 2011. **87**: p. II10-II13.
4. Karim, Q.A., A.B.M. Kharsany, J.A. Frohlich, L. Werner, M. Mashego, M. Mlotshwa, B.T. Madlala, F. Ntombela, and S.S.A. Karim, *Stabilizing HIV Prevalence Masks High HIV Incidence Rates Amongst Rural and Urban Women in Kwazulu-Natal, South Africa.* International Journal of Epidemiology, 2011. **40**(4): p. 922-930.
5. Stone, A., *Microbicides: A New Approach to Preventing HIV and Other Sexually Transmitted Infections.* Nature Reviews Drug Discovery, 2002. **1**(12): p. 977-985.
6. Bo, K. and M. Sherburn, *Evaluation of Female Pelvic-Floor Muscle Function and Strength.* Physical Therapy, 2005. **85**(3): p. 269-282.
7. Lederman, M.M., R.E. Offord, and O. Hartley, *Microbicides and Other Topical Strategies to Prevent Vaginal Transmission of HIV.* Nature Reviews Immunology, 2006. **6**(5): p. 371-382.
8. Cutler, B. and J. Justman, *Vaginal Microbicides and the Prevention of HIV Transmission.* Lancet Infectious Diseases, 2008. **8**(11): p. 685-697.

9. Hladik, F. and G.F. Doncel, *Preventing Mucosal HIV Transmission with Topical Microbicides: Challenges and Opportunities.* Antiviral Research, 2010. **88**: p. S3-S9.

10. Hurwitz, J.L., X. Zhan, S.A. Brown, M. Bonsignori, J. Stambas, T.D. Lockey, R. Sealy, S. Surman, P. Freiden, B. Jones, L. Martin, J. Blanchard, and K.S. Slobod, *HIV-1 Vaccine Development: Tackling Virus Diversity with a Multi-Envelope Cocktail.* Frontiers in Bioscience-Landmark, 2008. **13**: p. 609-620.

11. Newman, P.A., N. Duan, K.J. Roberts, D. Seiden, E.T. Rudy, D. Swendeman, and S. Popova, *HIV Vaccine Trial Participation among Ethnic Minority Communities - Barriers, Motivators, and Implications for Recruitment.* Jaids-Journal of Acquired Immune Deficiency Syndromes, 2006. **41**(2): p. 210-217.

12. Harris, J.E., *Why We Don't Have an HIV Vaccine, and How We Can Develop One.* Health Affairs, 2009. **28**(6): p. 1642-1654.

13. Chin, H.B., T.A. Sipe, R. Elder, S.L. Mercer, S.K. Chattopadhyay, V. Jacob, H.R. Wethington, D. Kirby, D.B. Elliston, M. Griffith, S.O. Chuke, S.C. Briss, I. Ericksen, J.S. Galbraith, J.H. Herbst, R.L. Johnson, J.M. Kraft, S.M. Noar, L.M. Romero, J. Santelli, and T. Community Preventive Serv, *The Effectiveness of Group-Based Comprehensive Risk-Reduction and Abstinence Education Interventions to Prevent or Reduce the Risk of Adolescent Pregnancy, Human Immunodeficiency Virus, and Sexually Transmitted Infections Two Systematic Reviews for the Guide to Community Preventive Services.* American Journal of Preventive Medicine, 2012. **42**(3): p. 272-294.

14. Nobelius, A.M., B. Kalina, R. Pool, J. Whitworth, J. Chesters, and R. Power, *"The Young Ones Are the Condom Generation": Condom Use Amongst out-of-School Adolescents in Rural Southwest Uganda.* Journal of Sex Research, 2012. **49**(1): p. 88-102.

15. das Neves, J., B. Santos, T. Cunha, B. Teixeira, P. Rocha, and G. Dias, *Vaginal Microbicides: The Importance of Effective Distribution, Retention and Coating of the Mucosa.* AIDS, 2008. **22**(7): p. 908-909.

16. Kheyfets, V.O. and S.L. Kieweg, *Gravity-Driven Thin Film Flow of an Ellis Fluid.* Journal of Non-Newtonian Fluid Mechanics, 2013. **202**: p. 88-98.

17. Kheyfets, V.O. and S.L. Kieweg, *Experimental and Numerical Models of Three-Dimensional Gravity-Driven Flow of Shear-Thinning Polymer Solutions Used in Vaginal Delivery of Microbicides.* Journal of Biomechanical Engineering-Transactions of the Asme, 2013. **135**(6): p. 14.

18. Hu, B. and S.L. Kieweg, *The Effect of Surface Tension on the Gravity-Driven Thin Film Flow of Newtonian and Power-Law Fluids.* Computers & Fluids, 2012. **64**: p. 83-90.

19. Hu, B. and S.L. Kieweg, *Contact Line Instability of Gravity-Driven Flow of Power-Law Fluids.* Journal of Non-Newtonian Fluid Mechanics, 2015. **225**: p. 62-69.

20. Karri, S., *2d Thin-Film Flow of a Non-Newtonian Fluid between Elastic Boundaries,* Masters Thesis Thesis in Mechanical Engineering. 2011. University of Kansas

21. Szeri, A.J., S.C. Park, S. Verguet, A. Weiss, and D.F. Katz, *A Model of Transluminal Flow of an Anti-HIV Microbicide Vehicle: Combined Elastic Squeezing and Gravitational Sliding.* Physics of Fluids, 2008. **20**(8).

22. Anwar, M.R., K.V. Camarda, and S.L. Kieweg, *Mathematical Model of Microbicidal Flow Dynamics and Optimization of Rheological Properties for Intra-Vaginal Drug Delivery: Role of Tissue Mechanics and Fluid Rheology.* Journal of Biomechanics, 2015. **48**(9): p. 1625-1630.

23. Fleenor, J., *Numerical Simulation of 2-D Thin Film Squeeaing Flow of an Ellis Fluid between Viscoelastic Boundaries,* Masters Project Thesis in Mechanical Engineering. 2014. University of Kansas

24. Cosson, M., E. Lambaudie, M. Boukerrou, P. Lobry, G. Crepin, and A. Ego, *A Biomechanical Study of the Strength of Vaginal Tissues - Results on 16 Post-Menopausal Patients Presenting with Genital Prolapse.* European Journal of Obstetrics Gynecology and Reproductive Biology, 2004. **112**(2): p. 201-205.

25. Ettema, G.J.C., J.T.W. Goh, and M.R. Forwood, *A New Method to Measure Elastic Properties of Plastic-Viscoelastic Connective Tissue.* Medical Engineering & Physics, 1998. **20**(4): p. 308-314.

26. Goh, J.T.W., *Biomechanical Properties of Prolapsed Vaginal Tissue in Pre- and Post-Menopausal Women.* International Urogynecology Journal and Pelvic Floor Dysfunction, 2002. **13**(2): p. 76-79.

27. Martins, P., E. Pena, B. Calvo, M. Doblare, T. Mascarenhas, R.M.N. Jorge, and A. Ferreira, *Prediction of Nonlinear Elastic Behaviour of Vaginal Tissue: Experimental Results and Model Formulation.* Computer Methods in Biomechanics and Biomedical Engineering, 2010. **13**(3): p. 327-337.

28. Lei, L.L., Y.F. Song, and R.Q. Chen, *Biomechanical Properties of Prolapsed Vaginal Tissue in Pre- and Post-Menopausal Women.* International Urogynecology Journal, 2007. **18**(6): p. 603-607.

29. Rubod, C., M. Boukerrou, M. Brieu, C. Jean-Charles, P. Dubois, and M. Cosson, *Biomechanical Properties of Vaginal Tissue: Preliminary Results.* International Urogynecology Journal, 2008. **19**(6): p. 811-816.

30. Rubod, C., M. Boukerrou, M. Brieu, P. Dubois, and M. Cosson, *Biomechanical Properties of Vaginal Tissue. Part 1: New Experimental Protocol.* Journal of Urology, 2007. **178**(1): p. 320-325.

31. Epstein, L.B., C.A. Graham, and M.H. Heit, *Systemic and Vaginal Biomechanical Properties of Women with Normal Vaginal Support and Pelvic Organ Prolapse.* American Journal of Obstetrics and Gynecology, 2007. **197**(2): p. 6.

32. Mosier, E., R. Jerome, and X.J. Xie, *In-Vivo Btc-2000 Measurement of Anterior Vaginal Wall Biomechanical Properties in Prolapse Patients Undergoing Surgical Repair.* J Biotechnol Biomaterial, 2011. **1**(117).

33. Chuong, C.J., M. Ma, R.C. Eberhart, and P. Zimmern, *Viscoelastic Properties Measurement of the Prolapsed Anterior Vaginal Wall: A Patient-Directed Methodology.* European Journal of Obstetrics & Gynecology and Reproductive Biology, 2014. **173**: p. 106-112.

34. Bo, K., *Pressure Measurements During Pelvic Floor Muscle Contractions - the Effect of Different Positions of the Vaginal Measuring Device.* Neurourology and Urodynamics, 1992. **11**(2): p. 107-113.

35. Frawley, H.C., M.P. Galea, B.A. Phillips, M. Sherburn, and K. Bo, *Effect of Test Position on Pelvic Floor Muscle Assessment.* International Urogynecology Journal, 2006. **17**(4): p. 365-371.

36. Guaderrama, N.M., C.W. Nager, J.M. Liu, D.H. Pretorius, and R.K. Mittal, *The Vaginal Pressure Profile.* Neurourology and Urodynamics, 2005. **24**(3): p. 243-247.

37. Verelst, M. and G. Leivseth, *Force-Length Relationship in the Pelvic Floor Muscles under Transverse Vaginal Distension: A Method Study in Healthy Women.* Neurourology and Urodynamics, 2004. **23**(7): p. 662-667.

38. Parezanovic-Ilic, K., M. Jevtic, B. Jeremic, and S. Arsenijevic, *Muscle Strength Measurement of Pelvic Floor in Women by Vaginal Dynamometer.* Srpski Arhiv Za Celokupno Lekarstvo, 2009. **137**(9-10): p. 511-517.

39. Miller, J.M., J.A. Ashton-Miller, D. Perruchini, and I.O.J. DeLancey, *Test-Retest Reliability of an Instrumented Speculum for Measuring Vaginal Closure Force.* Neurourology and Urodynamics, 2007. **26**(6): p. 858-863.

40. Dumoulin, C., D. Bourbonnais, and M.C. Lemieux, *Development of a Dynamometer for Measuring the Isometric Force of the Pelvic Floor Musculature.* Neurourology and Urodynamics, 2003. **22**(7): p. 648-653.

41. Chamochumbi, C.C.M., F.R. Nunes, R.R.J. Guirro, and E.C.O. Guirro, *Comparison of Active and Passive Forces of the Pelvic Floor Muscles in Women with and without Stress Urinary Incontinence.* Revista Brasileira De Fisioterapia, 2012. **16**(4): p. 314-319.

42. Constantinou, C.E. and S. Omata, *Direction Sensitive Sensor Probe for the Evaluation of Voluntary and Reflex Pelvic Floor Contractions.* Neurourology and Urodynamics, 2007. **26**(3): p. 386-391.

43. Constantinou, C.E., S. Omata, Y. Yoshimura, and Q. Peng, *Evaluation of the Dynamic Responses of Female Pelvic Floor Using a Novel Vaginal Probe,* in *Reproductive Biomechanics*, D. Elad and R.C. Young, Editors. 2007, Blackwell Publishing: Oxford. p. 297-315.

44. Shishido, K., Q.Y. Peng, R. Jones, S. Omata, and C.E. Constantinou, *Influence of Pelvic Floor Muscle Contraction on the Profile of Vaginal Closure Pressure in Continent and Stress Urinary Incontinent Women.* Journal of Urology, 2008. **179**(5): p. 1917-1922.

45. Egorov, V., H. van Raalte, and V. Lucente, *Quantifying Vaginal Tissue Elasticity under Normal and Prolapse Conditions by Tactile Imaging.* International Urogynecology Journal, 2012. **23**(4): p. 459-466.

46. Egorov, V., H. van Raalte, and A.P. Sarvazyan, *Vaginal Tactile Imaging.* IEEE Transactions on Biomedical Engineering, 2010. **57**(7): p. 1736-1744.

47. Egorov, V. and A.P. Sarvazyan. *Methods for Characterizing Vaginal Tissue Elasticity.* US Patent 8,052,622. November 8, 2011.

48. Egorov, V., H. van Raalte, and A.P. Sarvazyan. *Methods for Assessment of Pelvic Organ Conditions Affecting the Vagina.* US Patent 8,187,208. May 29.2012.

49. Egorov, V. and A.P. Sarvazyan. *Method and Device for Measuring Tactile Profile of Vagina.* US Patent 8,840,571. September 23, 2014.

50. Hall, T.J., M. Bilgen, M.F. Insana, and T.A. Krouskop, *Phantom Materials for Elastography.* IEEE Transactions on Ultrasonics Ferroelectrics and Frequency Control, 1997. **44**(6): p. 1355-1365.

51. Sridhar, M., J. Liu, and M.F. Insana, *Viscoelasticity Imaging Using Ultrasound: Parameters and Error Analysis.* Physics in Medicine and Biology, 2007. **52**(9): p. 2425-2443.

52. Kwon, J. and G. Subhash, *Compressive Strain Rate Sensitivity of Ballistic Gelatin.* Journal of Biomechanics, 2010. **43**(3): p. 420-425.

53. Devi, C.U., R.M. Vasu, and A.K. Sood, *Design, Fabrication, and Characterization of a Tissue-Equivalent Phantom for Optical Elastography.* Journal of Biomedical Optics, 2005. **10**(4): p. 10.

54. Tabor, B.E., *Crosslinking Efficiency of Gelatin Hardners.* Journal of Applied Polymer Science, 1968. **12**(8): p. 1967.

55. Melendez, J., *Finite Element Analysis Simulating Indentation Testing of Human Vaginal Tissue,* Masters Thesis in Bioengineering. 2015. University of Kansas

Appendix A) Mechanical Design Drawings

Driving End

Technical drawings of the custom machined pieces of the driving end referred to in Chapter 2) Instrument Design Process

Probe End

Technical drawings of the custom machined pieces of the probe end referred to in Chapter 2) Instrument Design Process

Calibration Instrument

Technical drawings of the custom machined pieces of the calibration instrument referred to in Chapter 4) Design Process for Calibration Instrument and Procedure.

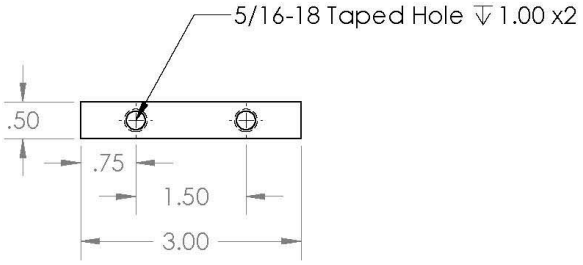

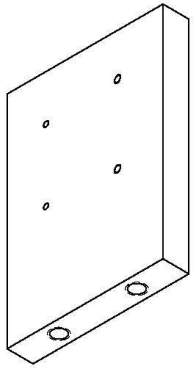

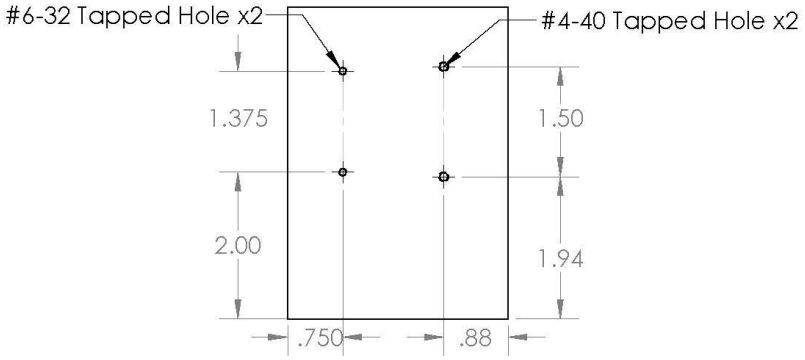

		UNLESS OTHERWISE SPECIFIED:		NAME	DATE
		DIMENSIONS ARE IN INCHES TOLERANCES: FRACTIONAL ± ANGULAR: MACH ± BEND ± TWO PLACE DECIMAL ±.010 THREE PLACE DECIMAL ±.005	DRAWN		
			CHECKED		TITLE:
			ENG APPR.		
			MFG APPR.		
		INTERPRET GEOMETRIC TOLERANCING PER:	Q.A.		
		MATERIAL Al - 6061	COMMENTS:		SIZE DWG. NO. REV ACalibBackE2
NEXT ASSY	USED ON	FINISH			
APPLICATION		DO NOT SCALE DRAWING			SCALE: 1:2 WEIGHT: SHEET 1 OF 1

5 4 3 2 1

Phantom Mold

Technical drawings of the custom machined pieces of the driving end referred to in Chapter 3)

Tissue Phantom Validation Design Process

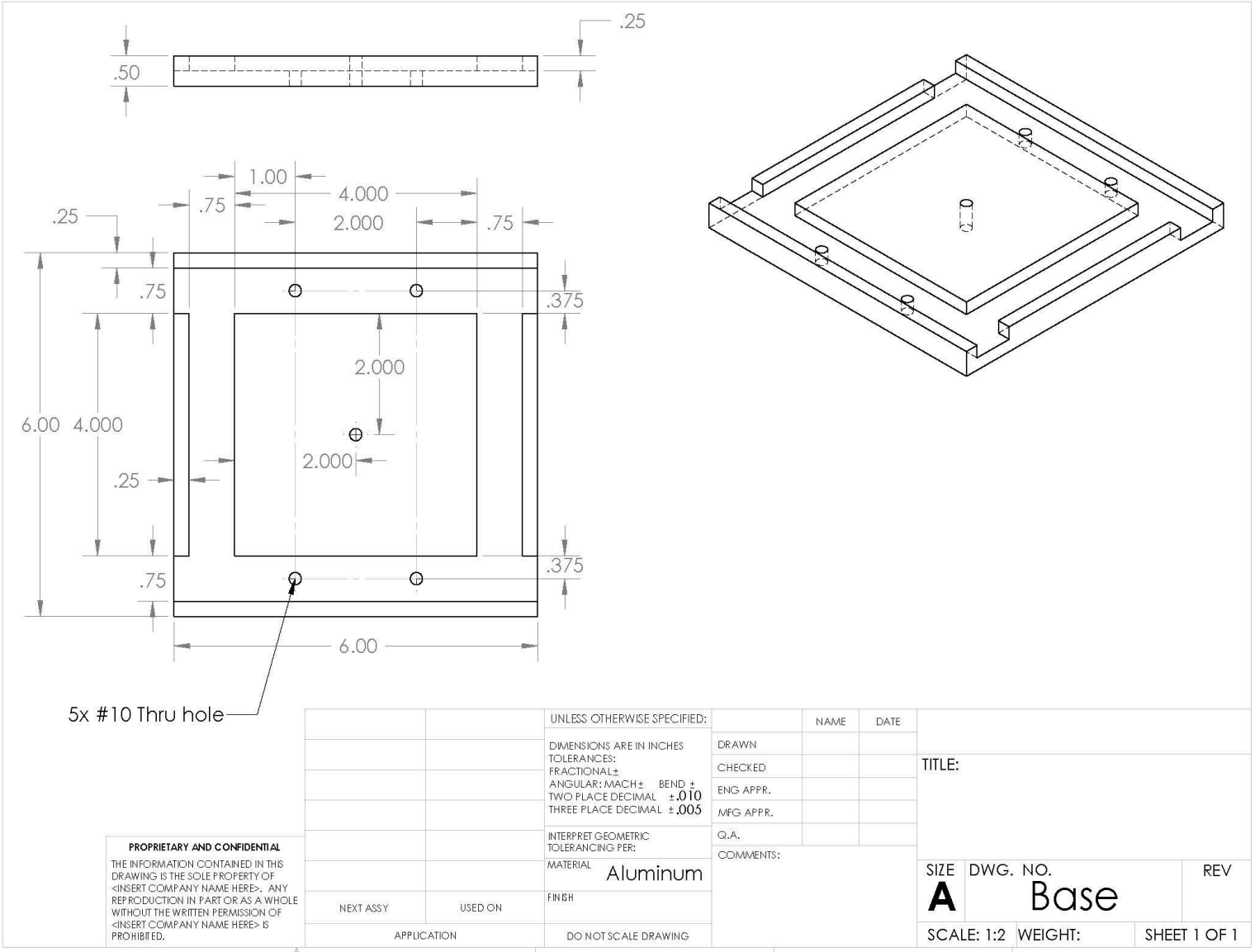

		UNLESS OTHERWISE SPECIFIED:		NAME	DATE
		DIMENSIONS ARE IN INCHES TOLERANCES: FRACTIONAL ± ANGULAR: MACH ± BEND ± TWO PLACE DECIMAL ±.010 THREE PLACE DECIMAL ±.005	DRAWN		
			CHECKED		TITLE:
			ENG APPR.		
			MFG APPR.		
		INTERPRET GEOMETRIC TOLERANCING PER:	Q.A.		
		MATERIAL Aluminum	COMMENTS:		SIZE A / DWG. NO. Base / REV
NEXT ASSY	USED ON	FINISH			
APPLICATION		DO NOT SCALE DRAWING			SCALE: 1:2 / WEIGHT: / SHEET 1 OF 1

5 4 3 2 1

Appendix B) Computer Code

CalAndCheck.vi

CalAndCheck.vi is an analysis program that was used in order to verify an eight parameter calibration model's accuracy. This was utilized in Chapter 4) to help determine relevant variables. Input into the .vi are two files, one data from a calibration protocol, and the second data from a test associated with that calibration. The program then processes the calibration data and obtains the proper calibration parameters. Then, the test data is sent through the calibration equation to obtain probe end force and position. These calculated force and position values are then compared to the measured force and position of the calibration instrument on a plot and through coefficients of determination.

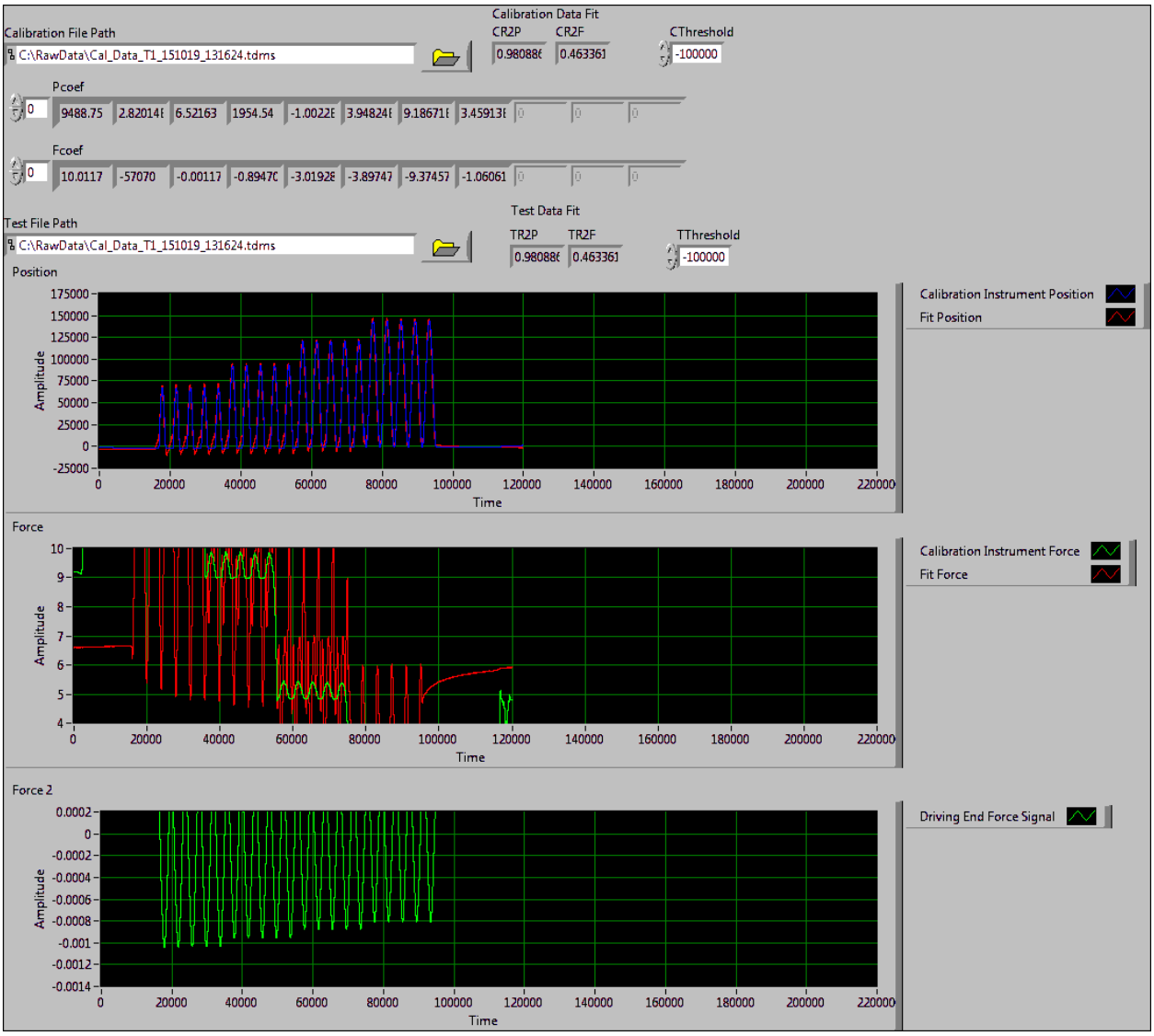

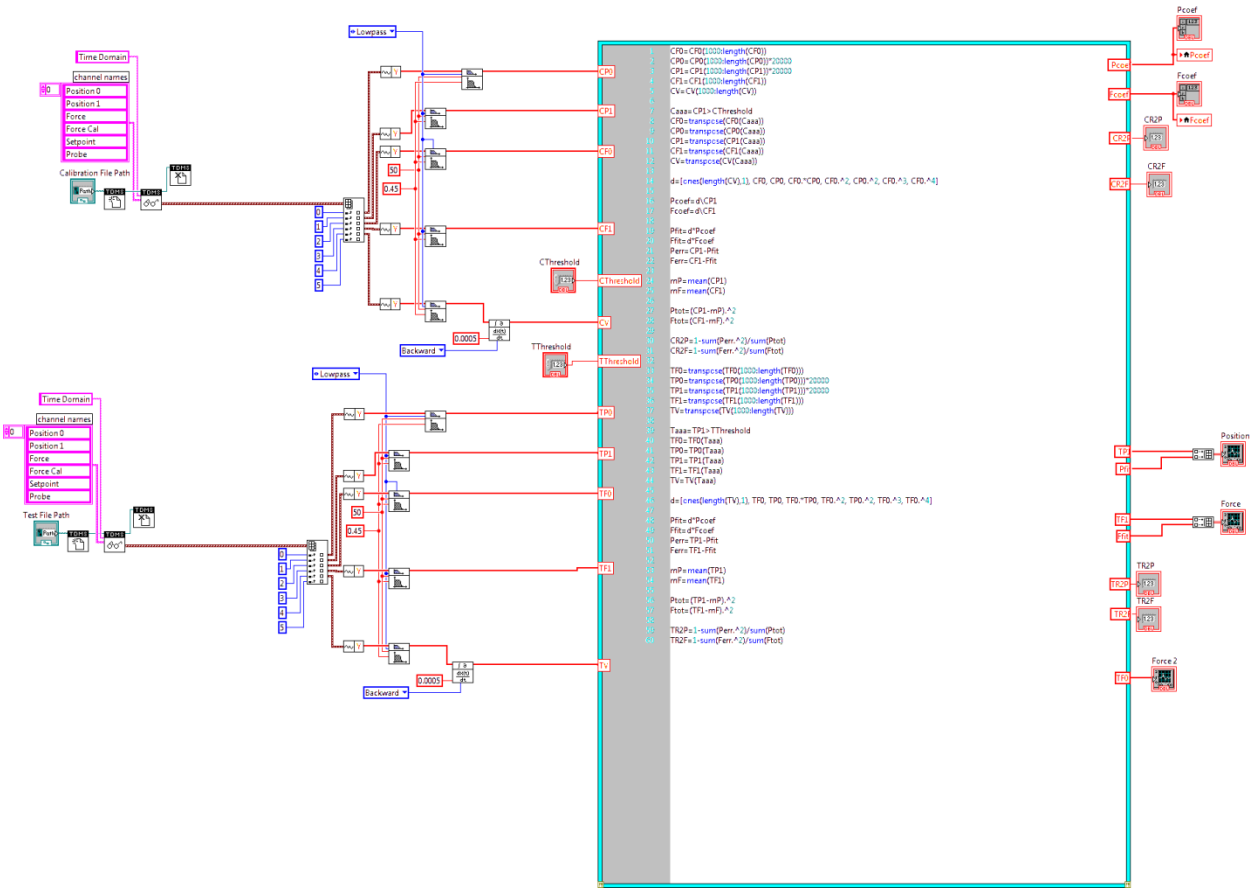

MathScript Text:

```
CF0=CF0(1000:length(CF0))
CP0=CP0(1000:length(CP0))*20000
CP1=CP1(1000:length(CP1))*20000
CF1=CF1(1000:length(CF1))
CV=CV(1000:length(CV))

Caaa=CP1>CThreshold
CF0=transpose(CF0(Caaa))
CP0=transpose(CP0(Caaa))
CP1=transpose(CP1(Caaa))
CF1=transpose(CF1(Caaa))
CV=transpose(CV(Caaa))

d=[ones(length(CV),1), CF0, CP0, CF0.*CP0, CF0.^2, CP0.^2, CF0.^3, CF0.^4]

Pcoef=d\CP1
Fcoef=d\CF1

Pfit=d*Pcoef
Ffit=d*Fcoef
Perr=CP1-Pfit
```

```
Ferr=CF1-Ffit

mP=mean(CP1)
mF=mean(CF1)

Ptot=(CP1-mP).^2
Ftot=(CF1-mF).^2

CR2P=1-sum(Perr.^2)/sum(Ptot)
CR2F=1-sum(Ferr.^2)/sum(Ftot)

TF0=transpose(TF0(1000:length(TF0)))
TP0=transpose(TP0(1000:length(TP0)))*20000
TP1=transpose(TP1(1000:length(TP1)))*20000
TF1=transpose(TF1(1000:length(TF1)))
TV=transpose(TV(1000:length(TV)))


Taaa=TP1>TThreshold
TF0=TF0(Taaa)
TP0=TP0(Taaa)
TP1=TP1(Taaa)
TF1=TF1(Taaa)
TV=TV(Taaa)

d=[ones(length(TV),1), TF0, TP0, TF0.*TP0, TF0.^2, TP0.^2, TF0.^3, TF0.^4]

Pfit=d*Pcoef
Ffit=d*Fcoef
Perr=TP1-Pfit
Ferr=TF1-Ffit

mP=mean(TP1)
mF=mean(TF1)

Ptot=(TP1-mP).^2
Ftot=(TF1-mF).^2

TR2P=1-sum(Perr.^2)/sum(Ptot)
TR2F=1-sum(Ferr.^2)/sum(Ftot)
```

Host Calibration Process2.vi

HostCalibrationProcess2.vi is a support program made to be used with the eight parameter calibration process. This .vi takes in the calibration data and outputs the calibration parameters both to the user and, optionally, sent to the FPGA. There is also a warning light that triggers if the calibration parameters are outside the range of the fixedpoint number that they are sent to in the FPGA.

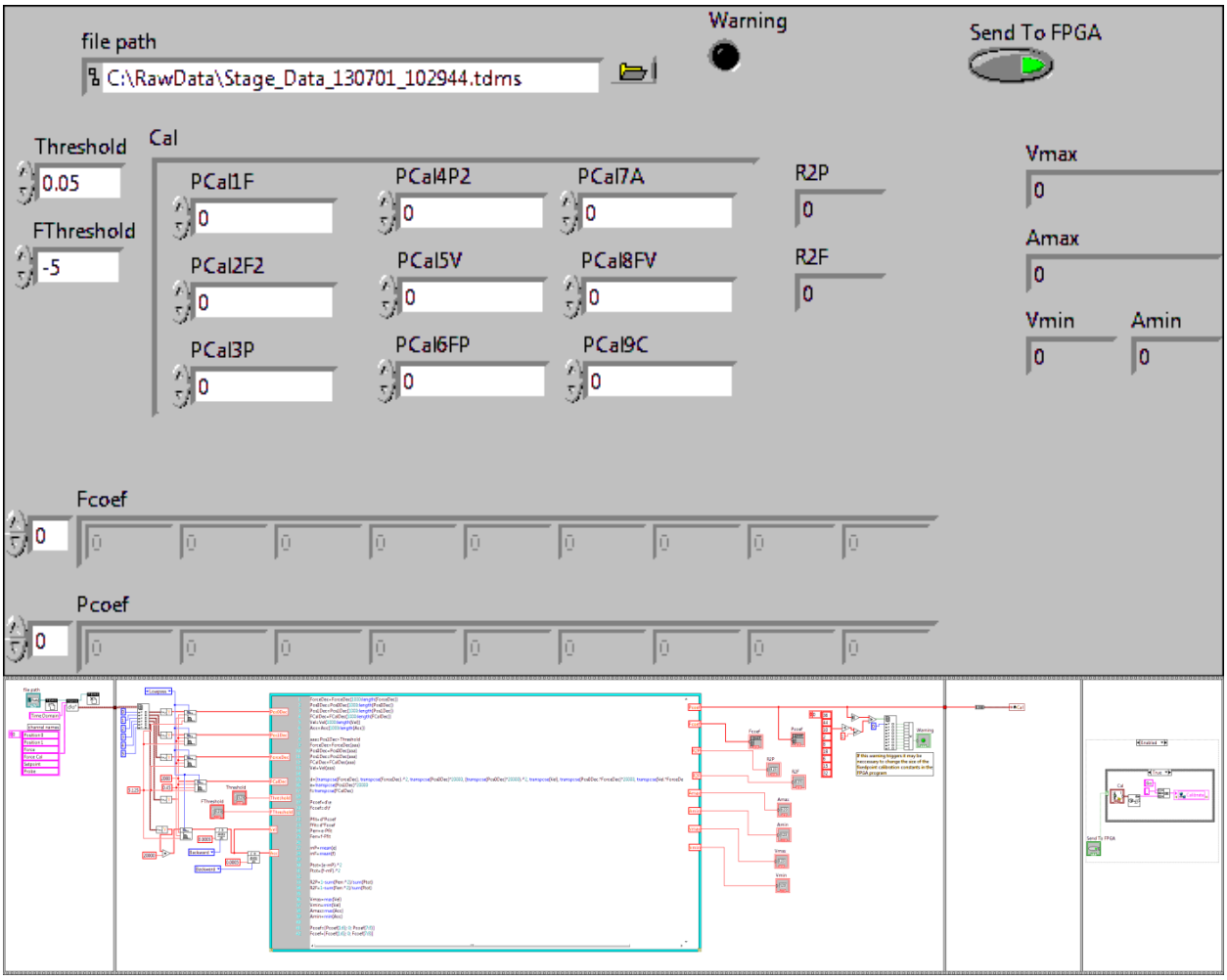

MathScript Text:

```
ForceDec=ForceDec(1000:length(ForceDec))
Pos0Dec=Pos0Dec(1000:length(Pos0Dec))
Pos1Dec=Pos1Dec(1000:length(Pos1Dec))
FCalDec=FCalDec(1000:length(FCalDec))
Vel=Vel(1000:length(Vel))
Acc=Acc(1000:length(Acc))

aaa=Pos1Dec>Threshold
ForceDec=ForceDec(aaa)
Pos0Dec=Pos0Dec(aaa)
Pos1Dec=Pos1Dec(aaa)
```

```
FCalDec=FCalDec(aaa)
Vel=Vel(aaa)

d=[transpose(ForceDec), transpose(ForceDec).^2, transpose(Pos0Dec)*20000,
(transpose(Pos0Dec)*20000).^2, transpose(Vel), transpose(Pos0Dec.*ForceDec)*20000,
transpose(Vel.*ForceDec), ones(length(ForceDec),1)]
e=transpose(Pos1Dec)*20000
f=transpose(FCalDec)

Pcoef=d\e
Fcoef=d\f

Pfit=d*Pcoef
Ffit=d*Fcoef
Perr=e-Pfit
Ferr=f-Ffit

mP=mean(e)
mF=mean(f)

Ptot=(e-mP).^2
Ftot=(f-mF).^2

R2P=1-sum(Perr.^2)/sum(Ptot)
R2F=1-sum(Ferr.^2)/sum(Ftot)

Vmax=max(Vel)
Vmin=min(Vel)
Amax=max(Acc)
Amin=min(Acc)

Pcoef=[Pcoef(1:6); 0; Pcoef(7:8)]
Fcoef=[Fcoef(1:6); 0; Fcoef(7:8)]
```

Slopes2.vi

Slopes2.vi is a data processing program. It takes in the .tdms file of a calibration test, plots the relevant raw data, finds the proper loading segments, plots those loading segments as Force vs Displacement curves, finds the slope of those Force vs Displacement Curves, plots those slopes as calibration E vs driving E, and reports the slopes for other programs to employ. The program can also, optionally, output the force and displacement data as a .txt file if MATLAB or other processing is required.

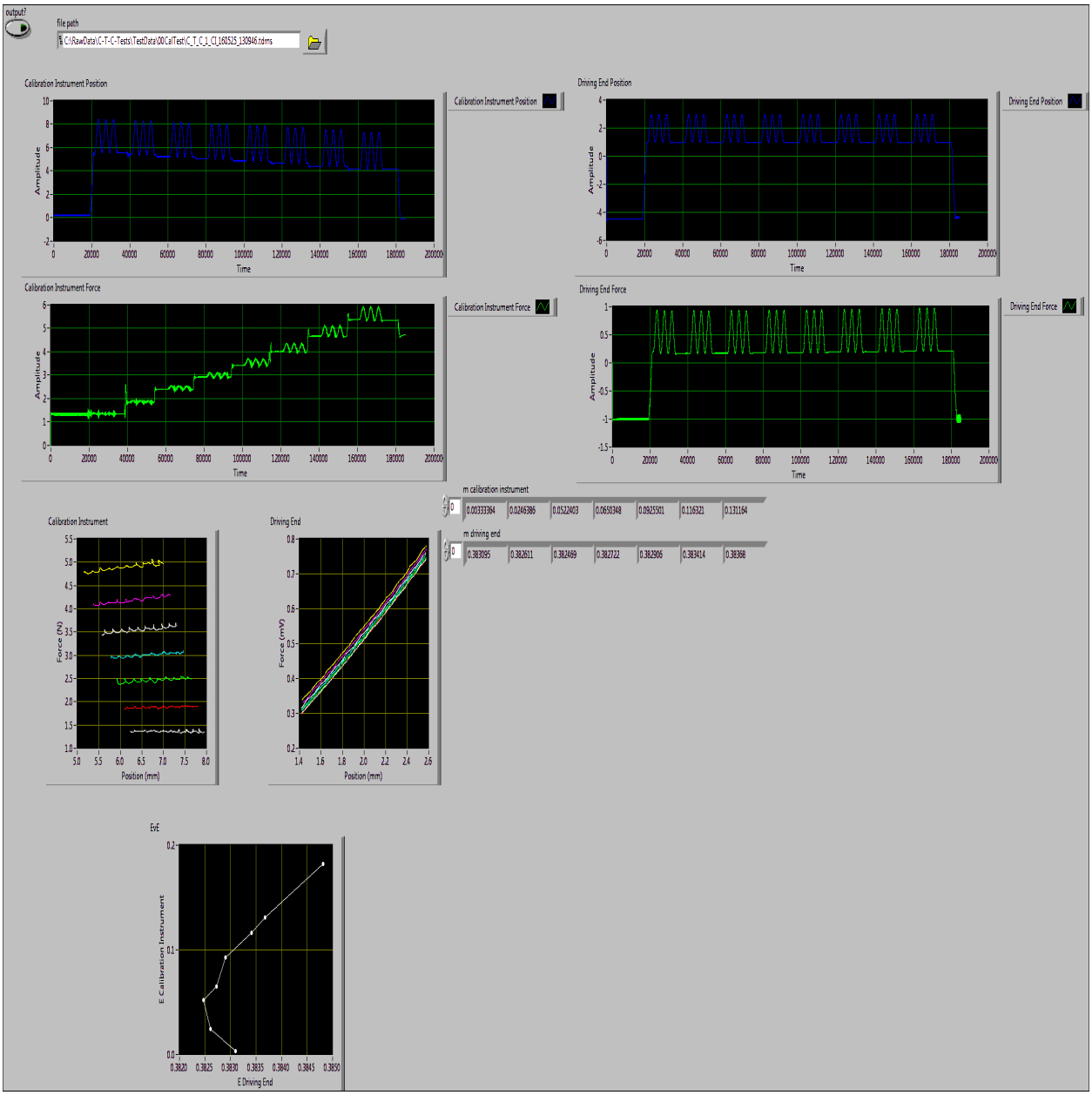

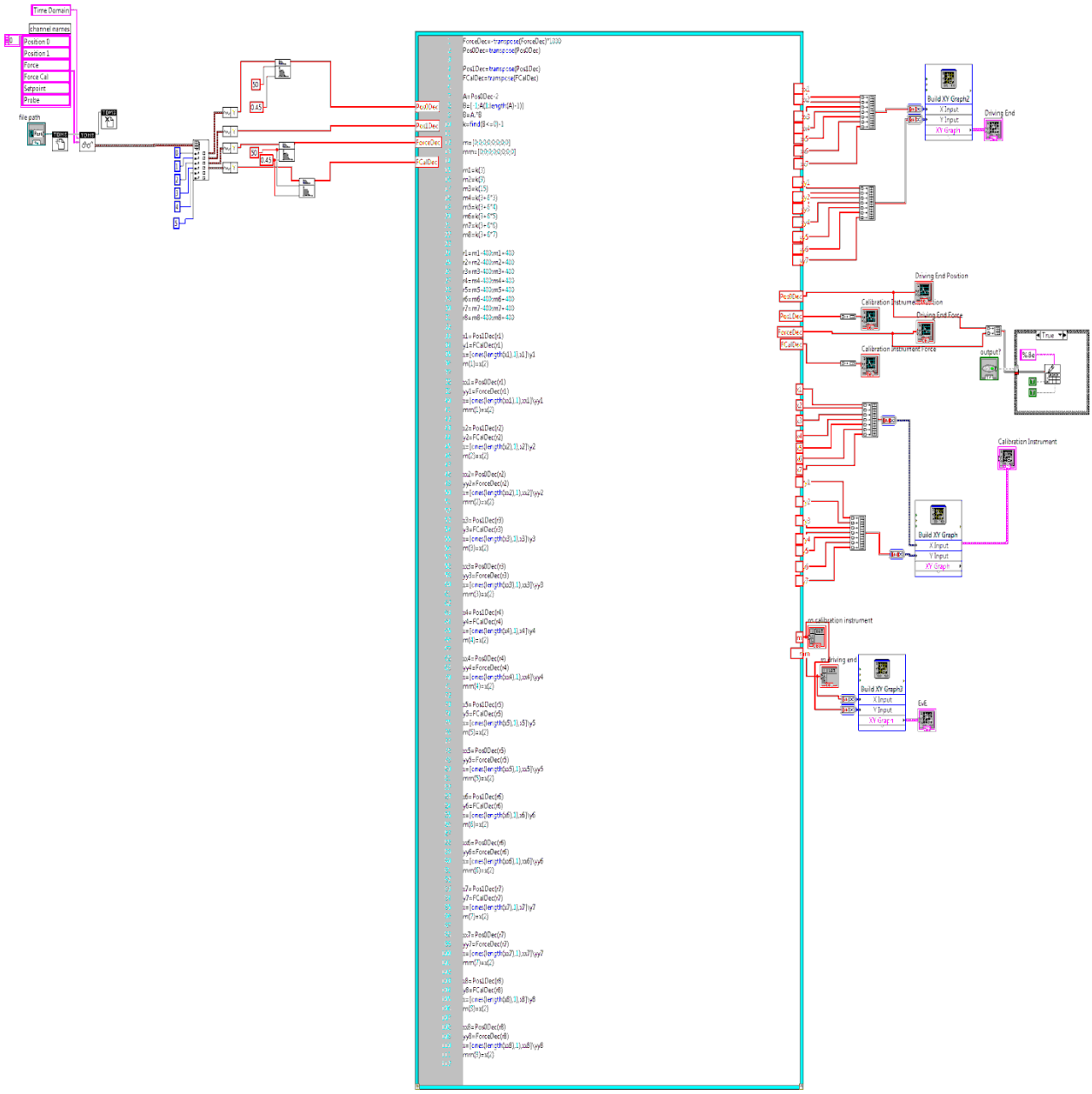

MathScript Text:

```
ForceDec=-transpose(ForceDec)*1000
Pos0Dec=transpose(Pos0Dec)

Pos1Dec=transpose(Pos1Dec)
FCalDec=transpose(FCalDec)

A=Pos0Dec-2
B=[-1;A(1:length(A)-1)]
B=A.*B
k=find(B<=0)-1
```

```
m=[0;0;0;0;0;0;0;0]
mm=[0;0;0;0;0;0;0;0]

m1=k(3)
m2=k(9)
m3=k(15)
m4=k(3+6*3)
m5=k(3+6*4)
m6=k(3+6*5)
m7=k(3+6*6)
m8=k(3+6*7)

r1=m1-400:m1+400
r2=m2-400:m2+400
r3=m3-400:m3+400
r4=m4-400:m4+400
r5=m5-400:m5+400
r6=m6-400:m6+400
r7=m7-400:m7+400
r8=m8-400:m8+400

x1=Pos1Dec(r1)
y1=FCalDec(r1)
x=[ones(length(x1),1),x1]\y1
m(1)=x(2)

xx1=Pos0Dec(r1)
yy1=ForceDec(r1)
x=[ones(length(xx1),1),xx1]\yy1
mm(1)=x(2)
x2=Pos1Dec(r2)
y2=FCalDec(r2)
x=[ones(length(x2),1),x2]\y2
m(2)=x(2)

xx2=Pos0Dec(r2)
yy2=ForceDec(r2)
x=[ones(length(xx2),1),xx2]\yy2
mm(2)=x(2)

x3=Pos1Dec(r3)
y3=FCalDec(r3)
x=[ones(length(x3),1),x3]\y3
m(3)=x(2)
```

```
xx3=Pos0Dec(r3)
yy3=ForceDec(r3)
x=[ones(length(xx3),1),xx3]\yy3
mm(3)=x(2)

x4=Pos1Dec(r4)
y4=FCalDec(r4)
x=[ones(length(x4),1),x4]\y4
m(4)=x(2)

xx4=Pos0Dec(r4)
yy4=ForceDec(r4)
x=[ones(length(xx4),1),xx4]\yy4
mm(4)=x(2)

x5=Pos1Dec(r5)
y5=FCalDec(r5)
x=[ones(length(x5),1),x5]\y5
m(5)=x(2)

xx5=Pos0Dec(r5)
yy5=ForceDec(r5)
x=[ones(length(xx5),1),xx5]\yy5
mm(5)=x(2)

x6=Pos1Dec(r6)
y6=FCalDec(r6)
x=[ones(length(x6),1),x6]\y6
m(6)=x(2)

xx6=Pos0Dec(r6)
yy6=ForceDec(r6)
x=[ones(length(xx6),1),xx6]\yy6
mm(6)=x(2)

x7=Pos1Dec(r7)
y7=FCalDec(r7)
x=[ones(length(x7),1),x7]\y7
m(7)=x(2)

xx7=Pos0Dec(r7)
yy7=ForceDec(r7)
x=[ones(length(xx7),1),xx7]\yy7
mm(7)=x(2)

x8=Pos1Dec(r8)
```

```
y8=FCalDec(r8)
x=[ones(length(x8),1),x8]\y8
m(8)=x(2)

xx8=Pos0Dec(r8)
yy8=ForceDec(r8)
x=[ones(length(xx8),1),xx8]\yy8
mm(8)=x(2)
```

DriftAnalysis.vi

DriftAnalysis.vi is an analysis program that is used with the Drift protocol discussed in Chapter 5. The .vi takes inputs of the first and second file names from a drift test, as well as the number of files to be processed. The .vi then automatically generates the names for the other files that were not input by the user based on the second file's name. Each file is then simplified to four points, which are the average of driving force, driving position, calibration force, and calibration position, by averaging a specific stretch of data. After all of these points are collected time stamps, time values for each point are calculated. Each of the four data points are then plotted, and the values are sent to a generated .txt file for later analysis.

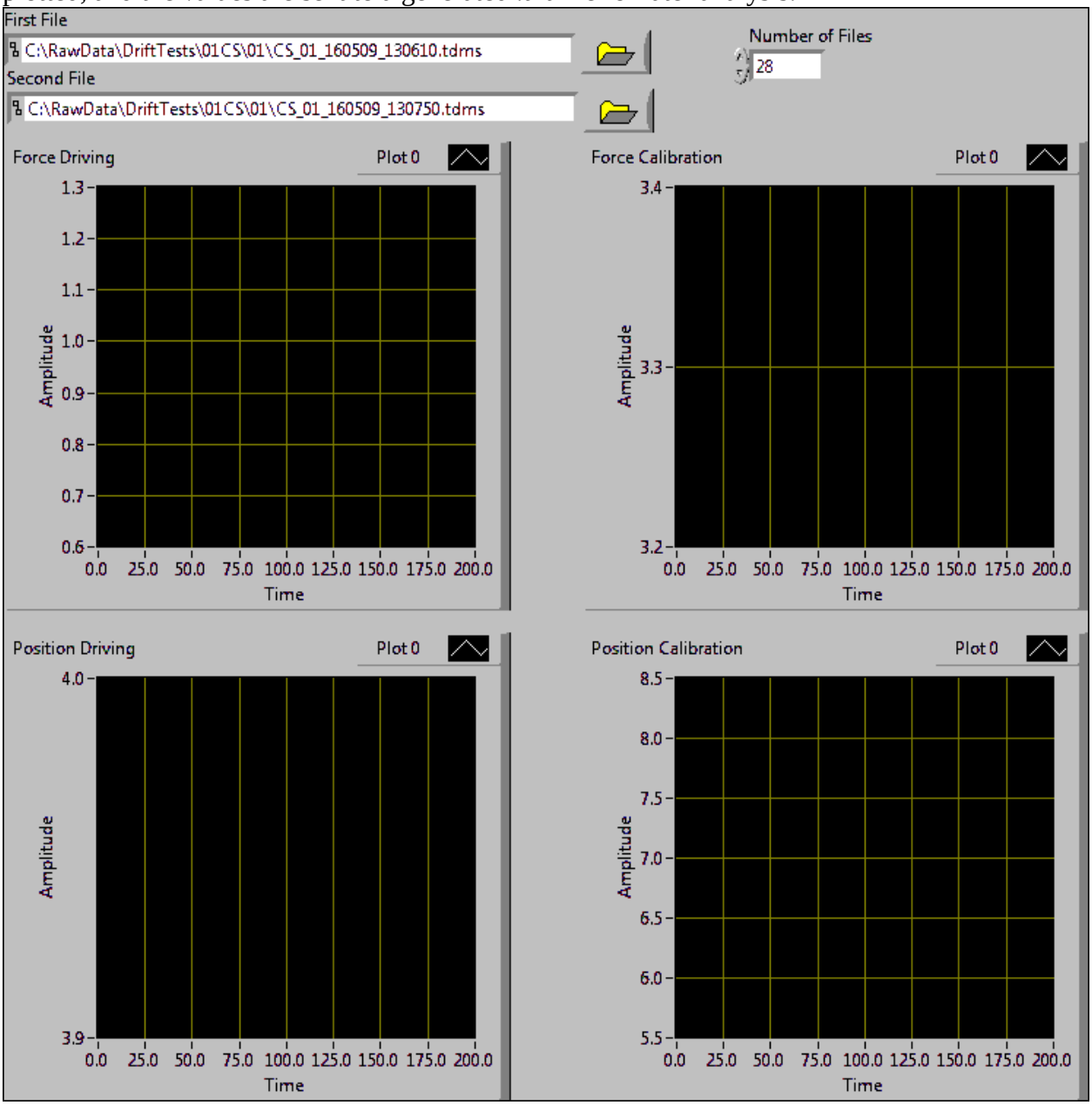

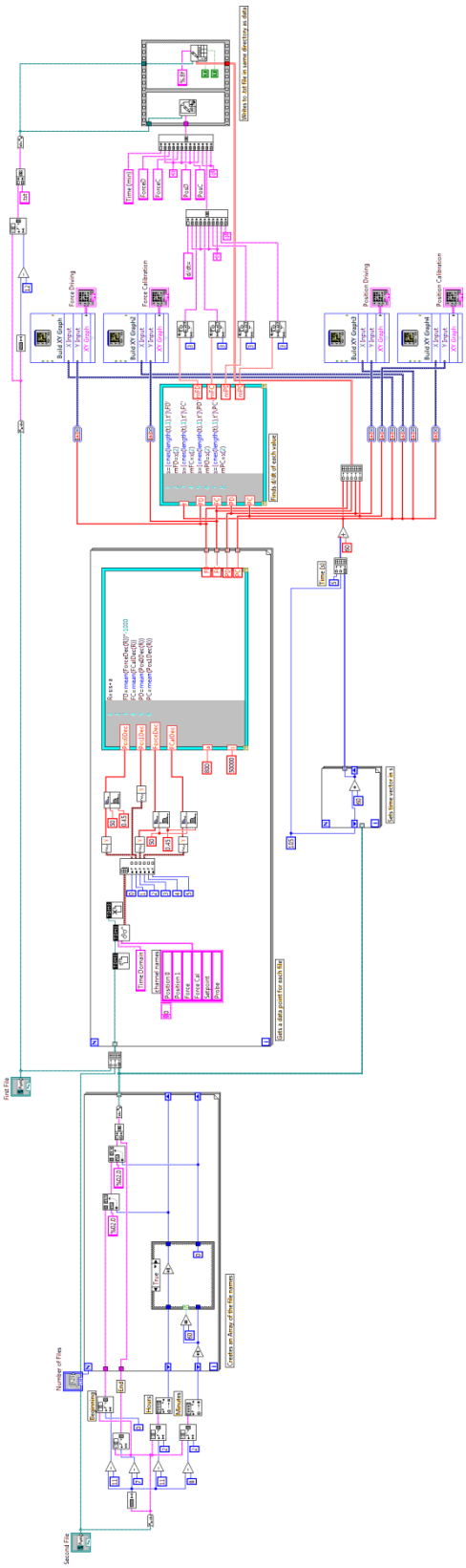

CTC_Analysis.vi

CTC_Analysis.vi is made to be run with the calibrate-test-calibrate testing procedure discussed in Chapter 5. Three files are input into the .vi and each analyzed the same way. First, the raw data is plotted. Next, the program automatically identifies the loading segments of interest. Those segments are then plotted as force vs displacement curves. The slopes of these curves is then calculated and plotted on the E calibration vs E driving plot. After this is done for each file the three comparative elasticity plots are combined and plotted together. Finally, the E driving and E calibration values are saved into a .txt file for future processing.

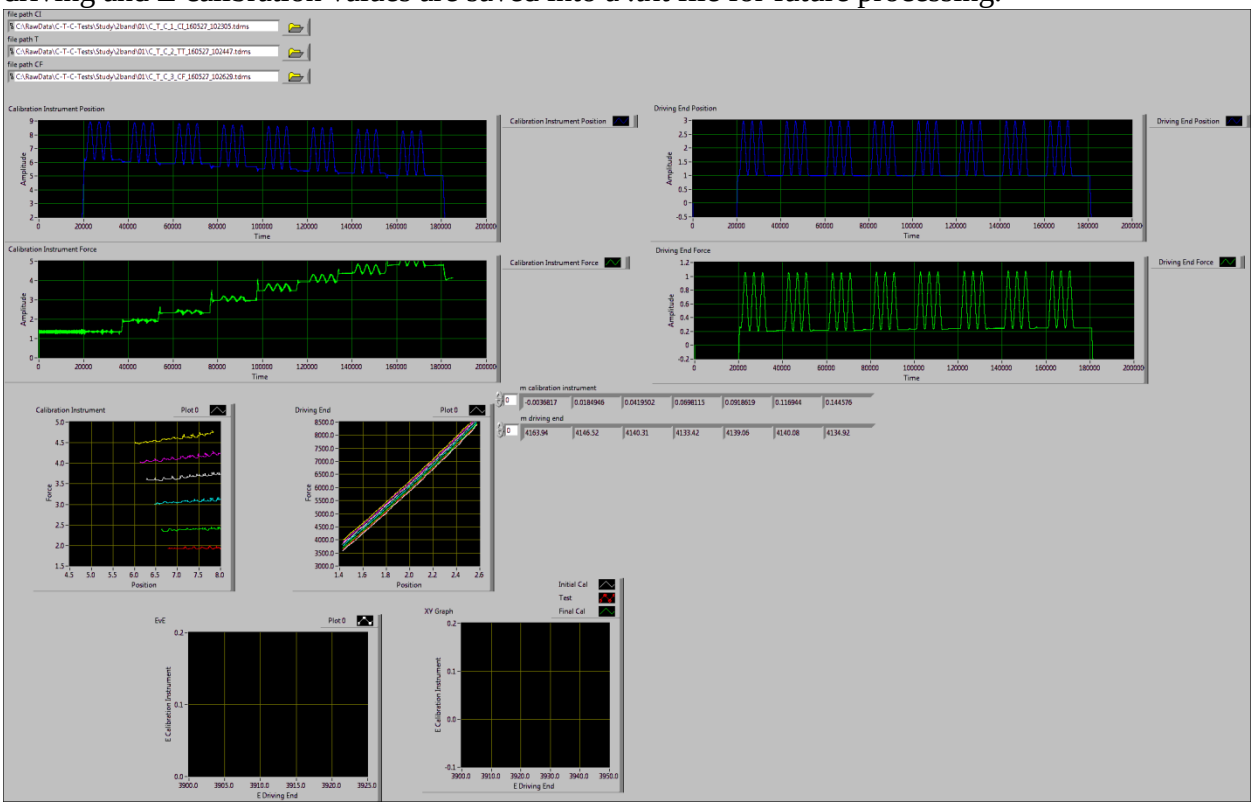

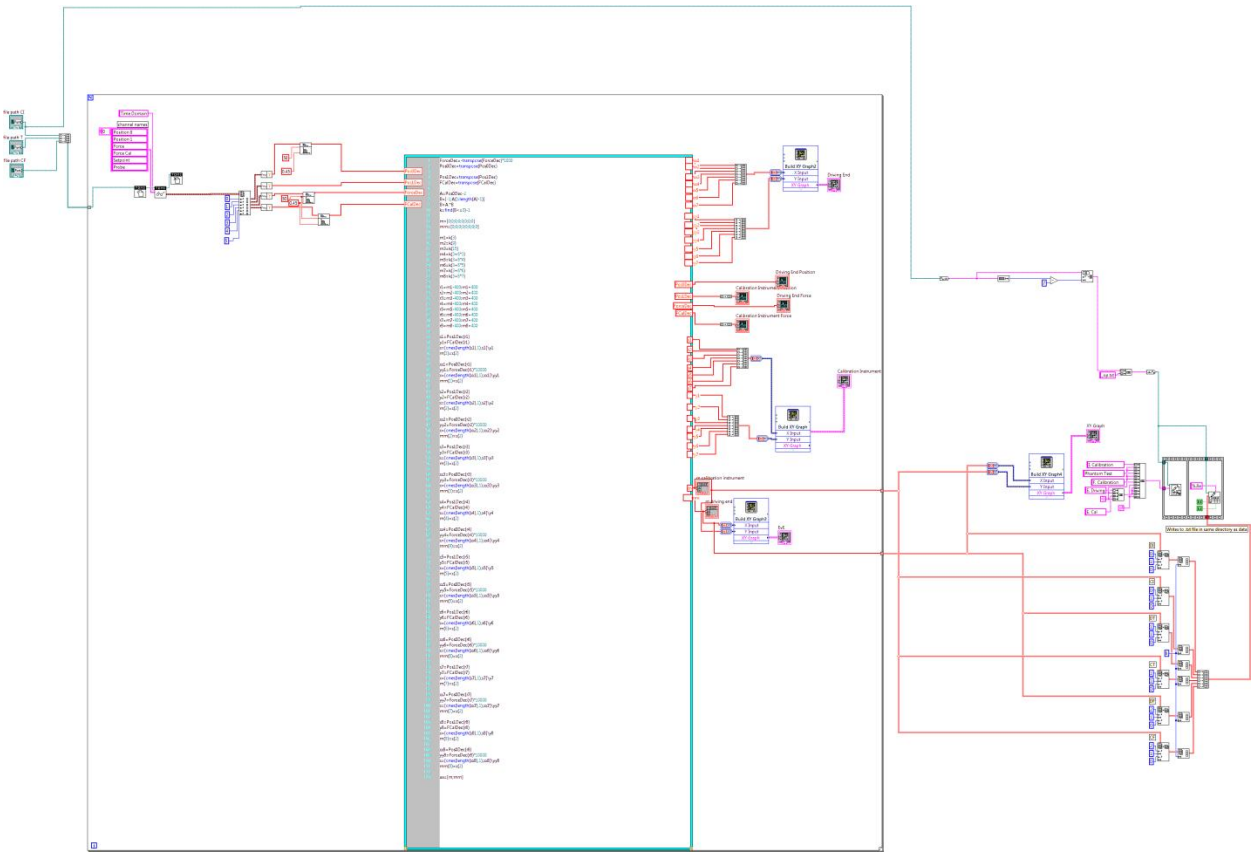

MathScript Text:
ForceDec=-transpose(ForceDec)*1000
Pos0Dec=transpose(Pos0Dec)

Pos1Dec=transpose(Pos1Dec)
FCalDec=transpose(FCalDec)

A=Pos0Dec-2
B=[-1;A(1:length(A)-1)]
B=A.*B
k=find(B<=0)-1

m=[0;0;0;0;0;0;0;0;0]
mm=[0;0;0;0;0;0;0;0;0]

m1=k(3)
m2=k(9)
m3=k(15)
m4=k(3+6*3)
m5=k(3+6*4)
m6=k(3+6*5)
m7=k(3+6*6)

```
m8=k(3+6*7)

r1=m1-400:m1+400
r2=m2-400:m2+400
r3=m3-400:m3+400
r4=m4-400:m4+400
r5=m5-400:m5+400
r6=m6-400:m6+400
r7=m7-400:m7+400
r8=m8-400:m8+400

x1=Pos1Dec(r1)
y1=FCalDec(r1)
x=[ones(length(x1),1),x1]\y1
m(1)=x(2)

xx1=Pos0Dec(r1)
yy1=ForceDec(r1)*10000
x=[ones(length(xx1),1),xx1]\yy1
mm(1)=x(2)

x2=Pos1Dec(r2)
y2=FCalDec(r2)
x=[ones(length(x2),1),x2]\y2
m(2)=x(2)

xx2=Pos0Dec(r2)
yy2=ForceDec(r2)*10000
x=[ones(length(xx2),1),xx2]\yy2
mm(2)=x(2)

x3=Pos1Dec(r3)
y3=FCalDec(r3)
x=[ones(length(x3),1),x3]\y3
m(3)=x(2)

xx3=Pos0Dec(r3)
yy3=ForceDec(r3)*10000
x=[ones(length(xx3),1),xx3]\yy3
mm(3)=x(2)

x4=Pos1Dec(r4)
y4=FCalDec(r4)
x=[ones(length(x4),1),x4]\y4
m(4)=x(2)
```

```
xx4=Pos0Dec(r4)
yy4=ForceDec(r4)*10000
x=[ones(length(xx4),1),xx4]\yy4
mm(4)=x(2)

x5=Pos1Dec(r5)
y5=FCalDec(r5)
x=[ones(length(x5),1),x5]\y5
m(5)=x(2)

xx5=Pos0Dec(r5)
yy5=ForceDec(r5)*10000
x=[ones(length(xx5),1),xx5]\yy5
mm(5)=x(2)

x6=Pos1Dec(r6)
y6=FCalDec(r6)
x=[ones(length(x6),1),x6]\y6
m(6)=x(2)

xx6=Pos0Dec(r6)
yy6=ForceDec(r6)*10000
x=[ones(length(xx6),1),xx6]\yy6
mm(6)=x(2)

x7=Pos1Dec(r7)
y7=FCalDec(r7)
x=[ones(length(x7),1),x7]\y7
m(7)=x(2)

xx7=Pos0Dec(r7)
yy7=ForceDec(r7)*10000
x=[ones(length(xx7),1),xx7]\yy7
mm(7)=x(2)

x8=Pos1Dec(r8)
y8=FCalDec(r8)
x=[ones(length(x8),1),x8]\y8
m(8)=x(2)

xx8=Pos0Dec(r8)
yy8=ForceDec(r8)*10000
x=[ones(length(xx8),1),xx8]\yy8
mm(8)=x(2)

aa=[m;mm]
```

Appendix C) Example Data

Drift Tests

Values over time (min) for the values of driving force (ForceD in mV), calibration instrument force (ForceC in N), driving position (PosD in mm), and calibration instrument position (PosC in mm) referenced in Chapter 5. Triplicate tests for the isolated driving load cell, drained isolated driving bellows, short nylon tubing with 3mm displacement, long nylon tubing with 3 and 4 mm displacement and copper tubing with 3 and 4mm displacement.

Load Cell Test Trial 1

Time (min)	ForceD	ForceC	PosD	PosC
d/dt=	-4.442E-6	-402.691E-6	42.126E-6	-22.703E-6
0.08333333	0.12319196	2.26297885	3.99722523	0.00002928
1.75000000	0.12326124	2.26716849	3.99609035	-0.00002191
2.75000000	0.12329373	2.26795000	3.99508989	-0.00004944
3.75000000	0.12326558	2.26836481	3.99572250	-0.00006536
4.75000000	0.12328634	2.26893777	3.99544005	-0.00010031
5.75000000	0.12333924	2.26932992	3.99207003	-0.00013602
6.75000000	0.12328833	2.26863766	3.99286013	-0.00015225
7.75000000	0.12329354	2.26910947	3.99429286	-0.00018783
8.75000000	0.12334060	2.26781152	3.99398220	-0.00020194
9.75000000	0.12333891	2.26821631	3.99481198	-0.00023926
10.75000000	0.12333219	2.26588962	3.99469232	-0.00025125
11.75000000	0.12331220	2.26582893	3.99393214	-0.00028190
12.75000000	0.12334492	2.26568483	3.99464370	-0.00030025
13.75000000	0.12331296	2.26491721	3.99500107	-0.00032172
14.75000000	0.12331962	2.26441872	3.99418374	-0.00034775
15.75000000	0.12326642	2.26416762	3.99579436	-0.00036099
16.75000000	0.12326162	2.26361697	3.99443164	-0.00039757
17.75000000	0.12320817	2.26244067	3.99506017	-0.00040874
18.75000000	0.12325751	2.26209810	3.99471070	-0.00044076
19.75000000	0.12325158	2.26129274	3.99503144	-0.00045106
20.75000000	0.12322565	2.26172239	3.99613415	-0.00047328
21.75000000	0.12319436	2.26128737	3.99613226	-0.00050075
22.75000000	0.12322596	2.26093633	3.99571671	-0.00052584
23.75000000	0.12317517	2.25996568	3.99657828	-0.00054806
24.75000000	0.12320234	2.25904692	3.99582327	-0.00055337
25.75000000	0.12319886	2.25830467	3.99601124	-0.00057534
26.75000000	0.12318127	2.25853280	3.99526028	-0.00059900
27.75000000	0.12314143	2.25777478	3.99528537	-0.00061273
28.75000000	0.12318857	2.25821438	3.99606635	-0.00063514
29.75000000	0.12319206	2.25705027	3.99651222	-0.00064925

Load Cell Test Trial 2:

Time (min)	ForceD	ForceC	PosD	PosC
d/dt=	-2.087E-6	-27.744E-6	-250.022E-6	-13.062E-6
0.08333333	0.12316837	2.25594854	3.99684305	-0.00008620
1.75000000	0.12319479	2.25602751	3.99628351	-0.00010044
2.75000000	0.12318345	2.25619171	3.99623065	-0.00010312
3.75000000	0.12317656	2.25589757	3.99698679	-0.00013983
4.75000000	0.12314681	2.25513691	3.99660330	-0.00015019
5.75000000	0.12315172	2.25539393	3.99517682	-0.00015487
6.75000000	0.12317536	2.25555510	3.98794717	-0.00018558
7.75000000	0.12320132	2.25473406	3.99160314	-0.00019126
8.75000000	0.12312561	2.25532889	3.98906780	-0.00019950
9.75000000	0.12309712	2.25428590	3.98920544	-0.00020031
10.75000000	0.12314994	2.25445554	3.98815120	-0.00020886
11.75000000	0.12320233	2.25407471	3.98912501	-0.00023683
12.75000000	0.12314364	2.25496899	3.99048931	-0.00024981
13.75000000	0.12313235	2.25566487	3.98884119	-0.00026735
14.75000000	0.12313265	2.25470328	3.98771519	-0.00029469
15.75000000	0.12316544	2.25501232	3.98856496	-0.00030069
16.75000000	0.12311197	2.25549821	3.98796148	-0.00030037
17.75000000	0.12313796	2.25433490	3.99088874	-0.00030680
18.75000000	0.12313352	2.25411101	3.99043784	-0.00033052
19.75000000	0.12309644	2.25497447	3.99114207	-0.00034894
20.75000000	0.12313485	2.25447934	3.98929860	-0.00036273
21.75000000	0.12313500	2.25505013	3.98848245	-0.00037004
22.75000000	0.12312702	2.25437829	3.98823354	-0.00039170
23.75000000	0.12316381	2.25531515	3.99090757	-0.00039607
24.75000000	0.12312410	2.25491408	3.98728534	-0.00040106
25.75000000	0.12311169	2.25431105	3.98872406	-0.00041373
26.75000000	0.12312814	2.25430463	3.98863566	-0.00044238
27.75000000	0.12312144	2.25501526	3.98803246	-0.00044963
28.75000000	0.12311095	2.25525761	3.98891438	-0.00045137
29.75000000	0.12311850	2.25588138	3.98844850	-0.00045743

Load Cell Test Trial 3:

Time (min)	ForceD	ForceC	PosD	PosC
d/dt=	-2.434E-6	-26.858E-6	-18.897E-6	-6.361E-6
0.08333333	0.12312002	2.25426556	3.99632679	0.00005768
1.75000000	0.12310894	2.25412552	3.99639208	0.00005137
2.75000000	0.12311561	2.25430848	3.99624004	0.00004925
3.75000000	0.12312089	2.25452732	3.99572761	0.00004469
4.75000000	0.12310381	2.25503575	3.99610532	0.00003433
5.75000000	0.12307828	2.25455682	3.99650661	0.00001242
6.75000000	0.12312306	2.25495882	3.99629912	0.00001548
7.75000000	0.12312331	2.25395396	3.99594677	0.00000137
8.75000000	0.12310558	2.25430191	3.99616977	-0.00000062
9.75000000	0.12309891	2.25431656	3.99608413	-0.00000268
10.75000000	0.12311855	2.25393080	3.99660959	-0.00001473
11.75000000	0.12309569	2.25402730	3.99640436	-0.00002915
12.75000000	0.12309173	2.25436428	3.99628926	-0.00002634
13.75000000	0.12306592	2.25445605	3.99630870	-0.00004295
14.75000000	0.12306826	2.25433945	3.99658286	-0.00004607
15.75000000	0.12309104	2.25446497	3.99623404	-0.00005037
16.75000000	0.12313044	2.25461504	3.99646561	-0.00005125
17.75000000	0.12305499	2.25423843	3.99666401	-0.00006242
18.75000000	0.12306610	2.25443370	3.99637726	-0.00006529
19.75000000	0.12309814	2.25450821	3.99632476	-0.00007072
20.75000000	0.12306931	2.25416503	3.99640425	-0.00007428
21.75000000	0.12304782	2.25405278	3.99603203	-0.00009238
22.75000000	0.12307363	2.25411981	3.99569598	-0.00009906
23.75000000	0.12309914	2.25334821	3.99579300	-0.00009919
24.75000000	0.12305162	2.25433625	3.99598645	-0.00009994
25.75000000	0.12308195	2.25371229	3.99587810	-0.00010218
26.75000000	0.12305609	2.25419241	3.99575646	-0.00010462
27.75000000	0.12305109	2.25293648	3.99573028	-0.00011679
28.75000000	0.12303995	2.25426008	3.99543801	-0.00011804
29.75000000	0.12303466	2.25324599	3.99558331	-0.00011991

Driving Bellows Test Trial 1:

Time (min)	ForceD	ForceC	PosD	PosC
d/dt=	-24.493E-6	-383.611E-6	-76.803E-6	-20.660E-6
0.08333333	0.10633603	2.22354051	3.97591520	-0.00001086
1.75000000	0.10601252	2.22852109	3.97353619	-0.00004370
2.75000000	0.10594568	2.22994903	3.97300950	-0.00005705
3.75000000	0.10593201	2.22975668	3.97276563	-0.00007210
4.75000000	0.10584265	2.22981410	3.97259097	-0.00010081
5.75000000	0.10583523	2.22844313	3.97187177	-0.00011985
6.75000000	0.10584000	2.22930846	3.97260800	-0.00014757
7.75000000	0.10581511	2.22889146	3.97199503	-0.00016355
8.75000000	0.10572952	2.22734731	3.97068483	-0.00019213
9.75000000	0.10574391	2.22827065	3.97121199	-0.00020418
10.75000000	0.10568057	2.22650944	3.97008560	-0.00022990
11.75000000	0.10569581	2.22651797	3.97139823	-0.00025375
12.75000000	0.10568520	2.22516571	3.97135259	-0.00027697
13.75000000	0.10563915	2.22477646	3.97102748	-0.00029931
14.75000000	0.10559906	2.22431830	3.97097773	-0.00030624
15.75000000	0.10556764	2.22399386	3.96995244	-0.00034007
16.75000000	0.10555636	2.22290127	3.97012310	-0.00035512
17.75000000	0.10554146	2.22195306	3.97112287	-0.00039089
18.75000000	0.10552462	2.22143929	3.97159346	-0.00040306
19.75000000	0.10544872	2.22042342	3.97003416	-0.00042559
20.75000000	0.10543556	2.22169736	3.97031391	-0.00044825
21.75000000	0.10544037	2.22078508	3.97062751	-0.00045612
22.75000000	0.10541541	2.21991636	3.96992536	-0.00048596
23.75000000	0.10544173	2.22112412	3.97157554	-0.00050062
24.75000000	0.10540315	2.21999326	3.97127326	-0.00051461
25.75000000	0.10541651	2.22057747	3.97115132	-0.00054201
26.75000000	0.10547676	2.22118120	3.97225068	-0.00055175
27.75000000	0.10543893	2.22030610	3.97164061	-0.00057491
28.75000000	0.10539294	2.21910059	3.97171920	-0.00059039
29.75000000	0.10533921	2.21838773	3.97100284	-0.00060499

Driving Bellows Test Trial 2:

Time (min)	ForceD	ForceC	PosD	PosC
d/dt=	-12.865E-6	-22.103E-6	218.833E-9	-10.822E-6
0.08333333	0.11916125	2.21717778	3.96726964	0.00003190
1.75000000	0.11894664	2.21490484	3.96919584	-0.00000106
2.75000000	0.11882731	2.21357218	3.96922577	-0.00001598
3.75000000	0.11881244	2.21545109	3.96853748	-0.00004582
4.75000000	0.11874160	2.21492988	3.96725162	-0.00005212
5.75000000	0.11871758	2.21556562	3.96686408	-0.00006429
6.75000000	0.11872906	2.21570697	3.96684570	-0.00009095
7.75000000	0.11871302	2.21404522	3.96675675	-0.00009844
8.75000000	0.11869243	2.21429179	3.96687538	-0.00010075
9.75000000	0.11866884	2.21483805	3.96547197	-0.00010755
10.75000000	0.11860187	2.21610754	3.96512601	-0.00011629
11.75000000	0.11862992	2.21566070	3.96604642	-0.00014395
12.75000000	0.11860396	2.21517416	3.96562721	-0.00014856
13.75000000	0.11860734	2.21491523	3.96578901	-0.00015050
14.75000000	0.11856115	2.21539464	3.96516442	-0.00015268
15.75000000	0.11858709	2.21488602	3.96570014	-0.00016779
16.75000000	0.11858535	2.21538460	3.96570982	-0.00018065
17.75000000	0.11857562	2.21481766	3.96566582	-0.00018620
18.75000000	0.11861373	2.21498352	3.96656523	-0.00020050
19.75000000	0.11862426	2.21403552	3.96818769	-0.00020581
20.75000000	0.11858311	2.21492882	3.96704461	-0.00022865
21.75000000	0.11855743	2.21600585	3.96669020	-0.00023777
22.75000000	0.11855254	2.21457357	3.96746546	-0.00024988
23.75000000	0.11853555	2.21453425	3.96634461	-0.00025337
24.75000000	0.11862133	2.21416923	3.96763176	-0.00026854
25.75000000	0.11857754	2.21440802	3.96746148	-0.00028714
26.75000000	0.11857503	2.21572124	3.96841661	-0.00029195
27.75000000	0.11856440	2.21497262	3.96804880	-0.00029270
28.75000000	0.11849750	2.21470124	3.96766582	-0.00029881
29.75000000	0.11848070	2.21433058	3.96752043	-0.00030387

Driving Bellows Test Trial 3:

Time (min)	ForceD	ForceC	PosD	PosC
d/dt=	-10.389E-6	31.350E-6	-65.401E-6	-6.193E-6
0.08333333	0.12228252	2.21319660	3.96776952	-0.00006273
1.75000000	0.12212625	2.21349810	3.96809663	-0.00009388
2.75000000	0.12217944	2.21392457	3.96944402	-0.00009881
3.75000000	0.12213541	2.21419022	3.96996764	-0.00010050
4.75000000	0.12205616	2.21321016	3.96757506	-0.00010381
5.75000000	0.12203632	2.21387570	3.96825286	-0.00011829
6.75000000	0.12209225	2.21348817	3.96990722	-0.00013639
7.75000000	0.12204697	2.21320410	3.96888289	-0.00014688
8.75000000	0.12206599	2.21418197	3.97002910	-0.00014825
9.75000000	0.12199669	2.21331221	3.96851483	-0.00015187
10.75000000	0.12202067	2.21405527	3.96797948	-0.00015350
11.75000000	0.12196310	2.21365244	3.96783270	-0.00016055
12.75000000	0.12194458	2.21310319	3.96960604	-0.00016523
13.75000000	0.12192615	2.21403528	3.96683075	-0.00018820
14.75000000	0.12194164	2.21387262	3.96646820	-0.00018914
15.75000000	0.12202240	2.21379507	3.97007824	-0.00019844
16.75000000	0.12196214	2.21434633	3.96758857	-0.00019919
17.75000000	0.12194061	2.21376369	3.96629303	-0.00019806
18.75000000	0.12191191	2.21322756	3.96654576	-0.00019994
19.75000000	0.12190264	2.21370376	3.96565920	-0.00020000
20.75000000	0.12193494	2.21418199	3.96900480	-0.00020256
21.75000000	0.12190690	2.21370313	3.96621512	-0.00021960
22.75000000	0.12186362	2.21382952	3.96769213	-0.00024045
23.75000000	0.12187338	2.21421168	3.96703950	-0.00023908
24.75000000	0.12184018	2.21565700	3.96616148	-0.00024207
25.75000000	0.12200513	2.21486131	3.97031816	-0.00024707
26.75000000	0.12186865	2.21412692	3.96717008	-0.00024919
27.75000000	0.12185449	2.21458673	3.96492439	-0.00025037
28.75000000	0.12189736	2.21375174	3.96796037	-0.00025000
29.75000000	0.12190314	2.21415252	3.96838097	-0.00025599

Short Tubing 4mm Displacement Test Trial 1:

Time (min)	ForceD	ForceC	PosD	PosC
d/dt=	-17.500E-3	104.869E-6	-664.066E-6	-51.812E-3
0.08333333	1.39321524	2.33515667	3.94218478	9.14985518
1.75000000	1.30628305	2.31172380	3.96674681	9.09974288
2.75000000	1.27158155	2.29644624	3.96674718	9.06305424
3.75000000	1.24379502	2.31121928	3.97371877	9.02391124
4.75000000	1.21536989	2.31211556	3.97441676	8.97866623
5.75000000	1.18967845	2.30970796	3.97607405	8.93335874
6.75000000	1.17006796	2.30572273	3.98643393	8.89392047
7.75000000	1.14775771	2.33624739	3.98782237	8.84020106
8.75000000	1.12916946	2.30575410	3.99564663	8.80083839
9.75000000	1.11051602	2.29802959	3.99998149	8.75566086
10.75000000	1.09132453	2.33278037	3.99993850	8.69849607
11.75000000	1.05478614	2.31472754	3.95967879	8.60251910
12.75000000	1.03734459	2.32101103	3.95929013	8.54712054
13.75000000	1.02102855	2.32435607	3.95935086	8.49244744
14.75000000	1.00495827	2.31180998	3.95942184	8.44081929
15.75000000	0.98987101	2.31437422	3.95934699	8.38614888
16.75000000	0.97507690	2.29682499	3.95938796	8.33672422
17.75000000	0.96108307	2.30688520	3.95934289	8.28163208
18.75000000	0.94736308	2.31147663	3.95912430	8.22764763
19.75000000	0.93429829	2.32818409	3.95901683	8.17155581
20.75000000	0.92164203	2.33454457	3.95905141	8.11877622
21.75000000	0.90901766	2.31572733	3.95917250	8.07254288
22.75000000	0.89698835	2.31812257	3.95909840	8.02206017
23.75000000	0.88513124	2.31343888	3.95918113	7.97384938
24.75000000	0.87355236	2.30813902	3.95925781	7.92715843
25.75000000	0.86228308	2.30397401	3.95929349	7.88097372
26.75000000	0.85183129	2.32745607	3.95927149	7.82869270
27.75000000	0.84103249	2.31531341	3.95926130	7.78557272
28.75000000	0.83058047	2.31351876	3.95940108	7.74153421
29.75000000	0.82144841	2.32251652	3.95948124	7.69786255

Short Tubing 4mm Displacement Test Trial 2:

Time (min)	ForceD	ForceC	PosD	PosC
d/dt=	-12.419E-3	232.640E-6	-547.545E-6	-39.604E-3
0.08333333	1.31454815	2.32360795	3.96164573	8.95803052
1.75000000	1.24835306	2.31151284	3.96570034	8.87573102
2.75000000	1.22895756	2.33537092	3.96556325	8.83729576
3.75000000	1.21055959	2.32317270	3.96504780	8.80269189
4.75000000	1.19403916	2.29183347	3.96598508	8.77164906
5.75000000	1.17882330	2.29067516	3.96740884	8.73690131
6.75000000	1.17111946	2.31476532	3.98323122	8.71213121
7.75000000	1.15670537	2.32435912	3.98434994	8.67454938
8.75000000	1.14255629	2.30967794	3.98506786	8.64044295
9.75000000	1.12905857	2.30380435	3.98575207	8.60414919
10.75000000	1.11619789	2.31650150	3.98641519	8.56408452
11.75000000	1.10351787	2.31026647	3.98739498	8.52727085
12.75000000	1.07989555	2.31781805	3.96242574	8.45534969
13.75000000	1.06817672	2.32532478	3.96214208	8.41315749
14.75000000	1.05636351	2.31902430	3.96164004	8.37356648
15.75000000	1.04490005	2.30930810	3.96144531	8.33522703
16.75000000	1.03351477	2.30070449	3.96091475	8.29693527
17.75000000	1.02272507	2.30495965	3.96073619	8.25635861
18.75000000	1.01243060	2.31305218	3.96092467	8.21547921
19.75000000	1.00239015	2.32783716	3.96074749	8.17252278
20.75000000	0.99245048	2.33629700	3.96078237	8.13132253
21.75000000	0.98238464	2.33164440	3.96056575	8.09342079
22.75000000	0.97270418	2.32763864	3.96053254	8.05561548
23.75000000	0.96311079	2.32409590	3.96040219	8.01787547
24.75000000	0.95363161	2.31396233	3.96015286	7.98175743
25.75000000	0.94460856	2.31355742	3.96024605	7.94506386
26.75000000	0.93557556	2.30734530	3.96015562	7.90882815
27.75000000	0.92671758	2.30651537	3.95987159	7.87165574
28.75000000	0.91848619	2.32711690	3.95984207	7.83135705
29.75000000	0.90990055	2.32380828	3.95989143	7.79592029

Short Tubing 4mm Displacement Test Trial 3:

Time (min)	ForceD	ForceC	PosD	PosC
d/dt=	-10.155E-3	126.760E-6	-612.632E-6	-32.443E-3
0.08333333	1.31089916	2.32998637	3.95993022	8.89018458
1.75000000	1.25787885	2.31891383	3.96852936	8.81142228
2.75000000	1.24292932	2.31515870	3.96880936	8.78189301
3.75000000	1.22907337	2.30772881	3.96899193	8.75324657
4.75000000	1.21630751	2.30937404	3.96928705	8.72342260
5.75000000	1.20412103	2.32792581	3.96975933	8.69038845
6.75000000	1.19282446	2.32868835	3.97103030	8.66143939
7.75000000	1.18149701	2.32185155	3.97182822	8.63274963
8.75000000	1.17005776	2.30813431	3.97185643	8.60426904
9.75000000	1.15945995	2.30673152	3.97244680	8.57414838
10.75000000	1.14920412	2.29685363	3.97328940	8.54600000
11.75000000	1.13948799	2.29762079	3.97457505	8.51624988
12.75000000	1.13462859	2.30259630	3.98611309	8.49820949
13.75000000	1.12494804	2.29826915	3.98683941	8.46854045
14.75000000	1.11584682	2.31493489	3.98779321	8.43467815
15.75000000	1.10819327	2.31098434	3.99160636	8.40853571
16.75000000	1.08452867	2.30870679	3.95916114	8.33268652
17.75000000	1.07571946	2.30933655	3.95868517	8.30047959
18.75000000	1.06680880	2.30911452	3.95772026	8.26781323
19.75000000	1.05811378	2.32045139	3.95733708	8.23302640
20.75000000	1.04983800	2.33482587	3.95665739	8.19746049
21.75000000	1.04152490	2.32686039	3.95658999	8.16715318
22.75000000	1.03341104	2.32382245	3.95642445	8.13690206
23.75000000	1.02540686	2.32064813	3.95638994	8.10617615
24.75000000	1.01803117	2.32536909	3.95664440	8.07458801
25.75000000	1.01047626	2.31971774	3.95709104	8.04633240
26.75000000	1.00303744	2.31756653	3.95733382	8.01676941
27.75000000	0.99565332	2.31912019	3.95719488	7.98560955
28.75000000	0.98825690	2.31576136	3.95703924	7.95616117
29.75000000	0.98095490	2.30882890	3.95707927	7.92776448

Long Tubing 3mm Displacement Test Trial 1:

Time (min)	ForceD	ForceC	PosD	PosC
d/dt=	-6.295E-3	-243.514E-6	739.225E-6	-27.888E-3
0.08333333	0.88001204	3.30973947	2.96118692	7.41098920
1.75000000	0.83818438	3.31130646	2.96145024	7.27356561
2.75000000	0.82706567	3.29440529	2.96150378	7.23571030
3.75000000	0.81739461	3.30043037	2.96157207	7.19543851
4.75000000	0.80871118	3.32860387	2.96159858	7.15181554
5.75000000	0.80016275	3.32166333	2.96153016	7.11839906
6.75000000	0.79229123	3.31737993	2.96151007	7.08578745
7.75000000	0.78464346	3.30951313	2.96150333	7.05541336
8.75000000	0.77727981	3.30515699	2.96156206	7.02517179
9.75000000	0.77032413	3.30575416	2.96176907	6.99439663
10.75000000	0.76360140	3.31552665	2.96170365	6.96182029
11.75000000	0.75678297	3.31281929	2.96170072	6.93322778
12.75000000	0.75031296	3.30380488	2.96171651	6.90615924
13.75000000	0.74379086	3.29555660	2.96192186	6.87977466
14.75000000	0.73731220	3.29016967	2.96145341	6.85265337
15.75000000	0.73145130	3.29512770	2.96217043	6.82328589
16.75000000	0.72554155	3.30790553	2.96167118	6.79260986
17.75000000	0.72503131	3.31093362	2.97647923	6.78460568
18.75000000	0.71926963	3.31363241	2.97633576	6.75778452
19.75000000	0.71384080	3.30807820	2.97684454	6.73412828
20.75000000	0.70827486	3.30596732	2.97654972	6.70850375
21.75000000	0.70291005	3.30615421	2.97670067	6.68411635
22.75000000	0.69765196	3.30931064	2.97669514	6.65819757
23.75000000	0.69241698	3.30811133	2.97660856	6.63442235
24.75000000	0.68720558	3.30008044	2.97664717	6.61203002
25.75000000	0.68193164	3.29535457	2.97640360	6.58952141
26.75000000	0.67713674	3.30038422	2.97663644	6.56445749
27.75000000	0.67240205	3.31296619	2.97671257	6.53835499
28.75000000	0.66741701	3.30560708	2.97648320	6.51697953
29.75000000	0.66277852	3.30380388	2.97689875	6.49574014

Long Tubing 3mm Displacement Test Trial 2:

Time (min)	ForceD	ForceC	PosD	PosC
d/dt=	-5.391E-3	-15.680E-6	19.979E-6	-23.793E-3
0.08333333	0.88992576	3.29322060	2.96120735	7.33809938
1.75000000	0.85859031	3.31136390	2.96137260	7.22790000
2.75000000	0.85095065	3.32926972	2.96138527	7.19362054
3.75000000	0.84398411	3.32834703	2.96142855	7.16587366
4.75000000	0.83733479	3.31576734	2.96146104	7.14253396
5.75000000	0.83098368	3.30777155	2.96141642	7.11809744
6.75000000	0.82473819	3.30326061	2.96141317	7.09329875
7.75000000	0.81880014	3.29816511	2.96148164	7.07005574
8.75000000	0.81294249	3.29806350	2.96141822	7.04500618
9.75000000	0.80741020	3.30307795	2.96142618	7.01885350
10.75000000	0.80199038	3.31870605	2.96152542	6.98989782
11.75000000	0.79649934	3.32745623	2.96146927	6.96363789
12.75000000	0.79113911	3.32611198	2.96152129	6.94017728
13.75000000	0.78558089	3.31779710	2.96130312	6.91861017
14.75000000	0.78019815	3.30049387	2.96143728	6.89904126
15.75000000	0.77498667	3.28710949	2.96137639	6.87964263
16.75000000	0.76982341	3.28733737	2.96126316	6.85610175
17.75000000	0.76481773	3.28537721	2.96127259	6.83430119
18.75000000	0.75999308	3.28819400	2.96114409	6.81118109
19.75000000	0.75536786	3.29501279	2.96138589	6.78700231
20.75000000	0.75051945	3.29577945	2.96131360	6.76465524
21.75000000	0.74596083	3.30065870	2.96161353	6.74238439
22.75000000	0.74122214	3.30754565	2.96109246	6.71818340
23.75000000	0.73692840	3.31383704	2.96169321	6.69583883
24.75000000	0.73239239	3.31786137	2.96133221	6.67362441
25.75000000	0.72827382	3.31954125	2.96211470	6.65301223
26.75000000	0.72360858	3.31444095	2.96171668	6.63318652
27.75000000	0.71938160	3.31495259	2.96218442	6.61272965
28.75000000	0.71484370	3.31526185	2.96162358	6.59118090
29.75000000	0.71110812	3.31850669	2.96291133	6.57190144

Long Tubing 3mm Displacement Test Trial 3:

Time (min)	ForceD	ForceC	PosD	PosC
d/dt=	-4.554E-3	-228.495E-6	10.646E-6	-20.419E-3
0.08333333	0.86585435	3.31902311	2.95935368	7.18180830
1.75000000	0.83678412	3.31079736	2.95945764	7.08132135
2.75000000	0.82986468	3.31437231	2.95935016	7.05298958
3.75000000	0.82379849	3.31423188	2.95930730	7.02839694
4.75000000	0.81823529	3.30623347	2.95939543	7.00707828
5.75000000	0.81291077	3.30571875	2.95938757	6.98491330
6.75000000	0.80782837	3.30713774	2.95936494	6.96289076
7.75000000	0.80293251	3.30767296	2.95941219	6.94108040
8.75000000	0.79805002	3.30658442	2.95932642	6.91937110
9.75000000	0.79331575	3.30305150	2.95916080	6.89965518
10.75000000	0.78859889	3.29573434	2.95929412	6.88107397
11.75000000	0.78399689	3.28981091	2.95920870	6.86206292
12.75000000	0.77945003	3.28910232	2.95924371	6.84193084
13.75000000	0.77505085	3.29066150	2.95924015	6.82168340
14.75000000	0.77079682	3.29810145	2.95912059	6.79936667
15.75000000	0.76664511	3.31041362	2.95923964	6.77655637
16.75000000	0.76267161	3.32500605	2.95934342	6.75310069
17.75000000	0.75839432	3.32264086	2.95936440	6.73425050
18.75000000	0.75423570	3.31190879	2.95949655	6.71740649
19.75000000	0.74998239	3.30577569	2.95943199	6.70029001
20.75000000	0.74586910	3.30379741	2.95954978	6.68202029
21.75000000	0.74187097	3.30623483	2.95947034	6.66209663
22.75000000	0.73790943	3.31623192	2.95945130	6.64059657
23.75000000	0.73410303	3.31586914	2.95957769	6.62237253
24.75000000	0.73012386	3.31225838	2.95964681	6.60511623
25.75000000	0.72629741	3.31137029	2.95959375	6.58703708
26.75000000	0.72318571	3.31057973	2.95966777	6.57172615
27.75000000	0.71920681	3.30177621	2.95971062	6.55501211
28.75000000	0.71525834	3.29032023	2.95948519	6.54021211
29.75000000	0.71144374	3.28082266	2.95957518	6.52538583

Long Tubing 4mm Displacement Test Trial 1:

Time (min)	ForceD	ForceC	PosD	PosC
d/dt=	-7.135E-3	-41.508E-6	-1.332E-3	-26.315E-3
0.08333333	1.21040533	3.30339558	3.96940423	8.36024825
1.75000000	1.16603460	3.29517818	3.97881165	8.25692016
2.75000000	1.15568840	3.29463403	3.97959421	8.22608552
3.75000000	1.14955217	3.29725441	3.98742970	8.20592441
4.75000000	1.14122949	3.29975397	3.98787155	8.17820974
5.75000000	1.13373083	3.30566065	3.98868172	8.15170312
6.75000000	1.12652524	3.31241169	3.98943434	8.12592890
7.75000000	1.11965335	3.30831688	3.99061883	8.10239488
8.75000000	1.11535413	3.31374177	3.99729606	8.08428546
9.75000000	1.10847290	3.29821556	3.99803854	8.06371923
10.75000000	1.10180532	3.29105711	3.99857293	8.04091280
11.75000000	1.09552788	3.28167548	3.99961801	8.01989070
12.75000000	1.08898655	3.27652660	3.99995547	7.99738845
13.75000000	1.08250272	3.28211337	3.99999712	7.97173283
14.75000000	1.07636288	3.29229745	3.99998039	7.94540549
15.75000000	1.05483074	3.30357212	3.95924231	7.86834114
16.75000000	1.04913210	3.30712555	3.95955513	7.84467878
17.75000000	1.04336272	3.31593902	3.95922139	7.81841161
18.75000000	1.03748024	3.31362831	3.95943889	7.79513983
19.75000000	1.03143252	3.30685252	3.95948769	7.77348021
20.75000000	1.02549197	3.29651236	3.95946704	7.75253702
21.75000000	1.01987354	3.30049376	3.95928770	7.72833702
22.75000000	1.01440577	3.31079336	3.95944649	7.70317310
23.75000000	1.00887085	3.31410593	3.95934189	7.67955449
24.75000000	1.00331268	3.30829723	3.95911943	7.65817990
25.75000000	0.99788161	3.30173287	3.95912309	7.63767566
26.75000000	0.99260567	3.30113655	3.95908853	7.61628402
27.75000000	0.98740154	3.29251416	3.95941645	7.59700893
28.75000000	0.98203068	3.28366474	3.95901499	7.57619482
29.75000000	0.97690062	3.28530271	3.95919877	7.55441754

Long Tubing 4mm Displacement Test Trial 2:

Time (min)	ForceD	ForceC	PosD	PosC
d/dt=	-5.531E-3	-17.006E-6	-194.297E-6	-20.332E-3
0.08333333	1.22188878	3.29419520	3.96847032	8.32118745
1.75000000	1.18521095	3.28473717	3.97695476	8.22721873
2.75000000	1.17699220	3.28672600	3.97698668	8.20131099
3.75000000	1.17035204	3.29853168	3.97727817	8.17747953
4.75000000	1.16420581	3.31513303	3.97747559	8.15357353
5.75000000	1.15829701	3.30924274	3.97786844	8.13497865
6.75000000	1.15259393	3.30291039	3.97817613	8.11711017
7.75000000	1.14699900	3.29663467	3.97853040	8.09949775
8.75000000	1.14165920	3.29374887	3.97906442	8.08100487
9.75000000	1.13633459	3.29218133	3.97954135	8.06248564
10.75000000	1.13120069	3.29175738	3.98024918	8.04381124
11.75000000	1.12628066	3.28976545	3.98144364	8.02636866
12.75000000	1.12328494	3.28228702	3.98779172	8.01556317
13.75000000	1.11811740	3.27314964	3.98825336	7.99875431
14.75000000	1.11311360	3.27662461	3.98871944	7.97927278
15.75000000	1.10846522	3.29305828	3.98942283	7.95715418
16.75000000	1.10362219	3.29708052	3.99014571	7.93798783
17.75000000	1.09905215	3.30227822	3.99093694	7.91863883
18.75000000	1.09659942	3.30440235	3.99757267	7.90722672
19.75000000	1.09151890	3.29173775	3.99799868	7.89103851
20.75000000	1.08648581	3.28280006	3.99859206	7.87357990
21.75000000	1.08164943	3.27704328	3.99909746	7.85624089
22.75000000	1.07692665	3.27442122	3.99988006	7.83830206
23.75000000	1.07251331	3.29432633	3.99997769	7.81505743
24.75000000	1.05268628	3.30500090	3.95938842	7.74155025
25.75000000	1.04813020	3.30167289	3.95940344	7.72403514
26.75000000	1.04332953	3.29626488	3.95915943	7.70612047
27.75000000	1.03877970	3.29275583	3.95908991	7.68809519
28.75000000	1.03423161	3.30019873	3.95875464	7.66781330
29.75000000	1.03019586	3.30385232	3.95927963	7.64895162

Long Tubing 4mm Displacement Test Trial 3:

Time (min)	ForceD	ForceC	PosD	PosC
d/dt=	-2.771E-3	-41.464E-6	-132.146E-6	-12.775E-3
0.08333333	1.22721841	3.28522653	3.96187356	8.31168414
1.75000000	1.19272551	3.31589554	3.96103989	8.20889625
2.75000000	1.18507291	3.31341007	3.96128974	8.18530256
3.75000000	1.17856306	3.30767017	3.96162471	8.16518021
4.75000000	1.17258890	3.29814199	3.96197426	8.14749625
5.75000000	1.16701633	3.28456273	3.96249743	8.13141248
6.75000000	1.16165248	3.27512820	3.96325148	8.11547903
7.75000000	1.15652106	3.26664352	3.96417494	8.09941948
8.75000000	1.15770267	3.27571912	3.98040759	8.09844975
9.75000000	1.15208771	3.26679246	3.98025144	8.08120868
10.75000000	1.14707677	3.26846484	3.98049789	8.06202409
11.75000000	1.14230673	3.28802215	3.98086464	8.04008002
12.75000000	1.13769289	3.30355699	3.98106663	8.01836273
13.75000000	1.13289927	3.30243943	3.98149749	8.00019032
14.75000000	1.12813740	3.29733782	3.98194048	7.98362622
15.75000000	1.12342478	3.28504209	3.98230705	7.96836885
16.75000000	1.11869984	3.27847042	3.98275729	7.95272154
17.75000000	1.11426678	3.27616867	3.98338042	7.93613427
18.75000000	1.10976512	3.27454743	3.98394043	7.91885811
19.75000000	1.10538101	3.28438083	3.98439106	7.89952335
20.75000000	1.10122980	3.28731702	3.98502008	7.88182753
21.75000000	1.09689852	3.28563849	3.98552912	7.86531348
22.75000000	1.09258771	3.27751376	3.98635782	7.85057622
23.75000000	1.09082702	3.27147255	3.99340822	7.84289551
24.75000000	1.08672150	3.26530496	3.99433261	7.82797022
25.75000000	1.07059723	3.30430856	3.96138645	7.76008571
26.75000000	1.06623344	3.29796244	3.96098540	7.74311423
27.75000000	1.06200730	3.29479386	3.96093411	7.72619107
28.75000000	1.05786137	3.29427927	3.96076868	7.70927066
29.75000000	1.05343689	3.29215536	3.96011919	7.69225543

Copper Tubing 3mm Displacement Test Trial 1:

Time (min)	ForceD	ForceC	PosD	PosC
d/dt=	-6.713E-3	-319.434E-6	27.469E-6	-29.857E-3
0.08333333	0.71513638	3.21804511	2.97861708	6.53884026
1.75000000	0.69289879	3.21050768	2.97847416	6.49140474
2.75000000	0.68271404	3.22793761	2.97863834	6.44829576
3.75000000	0.67318704	3.22627386	2.97859688	6.40999376
4.75000000	0.66432172	3.23202075	2.97856866	6.37124863
5.75000000	0.65570063	3.22784210	2.97852189	6.33627104
6.75000000	0.64736337	3.22644474	2.97859322	6.30051142
7.75000000	0.63925014	3.22117055	2.97851047	6.26713527
8.75000000	0.63169935	3.22615257	2.97869672	6.23196854
9.75000000	0.62420234	3.22727289	2.97868916	6.19841567
10.75000000	0.61699546	3.22176749	2.97872977	6.16776024
11.75000000	0.60979753	3.20876256	2.97886033	6.13970986
12.75000000	0.60274446	3.19995949	2.97879182	6.11062584
13.75000000	0.59614111	3.21276862	2.97887270	6.07663539
14.75000000	0.58974353	3.22862832	2.97881213	6.04241486
15.75000000	0.58325053	3.22168611	2.97884681	6.01505287
16.75000000	0.57690515	3.21982210	2.97885439	5.98660387
17.75000000	0.57085545	3.22306507	2.97887769	5.95716810
18.75000000	0.56476294	3.21084144	2.97887450	5.93240618
19.75000000	0.55884263	3.21032636	2.97892190	5.90594007
20.75000000	0.55316101	3.21335435	2.97907357	5.87807247
21.75000000	0.54760958	3.22005941	2.97909406	5.84988995
22.75000000	0.54212832	3.22768576	2.97916217	5.82156629
23.75000000	0.53651398	3.22261432	2.97916319	5.79684576
24.75000000	0.53106099	3.21862699	2.97918190	5.77262328
25.75000000	0.52568351	3.21825519	2.97914371	5.74692871
26.75000000	0.52051430	3.21818048	2.97923637	5.72207728
27.75000000	0.51531505	3.21153812	2.97926134	5.69930799
28.75000000	0.51011208	3.20841097	2.97925629	5.67614600
29.75000000	0.50527807	3.21202575	2.97920696	5.65089788

Copper Tubing 3mm Displacement Test Trial 2:

Time (min)	ForceD	ForceC	PosD	PosC
d/dt=	-5.023E-3	-167.076E-6	17.253E-6	-22.773E-3
0.08333333	0.67757778	3.24514956	2.97950912	7.01230630
1.75000000	0.66582659	3.23669317	2.97935916	6.98698689
2.75000000	0.65943596	3.22780496	2.97923417	6.96527684
3.75000000	0.65332978	3.22090421	2.97932087	6.94275262
4.75000000	0.64735348	3.21932919	2.97927269	6.91818240
5.75000000	0.64175109	3.22540800	2.97932852	6.89238277
6.75000000	0.63622860	3.23423470	2.97934899	6.86574494
7.75000000	0.63069277	3.23004487	2.97942019	6.84265062
8.75000000	0.62518866	3.22393600	2.97940396	6.82010100
9.75000000	0.61979207	3.22421406	2.97939391	6.79556586
10.75000000	0.61450336	3.22765318	2.97934794	6.77138215
11.75000000	0.60929838	3.22234105	2.97942953	6.74938252
12.75000000	0.60425287	3.22347568	2.97949730	6.72542316
13.75000000	0.59899291	3.22075806	2.97935022	6.70246673
14.75000000	0.59402912	3.22367790	2.97947868	6.67871105
15.75000000	0.58916739	3.23421205	2.97958822	6.65307772
16.75000000	0.58428401	3.23983002	2.97946087	6.62826211
17.75000000	0.57944949	3.23837605	2.97948911	6.60576273
18.75000000	0.57465714	3.23522322	2.97954670	6.58491492
19.75000000	0.56984627	3.22925263	2.97957920	6.56386174
20.75000000	0.56522630	3.22522004	2.97964284	6.54285393
21.75000000	0.56052884	3.22324183	2.97958620	6.52154426
22.75000000	0.55594454	3.21854734	2.97963886	6.50119201
23.75000000	0.55139840	3.21239672	2.97969843	6.48137953
24.75000000	0.54693898	3.21112320	2.97971105	6.46041586
25.75000000	0.54274834	3.22683880	2.97974339	6.43511717
26.75000000	0.53851778	3.23606275	2.97972474	6.41171923
27.75000000	0.53418168	3.23564927	2.97979419	6.39087322
28.75000000	0.52990394	3.23028554	2.97976838	6.37168159
29.75000000	0.52564497	3.22110880	2.97982294	6.35396248

Copper Tubing 3mm Displacement Test Trial 3:

Time (min)	ForceD	ForceC	PosD	PosC
d/dt=	-4.004E-3	325.240E-6	418.844E-6	-18.867E-3
0.08333333	0.61996366	3.22316062	2.91672311	6.72684295
1.75000000	0.62759708	3.24137230	2.97893731	6.76649151
2.75000000	0.62250811	3.22869843	2.97888663	6.75043995
3.75000000	0.61749574	3.21781250	2.97888498	6.73288614
4.75000000	0.61278528	3.21683319	2.97889504	6.71239594
5.75000000	0.60819053	3.22941693	2.97890327	6.68793340
6.75000000	0.60372310	3.25010965	2.97889960	6.66218583
7.75000000	0.59920225	3.24997782	2.97882580	6.64097278
8.75000000	0.59467814	3.24701476	2.97883485	6.62129276
9.75000000	0.59023530	3.23913489	2.97890343	6.60335537
10.75000000	0.58591515	3.23424416	2.97881453	6.58451223
11.75000000	0.58147568	3.22681765	2.97882732	6.56588589
12.75000000	0.57714300	3.22623169	2.97877072	6.54612959
13.75000000	0.57286226	3.22393152	2.97881824	6.52694906
14.75000000	0.56871963	3.22448074	2.97875959	6.50717328
15.75000000	0.56465379	3.22737210	2.97879548	6.48717672
16.75000000	0.56061582	3.23188188	2.97871155	6.46621099
17.75000000	0.55675060	3.22996654	2.97878383	6.44762584
18.75000000	0.55267931	3.22607097	2.97877632	6.43013015
19.75000000	0.54879346	3.21964696	2.97878752	6.41303502
20.75000000	0.54535048	3.22271079	2.97881101	6.39517778
21.75000000	0.54166319	3.23303227	2.97890715	6.37367740
22.75000000	0.53783232	3.24028102	2.97886938	6.35348839
23.75000000	0.53413181	3.24129302	2.97887157	6.33492547
24.75000000	0.53044064	3.23632477	2.97888588	6.31844164
25.75000000	0.52683303	3.23133398	2.97898670	6.30275930
26.75000000	0.52324089	3.23333658	2.97903462	6.28455094
27.75000000	0.51976356	3.24018405	2.97897992	6.26478221
28.75000000	0.51637528	3.25093669	2.97901076	6.24455393
29.75000000	0.51300836	3.25323465	2.97915481	6.22663233

Copper Tubing 4mm Displacement Test Trial 1:

Time (min)	ForceD	ForceC	PosD	PosC
d/dt=	-5.151E-3	-158.581E-6	-29.718E-6	-21.137E-3
0.08333333	0.92359938	3.24286178	3.96085170	7.69229800
1.75000000	0.90953216	3.23743052	3.96062304	7.67843190
2.75000000	0.90304066	3.22862791	3.96072958	7.66070156
3.75000000	0.89687005	3.22981542	3.96073698	7.63865936
4.75000000	0.89111600	3.24441103	3.96086921	7.61280612
5.75000000	0.88510623	3.25350556	3.96078812	7.58825793
6.75000000	0.87925882	3.25226586	3.96074964	7.56608358
7.75000000	0.87341980	3.24512126	3.96080625	7.54543521
8.75000000	0.86790286	3.24348092	3.96081312	7.52368315
9.75000000	0.86238458	3.25507894	3.96078844	7.49872197
10.75000000	0.85711528	3.26406628	3.96062997	7.47384750
11.75000000	0.85184815	3.25529823	3.96074560	7.45467659
12.75000000	0.84635888	3.23963791	3.96048816	7.43656873
13.75000000	0.84110887	3.22770787	3.96059162	7.41851155
14.75000000	0.83593701	3.22283339	3.96062757	7.39781124
15.75000000	0.83084681	3.22201949	3.96026560	7.37691767
16.75000000	0.82579304	3.22427587	3.96028417	7.35409120
17.75000000	0.82096950	3.22542863	3.96044240	7.33335811
18.75000000	0.81600466	3.22338131	3.96053481	7.31223814
19.75000000	0.81112795	3.22874029	3.96051077	7.28940605
20.75000000	0.80652077	3.23843842	3.96051807	7.26684700
21.75000000	0.80208868	3.23815464	3.96128784	7.24636860
22.75000000	0.79707143	3.23517018	3.95994040	7.22574082
23.75000000	0.79262022	3.23885551	3.95998746	7.20529463
24.75000000	0.78830727	3.23736947	3.96047558	7.18578177
25.75000000	0.78369757	3.23642233	3.96007129	7.16570574
26.75000000	0.77921663	3.23844355	3.95987744	7.14535075
27.75000000	0.77492485	3.24255421	3.95999210	7.12399338
28.75000000	0.77068188	3.24803446	3.95976465	7.10363052
29.75000000	0.76646046	3.24908946	3.96004502	7.08377840

Copper Tubing 4mm Displacement Test Trial 2:

Time (min)	ForceD	ForceC	PosD	PosC
d/dt=	-4.224E-3	255.461E-6	-20.361E-6	-18.314E-3
0.08333333	0.87374749	3.23025087	3.96075775	7.44557010
1.75000000	0.86314293	3.23741317	3.96122581	7.42723283
2.75000000	0.85806523	3.24136303	3.96158443	7.40822778
3.75000000	0.85294362	3.23551844	3.96144037	7.39091529
4.75000000	0.84793124	3.23090093	3.96130775	7.37320587
5.75000000	0.84319381	3.23227725	3.96097481	7.35273390
6.75000000	0.83854019	3.23236426	3.96105690	7.33285986
7.75000000	0.83398097	3.23857282	3.96104056	7.31285474
8.75000000	0.82950789	3.24059145	3.96118008	7.29275468
9.75000000	0.82488021	3.23995737	3.96065368	7.27315312
10.75000000	0.82038343	3.24030438	3.96069282	7.25474170
11.75000000	0.81615161	3.23789509	3.96104182	7.23669401
12.75000000	0.81182956	3.23680485	3.96128891	7.21811604
13.75000000	0.80751412	3.23693199	3.96086493	7.19844538
14.75000000	0.80358509	3.24524530	3.96132513	7.17918633
15.75000000	0.79926347	3.24705698	3.96086930	7.15943371
16.75000000	0.79526385	3.24694866	3.96131349	7.14183464
17.75000000	0.79112747	3.24380614	3.96098380	7.12355350
18.75000000	0.78716650	3.23961334	3.96109076	7.10743346
19.75000000	0.78308100	3.23699064	3.96057612	7.08986841
20.75000000	0.77915791	3.24397035	3.96095274	7.07029507
21.75000000	0.77524795	3.24808477	3.96060558	7.05138883
22.75000000	0.77144877	3.24234808	3.96087046	7.03517965
23.75000000	0.76755760	3.24102285	3.96065771	7.01790368
24.75000000	0.76362574	3.23313693	3.96071247	7.00232341
25.75000000	0.76002978	3.23088934	3.96118380	6.98657428
26.75000000	0.75619890	3.22933739	3.96062328	6.96992903
27.75000000	0.75263541	3.23820499	3.96083602	6.95139526
28.75000000	0.74896152	3.24848235	3.96049897	6.93089750
29.75000000	0.74539862	3.25294130	3.96030916	6.91228539

Copper Tubing 4mm Displacement Test Trial 3:

Time (min)	ForceD	ForceC	PosD	PosC
d/dt=	-1.931E-3	52.889E-6	-187.764E-6	-10.056E-3
0.08333333	0.85322695	3.24935003	3.96202218	7.26225662
1.75000000	0.84373122	3.23390112	3.96211672	7.25344913
2.75000000	0.83921917	3.22404694	3.96236865	7.24045212
3.75000000	0.83497365	3.21579913	3.96255697	7.22603102
4.75000000	0.83082507	3.21381714	3.96286437	7.20974963
5.75000000	0.82666298	3.22194108	3.96256249	7.18975699
6.75000000	0.82269999	3.23723935	3.96253201	7.16905350
7.75000000	0.81882544	3.24805127	3.96255833	7.14870474
8.75000000	0.81479938	3.24887871	3.96240067	7.13091991
9.75000000	0.81081829	3.24561124	3.96260851	7.11488321
10.75000000	0.80686701	3.24194208	3.96239446	7.09887004
11.75000000	0.80310504	3.24631820	3.96237699	7.08136486
12.75000000	0.79940583	3.24948618	3.96269524	7.06414469
13.75000000	0.79573168	3.25033455	3.96255454	7.04662634
14.75000000	0.79204506	3.25912175	3.96259612	7.02791067
15.75000000	0.78841145	3.26525032	3.96244893	7.00983471
16.75000000	0.78468573	3.26016299	3.96234898	6.99433845
17.75000000	0.78110167	3.25445581	3.96257109	6.98019170
18.75000000	0.77731845	3.24421372	3.96224528	6.96634245
19.75000000	0.77361398	3.23281692	3.96207375	6.95329831
20.75000000	0.77010989	3.22433022	3.96219428	6.93945137
21.75000000	0.76671700	3.22886675	3.96235514	6.92303427
22.75000000	0.76346503	3.24016701	3.96247487	6.90429788
23.75000000	0.75984029	3.23915787	3.96184274	6.88761785
24.75000000	0.75663439	3.23775111	3.96211354	6.87306960
25.75000000	0.75296158	3.23436756	3.96183163	6.85807004
26.75000000	0.74932227	3.23175471	3.96058282	6.84198015
27.75000000	0.74696170	3.23057103	3.96398674	6.83046248
28.75000000	0.74380039	3.23166326	3.96433030	6.81513839
29.75000000	0.74098210	3.24416787	3.96548429	6.79727522

Calibrate-Test-Calibrate Bench Tests

Presented here are values from calibrate-test-calibrate bench testing, which was discussed in Chapter 5. Values for driving end elasticity (E. Driving in mV/mm) and calibration instrument elasticity (E. Cal in N/mm) for each of the three repetitions of the calibration procedure.

Calibrate-Test-Calibrate 2 Band Test 1:

I. Calibration		Band Test		F. Calibration	
E. Driving	E. Cal	E. Driving	E. Cal	E. Driving	E. Cal
4.21840481E+3	-2.55577492E-3	4.16422670E+3	4.93293853E-2	4.16394123E+3	-3.68169559E-3
4.19421861E+3	2.09856518E-2	4.15769824E+3	4.87984156E-2	4.14651717E+3	1.84945574E-2
4.17967347E+3	4.91757165E-2	4.15309381E+3	5.09278939E-2	4.14030686E+3	4.19501906E-2
4.17553248E+3	6.98137910E-2	4.14994436E+3	4.44624911E-2	4.13342258E+3	6.98114567E-2
4.17060420E+3	9.15109075E-2	4.14762206E+3	4.61740599E-2	4.13906264E+3	9.18619189E-2
4.16613489E+3	1.19554112E-1	4.14685305E+3	4.63430636E-2	4.14008331E+3	1.16943515E-1
4.16412521E+3	1.35648536E-1	4.14682857E+3	4.33539703E-2	4.13492078E+3	1.44576343E-1
4.16610483E+3	1.59619101E-1	4.14482236E+3	5.13539684E-2	4.13673694E+3	1.60565137E-1

Calibrate-Test-Calibrate 2 Band Test 2:

I. Calibration		Band Test		F. Calibration	
E. Driving	E. Cal	E. Driving	E. Cal	E. Driving	E. Cal
4.06643040E+3	3.86961612E-4	4.05526833E+3	4.31919146E-2	4.11563317E+3	6.42628795E-4
4.06239253E+3	2.67271972E-2	4.05565268E+3	4.96371999E-2	4.10828267E+3	1.73939649E-2
4.05556375E+3	4.34892676E-2	4.05239327E+3	5.24477095E-2	4.10688856E+3	3.44192400E-2
4.05715461E+3	6.53489177E-2	4.04979607E+3	4.60366928E-2	4.09989741E+3	5.92991946E-2
4.06166309E+3	8.54248943E-2	4.04988669E+3	6.30883373E-2	4.10032418E+3	8.65562479E-2
4.06314613E+3	1.18026652E-1	4.04660306E+3	5.06689040E-2	4.09928396E+3	1.12297173E-1
4.06623110E+3	1.40746922E-1	4.04501474E+3	5.73919627E-2	4.10049046E+3	1.37609675E-1
4.06609870E+3	1.60718942E-1	4.04348734E+3	5.09423915E-2	4.10375211E+3	1.57461109E-1

Calibrate-Test-Calibrate 2 Band Test 3:

I. Calibration		Band Test		F. Calibration	
E. Driving	E. Cal	E. Driving	E. Cal	E. Driving	E. Cal
4.53012953E+3	1.90507467E-3	4.42679810E+3	4.19483893E-2	4.39062310E+3	-3.84555238E-3
4.49204306E+3	1.95568513E-2	4.41517333E+3	4.00622709E-2	4.36782072E+3	1.88172057E-2
4.46522794E+3	3.49859360E-2	4.40971979E+3	4.09146910E-2	4.36217146E+3	5.28375065E-2
4.44636107E+3	6.81489660E-2	4.40562088E+3	4.85509343E-2	4.34738287E+3	6.64799961E-2
4.43058679E+3	8.78681668E-2	4.39183176E+3	4.47594884E-2	4.33804798E+3	9.17211840E-2
4.41707909E+3	1.05551008E-1	4.38709292E+3	4.60366313E-2	4.33546423E+3	1.11763724E-1
4.40568325E+3	1.30751473E-1	4.37999185E+3	4.32227333E-2	4.32637626E+3	1.39924072E-1
4.40280107E+3	1.59208861E-1	4.37378334E+3	4.56984107E-2	4.32978928E+3	1.60008539E-1

Calibrate-Test-Calibrate 5 Band Test 1:

I. Calibration		Band Test		F. Calibration	
E. Driving	E. Cal	E. Driving	E. Cal	E. Driving	E. Cal
4.52981196E+3	-7.27480497E-3	4.40946732E+3	9.89730317E-2	4.39831991E+3	-6.09205404E-4
4.49684341E+3	1.83891420E-2	4.40007930E+3	1.01887504E-1	4.37701742E+3	2.27444145E-2
4.47255446E+3	3.40020335E-2	4.39452131E+3	1.01013172E-1	4.36086400E+3	3.90356927E-2
4.45123589E+3	6.37727650E-2	4.39331101E+3	1.04815974E-1	4.35230349E+3	5.97317166E-2
4.43708429E+3	8.19844336E-2	4.38275684E+3	1.04412038E-1	4.34714526E+3	7.67029056E-2
4.42558493E+3	9.52142074E-2	4.38001087E+3	1.16623669E-1	4.34305143E+3	1.00539385E-1
4.41848370E+3	1.31697904E-1	4.37263588E+3	1.13158872E-1	4.33454417E+3	1.18742979E-1
4.41309082E+3	1.59774799E-1	4.36767771E+3	1.06546539E-1	4.33302465E+3	1.47429748E-1

Calibrate-Test-Calibrate 5 Band Test 2:

I. Calibration		Band Test		F. Calibration	
E. Driving	E. Cal	E. Driving	E. Cal	E. Driving	E. Cal
4.44139825E+3	-8.73667185E-3	4.34799835E+3	1.16941792E-1	4.34694882E+3	-4.77267039E-3
4.41261100E+3	2.29210931E-2	4.34137487E+3	1.13752039E-1	4.32504985E+3	1.61105162E-2
4.39458893E+3	4.10759445E-2	4.34439230E+3	1.20238067E-1	4.31593986E+3	3.83761529E-2
4.38102137E+3	6.59006639E-2	4.33837517E+3	1.17408125E-1	4.31354769E+3	6.16802624E-2
4.37318846E+3	8.99851872E-2	4.33222842E+3	1.17687009E-1	4.30203312E+3	7.42938286E-2
4.37035124E+3	1.10697347E-1	4.32766245E+3	1.15137869E-1	4.30395004E+3	1.07244739E-1
4.36279031E+3	1.40029887E-1	4.32362791E+3	1.16160175E-1	4.29861687E+3	1.34550977E-1
4.35624423E+3	1.56502566E-1	4.32205411E+3	1.17546659E-1	4.29905426E+3	1.58337312E-1

Calibrate-Test-Calibrate 5 Band Test 3:

I. Calibration		Band Test		F. Calibration	
E. Driving	E. Cal	E. Driving	E. Cal	E. Driving	E. Cal
4.88217436E+3	-9.85663597E-3	4.62672168E+3	1.08986276E-1	4.67837286E+3	-1.96284184E-3
4.82674550E+3	2.14329808E-2	4.60984796E+3	1.10195707E-1	4.64332816E+3	2.03648944E-2
4.76768046E+3	3.79199173E-2	4.61325234E+3	1.07042523E-1	4.60720847E+3	4.99977548E-2
4.72748527E+3	6.65596130E-2	4.60509587E+3	1.14426581E-1	4.58378438E+3	6.08347662E-2
4.67846348E+3	7.80799666E-2	4.59694812E+3	1.07697008E-1	4.56583352E+3	8.23958201E-2
4.64896930E+3	1.00387638E-1	4.58289580E+3	1.04413664E-1	4.54988600E+3	9.69481086E-2
4.63144857E+3	1.29204616E-1	4.57779389E+3	1.07616153E-1	4.54550482E+3	1.37500587E-1
4.60710857E+3	1.50895572E-1	4.57286722E+3	1.08759835E-1	4.53076217E+3	1.56278325E-1

Repeated Calibration

Presented here are data from the repeated calibration tests discussed in Chapter 5. Values for driving end elasticity (E. Driving in mV/mm) and calibration instrument elasticity (E. Cal in N/mm) for each of the ten repetitions of the calibration procedure.

Repeated Calibration Test 1:

01		02		03	
E. Driving	E. Cal	E. Driving	E. Cal	E. Driving	E. Cal
4.27683537E+3	6.94105781E-3	4.24753075E+3	4.69362513E-3	4.23065676E+3	5.12695114E-3
4.25897958E+3	3.27658606E-2	4.24154501E+3	2.39833511E-2	4.22160460E+3	1.72220197E-2
4.25525474E+3	5.40792532E-2	4.23673069E+3	5.15848585E-2	4.22421799E+3	6.15149406E-2
4.25218905E+3	7.18413451E-2	4.23597525E+3	8.15515450E-2	4.22196077E+3	7.58633103E-2
4.24727696E+3	8.98743308E-2	4.23199672E+3	8.84614009E-2	4.21543546E+3	9.07031424E-2
4.24985293E+3	1.13197000E-1	4.23194577E+3	1.03089036E-1	4.21681396E+3	1.15225192E-1
4.24405090E+3	1.38075149E-1	4.22860651E+3	1.31011315E-1	4.21616606E+3	1.28701557E-1
4.23824151E+3	1.52181742E-1	4.23017846E+3	1.62063823E-1	4.22082185E+3	1.57685937E-1

04		05		06	
E. Driving	E. Cal	E. Driving	E. Cal	E. Driving	E. Cal
4.20873660E+3	-1.34965851E-3	4.19360141E+3	1.12634366E-2	4.17368771E+3	6.16713740E-3
4.20660567E+3	2.55333848E-2	4.19408298E+3	2.54165188E-2	4.17639161E+3	2.31293431E-2
4.20422117E+3	5.00261844E-2	4.18396665E+3	4.04145857E-2	4.17052719E+3	4.22065009E-2
4.20018011E+3	6.00845988E-2	4.18891093E+3	6.78184168E-2	4.17272098E+3	7.22924306E-2
4.20028879E+3	8.63494489E-2	4.18548685E+3	9.06265449E-2	4.17056190E+3	9.13200960E-2
4.20153759E+3	1.13341265E-1	4.18735422E+3	1.22087128E-1	4.17238395E+3	1.16432855E-1
4.19946165E+3	1.34952026E-1	4.19225547E+3	1.49689239E-1	4.17303049E+3	1.40261169E-1
4.20428886E+3	1.63839161E-1	4.19234598E+3	1.62129515E-1	4.17863348E+3	1.60664178E-1

07		08		09	
E. Driving	E. Cal	E. Driving	E. Cal	E. Driving	E. Cal
4.15890142E+3	5.54438598E-3	4.14738740E+3	-5.72696091E-4	4.12566570E+3	1.04841594E-3
4.16165579E+3	2.60668479E-2	4.14414063E+3	2.19489038E-2	4.12755083E+3	2.44024912E-2
4.15472340E+3	3.95466049E-2	4.14195767E+3	5.14312688E-2	4.12901424E+3	5.05313673E-2
4.15630200E+3	7.60227619E-2	4.14931737E+3	7.69064082E-2	4.13330989E+3	7.96088041E-2
4.15689357E+3	8.77693417E-2	4.14397735E+3	9.65308307E-2	4.13208500E+3	1.00527797E-1
4.15855582E+3	1.06873337E-1	4.14740572E+3	1.23683277E-1	4.13655105E+3	1.27453518E-1
4.16280152E+3	1.35337653E-1	4.15337548E+3	1.58053338E-1	4.13506259E+3	1.41153641E-1
4.15954360E+3	1.48368836E-1	4.15351138E+3	1.61437572E-1	4.13731412E+3	1.61367032E-1

10	
E. Driving	E. Cal
4.11540638E+3	9.01106425E-3
4.11373397E+3	2.26489877E-2
4.11695846E+3	4.46883656E-2
4.11378315E+3	6.27927020E-2
4.11652540E+3	9.11610033E-2
4.11821075E+3	1.13119210E-1
4.12341627E+3	1.44940836E-1
4.12400423E+3	1.63918201E-1

Repeated Calibration Test 2:

01		02		03	
E. Driving	E. Cal	E. Driving	E. Cal	E. Driving	E. Cal
4.17059850E+3	3.62753086E-3	4.15642216E+3	3.55054759E-3	4.14095997E+3	6.97798257E-3
4.16576059E+3	2.54831057E-2	4.15091961E+3	3.00840668E-2	4.13749473E+3	2.28252574E-2
4.16205519E+3	4.38733061E-2	4.14679224E+3	5.18583274E-2	4.13227237E+3	3.83025227E-2
4.16009553E+3	6.27220543E-2	4.14968355E+3	7.75330501E-2	4.13219716E+3	7.07952138E-2
4.16219086E+3	9.40140013E-2	4.14321751E+3	8.66362451E-2	4.13421739E+3	9.03456553E-2
4.15769636E+3	1.15045655E-1	4.14961238E+3	1.21912893E-1	4.13637830E+3	1.13172519E-1
4.16051126E+3	1.32920449E-1	4.14804003E+3	1.44689521E-1	4.13572443E+3	1.33596319E-1
4.16085020E+3	1.55254688E-1	4.15328891E+3	1.59940301E-1	4.14086068E+3	1.62155889E-1

04		05		06	
E. Driving	E. Cal	E. Driving	E. Cal	E. Driving	E. Cal
4.12623848E+3	7.62728910E-3	4.11280163E+3	6.79789470E-3	4.10550613E+3	1.12318763E-2
4.12241088E+3	2.96346255E-2	4.10782268E+3	1.71989825E-2	4.09701028E+3	1.78783108E-2
4.12284581E+3	5.38960498E-2	4.11215899E+3	5.35124922E-2	4.09997916E+3	4.43020179E-2
4.12090232E+3	5.63329754E-2	4.10823921E+3	7.32001778E-2	4.09705010E+3	7.35361497E-2
4.12571347E+3	9.10521582E-2	4.11060397E+3	9.24581586E-2	4.10081230E+3	9.71367881E-2
4.12407280E+3	1.14102525E-1	4.11544036E+3	1.11130066E-1	4.10050359E+3	1.19954146E-1
4.12477692E+3	1.38302497E-1	4.11970783E+3	1.38104312E-1	4.10383936E+3	1.42615649E-1
4.13047680E+3	1.64471086E-1	4.11412120E+3	1.57258930E-1	4.10488508E+3	1.64428065E-1

07		08		09	
E. Driving	E. Cal	E. Driving	E. Cal	E. Driving	E. Cal
4.08749786E+3	6.21846758E-3	4.07404148E+3	1.22678430E-2	4.06165568E+3	7.68499494E-3
4.08804421E+3	2.71404027E-2	4.07438629E+3	2.22692495E-2	4.06012783E+3	2.40845304E-2
4.08408259E+3	4.12070240E-2	4.07091661E+3	4.31879597E-2	4.06305705E+3	4.97127312E-2
4.08320143E+3	6.59003044E-2	4.07473457E+3	6.54984020E-2	4.06842716E+3	7.59053229E-2
4.09249031E+3	9.78851750E-2	4.07395436E+3	8.56129950E-2	4.06646770E+3	1.09062068E-1
4.09125189E+3	1.18507953E-1	4.08106846E+3	1.17843643E-1	4.07151205E+3	1.23796843E-1
4.09304027E+3	1.41906950E-1	4.08274745E+3	1.32701322E-1	4.07488065E+3	1.45809035E-1
4.09430835E+3	1.64370851E-1	4.08548285E+3	1.64051031E-1	4.07083233E+3	1.60226355E-1

10	
E. Driving	E. Cal
4.04810299E+3	4.96632894E-3
4.04554216E+3	1.94973418E-2
4.04952178E+3	4.72215975E-2
4.05037473E+3	7.01302032E-2
4.05476338E+3	1.02055662E-1
4.05880829E+3	1.27797751E-1
4.05972936E+3	1.44249780E-1
4.06208083E+3	1.58185456E-1

Repeated Calibration Test 3:

01		02		03	
E. Driving	E. Cal	E. Driving	E. Cal	E. Driving	E. Cal
4.40799916E+3	5.80845492E-3	4.38502437E+3	1.59514632E-3	4.36176611E+3	8.38802307E-3
4.39630996E+3	2.40254486E-2	4.36465162E+3	2.68400077E-2	4.35800070E+3	2.36337194E-2
4.37306390E+3	3.77039084E-2	4.35980142E+3	5.04994720E-2	4.34779362E+3	4.31004888E-2
4.36791160E+3	6.18984802E-2	4.35617363E+3	6.82997460E-2	4.34661438E+3	6.81901399E-2
4.36206551E+3	7.65896265E-2	4.35234033E+3	8.62145108E-2	4.34142508E+3	8.72935665E-2
4.35608617E+3	1.06982621E-1	4.34981210E+3	1.12166149E-1	4.33727395E+3	1.06536198E-1
4.35128780E+3	1.28971040E-1	4.34514264E+3	1.29474840E-1	4.33439984E+3	1.24642957E-1
4.35198690E+3	1.45664790E-1	4.34472675E+3	1.47250286E-1	4.33290801E+3	1.57404614E-1

04		05		06	
E. Driving	E. Cal	E. Driving	E. Cal	E. Driving	E. Cal
4.34640647E+3	1.23000324E-3	4.32648261E+3	2.83368821E-3	4.30760163E+3	1.41095283E-2
4.33431853E+3	2.02544872E-2	4.32643301E+3	3.22564655E-2	4.30018242E+3	3.49742119E-2
4.33018286E+3	4.69702761E-2	4.31439914E+3	5.00486822E-2	4.29412137E+3	4.57835970E-2
4.32531306E+3	6.74248401E-2	4.31515458E+3	7.35336627E-2	4.29456239E+3	7.63990890E-2
4.32508559E+3	9.08424757E-2	4.30735952E+3	8.50346956E-2	4.29448415E+3	9.74910466E-2
4.31971421E+3	1.02692042E-1	4.30513463E+3	1.07877344E-1	4.29076691E+3	1.16219734E-1
4.31591134E+3	1.18503247E-1	4.30558831E+3	1.28958270E-1	4.29633711E+3	1.40264004E-1
4.31899454E+3	1.55273656E-1	4.30581394E+3	1.52880081E-1	4.29426028E+3	1.60175359E-1

07		08		09	
E. Driving	E. Cal	E. Driving	E. Cal	E. Driving	E. Cal
4.29448534E+3	7.90255605E-3	4.26710283E+3	4.27855931E-3	4.25585327E+3	6.68270073E-3
4.28600022E+3	3.07622449E-2	4.26603338E+3	2.07226707E-2	4.25049682E+3	2.91894692E-2
4.27916513E+3	4.19125097E-2	4.25795098E+3	4.99203339E-2	4.25405217E+3	5.65702413E-2
4.27357838E+3	6.73210581E-2	4.25985905E+3	7.09402696E-2	4.24960353E+3	7.05944988E-2
4.27519681E+3	8.10429117E-2	4.25844472E+3	8.76526621E-2	4.24791454E+3	9.06411870E-2
4.27852239E+3	1.05460402E-1	4.25980829E+3	1.06612810E-1	4.24804441E+3	1.13188943E-1
4.27786993E+3	1.31471715E-1	4.26447418E+3	1.36582141E-1	4.25014137E+3	1.27470119E-1
4.27927179E+3	1.59359778E-1	4.26293583E+3	1.58590302E-1	4.25142768E+3	1.58704936E-1

10	
E. Driving	E. Cal
4.23674786E+3	1.60937990E-3
4.24094275E+3	2.14967811E-2
4.23533238E+3	4.48103256E-2
4.23396475E+3	7.08613722E-2
4.23098509E+3	8.00060259E-2
4.23658233E+3	1.13416491E-1
4.23522982E+3	1.34376888E-1
4.23555232E+3	1.52349939E-1

Calibrate-Test-Calibrate Phantom Tests

Presented here are values from calibrate-test-calibrate phantom testing, which was discussed in Chapter 5. Values for driving end elasticity (E. Driving in mV/mm) and calibration instrument elasticity (E. Cal in N/mm) for each of the three repetitions of the calibration procedure.

Calibrate-Test-Calibrate Phantom 1 Test 1:

I. Calibration		Phantom Test		F. Calibration	
E. Driving	E. Cal	E. Driving	E. Cal	E. Driving	E. Cal
4.31905736E+3	-1.78151631E-3	4.33322448E+3	4.89426056E+0	4.28210449E+3	7.67516373E-3
4.30524265E+3	2.94349310E-2	4.33126793E+3	6.63033264E+1	4.27703498E+3	3.78447266E-2
4.29791717E+3	4.82954880E-2	4.32261204E+3	5.70960721E+0	4.27360047E+3	6.21918537E-2
4.29347366E+3	6.64710058E-2	4.32171496E+3	-7.20946409E+0	4.26914491E+3	9.12089639E-2
4.28393304E+3	9.12393279E-2	4.32163910E+3	5.55869586E+0	4.26587429E+3	9.96050926E-2
4.28660177E+3	1.15002903E-1	4.32159712E+3	-3.63249139E-1	4.26909789E+3	1.17096363E-1
4.27875186E+3	1.40270227E-1	4.31961111E+3	-1.55413050E+0	4.26427124E+3	1.38684269E-1
4.28334716E+3	1.60698096E-1	4.31761898E+3	-1.40431705E+0	4.26240247E+3	1.63524798E-1

Calibrate-Test-Calibrate Phantom 1 Test 2:

I. Calibration		Phantom Test		F. Calibration	
E. Driving	E. Cal	E. Driving	E. Cal	E. Driving	E. Cal
4.32384937E+3	6.45563889E-3	4.33551679E+3	2.22383571E+1	4.27724370E+3	1.58564348E-3
4.30592465E+3	3.45686327E-2	4.33517469E+3	-2.39641055E+0	4.26907528E+3	3.01702201E-2
4.30042020E+3	5.38960033E-2	4.33622834E+3	-3.68697366E+1	4.26523061E+3	6.42287800E-2
4.29517256E+3	7.91514429E-2	4.33284947E+3	1.61442639E+1	4.26027714E+3	8.25968534E-2
4.28735671E+3	9.04784502E-2	4.33350995E+3	1.35207906E+1	4.25979439E+3	1.05577242E-1
4.28213844E+3	1.11974421E-1	4.32829784E+3	2.78478913E+1	4.25784948E+3	1.20451011E-1
4.28151011E+3	1.40791087E-1	4.32413305E+3	7.19540508E+0	4.25467958E+3	1.41727885E-1
4.28109706E+3	1.57176447E-1	4.32658999E+3	-2.61890367E+1	4.25578648E+3	1.61665992E-1

Calibrate-Test-Calibrate Phantom 1 Test 3:

I. Calibration		Phantom Test		F. Calibration	
E. Driving	E. Cal	E. Driving	E. Cal	E. Driving	E. Cal
4.30315379E+3	5.91922596E-3	4.32135549E+3	3.43503637E+1	4.26304893E+3	9.19474846E-3
4.29064634E+3	2.46077046E-2	4.32199063E+3	1.55944939E+1	4.25181322E+3	2.91810542E-2
4.28757423E+3	4.54801511E-2	4.31796430E+3	-2.29495727E+1	4.24968135E+3	5.25237913E-2
4.27711116E+3	6.94778528E-2	4.31513336E+3	-6.61869648E+1	4.24923766E+3	7.03706589E-2
4.27154628E+3	9.40435908E-2	4.31468362E+3	-2.24783537E+1	4.24147763E+3	8.89765536E-2
4.26840492E+3	1.21624793E-1	4.31025869E+3	-1.57000717E+1	4.24292344E+3	1.18651706E-1
4.26898248E+3	1.42187162E-1	4.30360117E+3	-8.42714854E-1	4.24376211E+3	1.41856876E-1
4.26408519E+3	1.53582146E-1	4.30426427E+3	9.34212171E+0	4.24333223E+3	1.60449164E-1

Calibrate-Test-Calibrate Phantom 5 Test 1:

I. Calibration		Phantom Test		F. Calibration	
E. Driving	E. Cal	E. Driving	E. Cal	E. Driving	E. Cal
3.64280735E+3	1.31200338E-2	3.91691864E+3	-6.00972336E+0	3.57070116E+3	1.22289600E-2
3.63775597E+3	2.63839748E-2	3.89674479E+3	-3.25399838E+1	3.57826765E+3	4.28116748E-2
3.64040745E+3	5.72465923E-2	3.87687117E+3	-6.94023363E+0	3.58070504E+3	6.45620815E-2
3.64545445E+3	8.17680131E-2	3.87242876E+3	-3.84680533E+0	3.58568461E+3	7.62207681E-2
3.64824209E+3	1.00493875E-1	3.86864205E+3	-6.81569518E+1	3.59247020E+3	1.04890273E-1
3.65308799E+3	1.24588510E-1	3.86828646E+3	-4.24191963E+0	3.59494238E+3	1.27459994E-1
3.65155569E+3	1.43150712E-1	3.86738058E+3	-8.28104731E-1	3.60144673E+3	1.55570728E-1
3.66028970E+3	1.70814692E-1	3.86194787E+3	-1.00494382E+0	3.60414497E+3	1.67737955E-1

Calibrate-Test-Calibrate Phantom 5 Test 2:

I. Calibration		Phantom Test		F. Calibration	
E. Driving	E. Cal	E. Driving	E. Cal	E. Driving	E. Cal
3.57639963E+3	2.03058579E-2	3.85010534E+3	1.98346135E+0	3.55599125E+3	1.47574524E-2
3.57388479E+3	3.48338052E-2	3.85116711E+3	9.91231781E-1	3.56399786E+3	3.12142433E-2
3.57901003E+3	5.92133552E-2	3.84635097E+3	-7.34047327E+0	3.56298421E+3	4.07038831E-2
3.58789515E+3	8.80920306E-2	3.84072481E+3	4.70992160E+1	3.57835129E+3	7.60923786E-2
3.58809722E+3	1.07419400E-1	3.83482357E+3	9.24299171E-1	3.57598193E+3	9.34409611E-2
3.59497554E+3	1.32598754E-1	3.83503768E+3	3.59562595E+0	3.58398917E+3	1.16146285E-1
3.59567724E+3	1.49663162E-1	3.83098809E+3	1.13064352E+1	3.58568111E+3	1.40796514E-1
3.60061012E+3	1.72774587E-1	3.82449332E+3	1.19024172E+0	3.59116157E+3	1.68466049E-1

Calibrate-Test-Calibrate Phantom 5 Test 3:

I. Calibration		Phantom Test		F. Calibration	
E. Driving	E. Cal	E. Driving	E. Cal	E. Driving	E. Cal
3.58065506E+3	-1.39035371E-3	3.85899895E+3	-1.38490465E+1	3.57763509E+3	8.99433529E-3
3.58877063E+3	3.58142940E-2	3.86539913E+3	3.73609196E+0	3.58558931E+3	3.57510178E-2
3.59389373E+3	5.71153591E-2	3.86380761E+3	-2.40319625E-1	3.58792466E+3	6.62147993E-2
3.59738474E+3	8.23297167E-2	3.86299469E+3	1.54781262E+0	3.59099284E+3	8.07973675E-2
3.60360176E+3	1.06421039E-1	3.86368865E+3	-5.09057322E-1	3.59583890E+3	1.01795438E-1
3.60979774E+3	1.31014501E-1	3.86149634E+3	-4.48931337E+0	3.60240038E+3	1.15439003E-1
3.60944773E+3	1.49825528E-1	3.86131318E+3	2.22927961E+0	3.60941701E+3	1.51290406E-1
3.61861005E+3	1.73671799E-1	3.85973125E+3	-4.49861819E+0	3.61297144E+3	1.70963560E-1

Higher Elasticity Calibrate-Test-Calibrate Bench Tests

Presented here are values from calibrate-test-calibrate bench testing, which was discussed in Chapter 6. Values for driving end elasticity (E. Driving in mV/mm) and calibration instrument elasticity (E. Cal in N/mm) for each of the three repetitions of the calibration procedure.

Calibrate-Test-Calibrate 2 Band Test 1:

I. Calibration		Band Test		F. Calibration	
E. Driving	E. Cal	E. Driving	E. Cal	E. Driving	E. Cal
4.05476206E+3	1.52623402E-1	4.05550728E+3	2.79969384E-1	4.03243989E+3	1.53434229E-1
4.06500123E+3	2.88861428E-1	4.06174719E+3	2.85977708E-1	4.06411266E+3	2.91108561E-1
4.10402065E+3	4.50640496E-1	4.05952827E+3	2.81380328E-1	4.09924420E+3	4.43694171E-1
4.14172411E+3	5.97845677E-1	4.06552714E+3	2.90024990E-1	4.12305170E+3	5.67309269E-1
4.17894897E+3	7.17435869E-1	4.06110744E+3	2.84716191E-1	4.17534578E+3	7.33264926E-1
4.22952100E+3	8.52482092E-1	4.06743160E+3	2.93040727E-1	4.22471151E+3	8.53258757E-1
4.28221612E+3	9.93625298E-1	4.05761349E+3	2.96163387E-1	4.28138494E+3	9.96969712E-1
4.34759593E+3	1.18164285E+0	4.06362917E+3	3.01367300E-1	4.34126254E+3	1.16460534E+0

Calibrate-Test-Calibrate 2 Band Test 2:

I. Calibration		Band Test		F. Calibration	
E. Driving	E. Cal	E. Driving	E. Cal	E. Driving	E. Cal
4.01746206E+3	1.50688000E-1	4.02650429E+3	2.88478458E-1	4.00684789E+3	1.45959394E-1
4.04376058E+3	2.96577221E-1	4.03096025E+3	2.97389632E-1	4.03009240E+3	2.92565475E-1
4.07203065E+3	4.25486073E-1	4.03625660E+3	2.98757877E-1	4.06910065E+3	4.45213166E-1
4.10063666E+3	5.67812264E-1	4.03610654E+3	2.99264357E-1	4.10705285E+3	5.91218349E-1
4.15663978E+3	7.39417262E-1	4.03664194E+3	3.03520614E-1	4.15943527E+3	7.34673436E-1
4.21492232E+3	8.94038106E-1	4.03402537E+3	3.01377626E-1	4.19859217E+3	8.45379474E-1
4.27034743E+3	1.03329407E+0	4.03461524E+3	3.07562191E-1	4.25902513E+3	9.89847224E-1
4.33217970E+3	1.20038219E+0	4.03967321E+3	3.10023964E-1	4.31543873E+3	1.14659593E+0

Calibrate-Test-Calibrate 2 Band Test 3:

I. Calibration		Band Test		F. Calibration	
E. Driving	E. Cal	E. Driving	E. Cal	E. Driving	E. Cal
3.99054797E+3	1.54713782E-1	4.01225526E+3	2.93584019E-1	3.98783843E+3	1.54396236E-1
4.01456348E+3	2.83509030E-1	4.01362847E+3	2.99838436E-1	4.00706429E+3	2.88214387E-1
4.03776388E+3	4.29762495E-1	4.01182184E+3	3.00455550E-1	4.03492663E+3	4.32178995E-1
4.09287182E+3	5.99725023E-1	4.01370155E+3	3.02007433E-1	4.08084523E+3	5.81789634E-1
4.13787766E+3	7.42112839E-1	4.00718604E+3	2.87211569E-1	4.12038360E+3	7.19563104E-1
4.19551541E+3	9.00778720E-1	4.00867552E+3	2.95469407E-1	4.16008504E+3	8.72908404E-1
4.23769560E+3	1.06869615E+0	4.01190169E+3	3.01061511E-1	4.20121745E+3	1.02376727E+0
4.27966340E+3	1.22369448E+0	4.01016545E+3	3.05355540E-1	4.27644542E+3	1.19059459E+0

Calibrate-Test-Calibrate 5 Band Test 1:

I. Calibration		Band Test		F. Calibration	
E. Driving	E. Cal	E. Driving	E. Cal	E. Driving	E. Cal
3.99533517E+3	1.41499222E-1	4.13136625E+3	7.25653686E-1	3.98933689E+3	1.44775365E-1
4.01505068E+3	2.83855000E-1	4.13918938E+3	7.41620719E-1	4.01341716E+3	2.91420109E-1
4.04608257E+3	4.31095993E-1	4.14057093E+3	7.45469900E-1	4.04590862E+3	4.44180290E-1
4.08706414E+3	5.80274380E-1	4.13824498E+3	7.40360038E-1	4.08375657E+3	5.83254010E-1
4.13763780E+3	7.34456098E-1	4.14213920E+3	7.43820698E-1	4.13463257E+3	7.41097139E-1
4.18561483E+3	8.55398712E-1	4.13926006E+3	7.48657213E-1	4.18831066E+3	8.91995114E-1
4.24858072E+3	1.02406348E+0	4.14350944E+3	7.45002792E-1	4.24919288E+3	1.04731475E+0
4.30096462E+3	1.16118703E+0	4.13943708E+3	7.48914711E-1	4.31208985E+3	1.22174463E+0

Calibrate-Test-Calibrate 5 Band Test 2:

I. Calibration		Band Test		F. Calibration	
E. Driving	E. Cal	E. Driving	E. Cal	E. Driving	E. Cal
3.99477590E+3	1.53841233E-1	4.13344912E+3	7.43297338E-1	3.98717166E+3	1.52712024E-1
4.02408987E+3	3.04626357E-1	4.13678686E+3	7.45227562E-1	4.00877192E+3	2.98467022E-1
4.04839646E+3	4.32361855E-1	4.13545511E+3	7.46889893E-1	4.04881768E+3	4.61866188E-1
4.08617546E+3	5.85054727E-1	4.14008144E+3	7.53377366E-1	4.08199484E+3	6.08349739E-1
4.13280612E+3	7.30101436E-1	4.13630193E+3	7.48752983E-1	4.13186129E+3	7.44040828E-1
4.19753607E+3	8.96727375E-1	4.13477031E+3	7.49147174E-1	4.16762488E+3	8.81928960E-1
4.22873119E+3	1.02946316E+0	4.13849383E+3	7.54318373E-1	4.21168379E+3	1.04797421E+0
4.28133641E+3	1.19498092E+0	4.13550376E+3	7.46845353E-1	4.27557235E+3	1.20826755E+0

Calibrate-Test-Calibrate 5 Band Test 3:

I. Calibration		Band Test		F. Calibration	
E. Driving	E. Cal	E. Driving	E. Cal	E. Driving	E. Cal
3.98696073E+3	1.62138658E-1	4.12833580E+3	7.46406409E-1	3.97563107E+3	1.54272674E-1
4.01267319E+3	2.99960173E-1	4.12447977E+3	7.53892481E-1	4.00163198E+3	2.84251267E-1
4.03999612E+3	4.43065819E-1	4.12974421E+3	7.56519638E-1	4.03734488E+3	4.53572574E-1
4.08062337E+3	5.95349064E-1	4.12490272E+3	7.52039626E-1	4.06975739E+3	5.96508817E-1
4.12287809E+3	7.44089078E-1	4.11992963E+3	7.47253811E-1	4.11630258E+3	7.43261986E-1
4.18119075E+3	8.90363894E-1	4.12662375E+3	7.56182198E-1	4.15953338E+3	8.82648625E-1
4.22261799E+3	1.02070892E+0	4.12807282E+3	7.64885838E-1	4.19929598E+3	1.01849524E+0
4.26340784E+3	1.16896816E+0	4.12533671E+3	7.59780199E-1	4.25955791E+3	1.19197408E+0

Instrument Phantom Validation Tests

Presented here are values from calibrate-test-calibrate phantom testing, which was discussed in Chapter 6. Values for driving end elasticity (E. Driving in mV/mm) and calibration instrument elasticity (E. Cal in N/mm) for each of the three repetitions of the calibration procedure.

Calibrate-Test-Calibrate Phantom 1 Test 1:

I. Calibration		Phantom Test		F. Calibration	
E. Driving	E. Cal	E. Driving	E. Cal	E. Driving	E. Cal
3.51946703E+3	1.46583411E-1	3.52939238E+3	-1.94266304E+0	3.50469026E+3	1.42208024E-1
3.55897883E+3	2.94236942E-1	3.52799079E+3	-6.95047827E+0	3.54682979E+3	3.04152827E-1
3.61323749E+3	4.64623631E-1	3.52885031E+3	6.20622358E+0	3.59709611E+3	4.64867355E-1
3.66997865E+3	6.03879756E-1	3.52762192E+3	1.16916928E+1	3.66168526E+3	6.25482855E-1
3.73532199E+3	7.51344893E-1	3.52780196E+3	-2.93372225E+0	3.71698223E+3	7.58669426E-1
3.80577300E+3	9.39187780E-1	3.52608635E+3	3.36776227E+0	3.78489379E+3	8.89925094E-1
3.85668895E+3	1.05570318E+0	3.52215398E+3	7.52271002E+1	3.84303455E+3	1.05449285E+0
3.93687719E+3	1.22002172E+0	3.52815329E+3	2.95070610E+0	3.92238131E+3	1.24112087E+0

Calibrate-Test-Calibrate Phantom 1 Test 2:

I. Calibration		Phantom Test		F. Calibration	
E. Driving	E. Cal	E. Driving	E. Cal	E. Driving	E. Cal
3.50381902E+3	1.45795943E-1	3.51531615E+3	-1.28436975E+0	3.50031073E+3	1.46792098E-1
3.54161531E+3	2.80718584E-1	3.51497778E+3	-6.85507645E-2	3.54290268E+3	3.07121495E-1
3.59426785E+3	4.66225107E-1	3.51431454E+3	4.01187393E+0	3.59201674E+3	4.48716128E-1
3.66307222E+3	6.38680371E-1	3.51400537E+3	2.22137754E+0	3.64153836E+3	5.79100743E-1
3.71810054E+3	7.48503010E-1	3.51612655E+3	1.05275358E+0	3.71638637E+3	7.32963386E-1
3.79010901E+3	9.27907452E-1	3.51160864E+3	7.33472104E-1	3.77788101E+3	8.81899719E-1
3.83558651E+3	1.04005686E+0	3.51260071E+3	2.42279492E+0	3.84606365E+3	1.07140931E+0
3.90301959E+3	1.24168231E+0	3.51300254E+3	-3.01150076E+0	3.93948762E+3	1.18926408E+0

Calibrate-Test-Calibrate Phantom 1 Test 3:

I. Calibration		Phantom Test		F. Calibration	
E. Driving	E. Cal	E. Driving	E. Cal	E. Driving	E. Cal
3.50021441E+3	1.57028526E-1	3.50500961E+3	-2.51173559E+0	3.50047798E+3	1.58189419E-1
3.53160930E+3	2.86571500E-1	3.50586724E+3	1.72458337E+0	3.54575926E+3	3.23437624E-1
3.58864676E+3	4.52371320E-1	3.50291298E+3	-1.33091746E-1	3.58993256E+3	4.72033205E-1
3.64648950E+3	5.93197137E-1	3.50571268E+3	-1.85256602E+0	3.63681109E+3	5.99189711E-1
3.71532621E+3	7.41161467E-1	3.50647988E+3	-1.79113296E+0	3.69099924E+3	7.51231980E-1
3.76208937E+3	8.96607429E-1	3.50139569E+3	-1.49079594E+0	3.75249734E+3	9.16753687E-1
3.81681859E+3	1.06639847E+0	3.50637668E+3	7.00864115E+0	3.80812722E+3	1.06226211E+0
3.94806996E+3	1.20343335E+0	3.50721181E+3	8.50939121E-1	3.89126574E+3	1.25108808E+0

Calibrate-Test-Calibrate Phantom 2 Test 1:

I. Calibration		Phantom Test		F. Calibration	
E. Driving	E. Cal	E. Driving	E. Cal	E. Driving	E. Cal
3.66677524E+3	1.46195901E-1	3.70906092E+3	3.57851525E+0	3.66624730E+3	1.55272213E-1
3.70864898E+3	3.09573342E-1	3.71043182E+3	2.29870112E+0	3.70641509E+3	3.21746409E-1
3.74771728E+3	4.47540170E-1	3.70911786E+3	-7.20160549E+0	3.75476130E+3	4.82919931E-1
3.81517823E+3	6.29329749E-1	3.70909662E+3	7.63453422E+0	3.80436957E+3	6.13968450E-1
3.88484117E+3	7.91571558E-1	3.70901304E+3	1.35797308E+1	3.84004435E+3	7.45242847E-1
3.91419307E+3	8.56298494E-1	3.70822603E+3	3.41490746E+0	3.88648598E+3	8.85608458E-1
3.97663311E+3	1.03865639E+0	3.70489981E+3	6.95937776E+0	3.95462979E+3	1.01028301E+0
4.03739138E+3	1.21648618E+0	3.71078489E+3	1.32087327E+0	4.01493254E+3	1.20036382E+0

Calibrate-Test-Calibrate Phantom 2 Test 2:

I. Calibration		Phantom Test		F. Calibration	
E. Driving	E. Cal	E. Driving	E. Cal	E. Driving	E. Cal
3.66243891E+3	1.58507412E-1	3.69453300E+3	8.78837478E-1	3.65763471E+3	1.56856546E-1
3.70165709E+3	3.10076193E-1	3.69574074E+3	1.01731787E+1	3.69067041E+3	3.03508832E-1
3.74443393E+3	4.68492501E-1	3.69696177E+3	3.24668626E+0	3.73901448E+3	4.73783763E-1
3.80117720E+3	6.12306575E-1	3.69778548E+3	-7.71259239E+0	3.80472718E+3	6.36395507E-1
3.85309425E+3	7.33157177E-1	3.69636462E+3	2.32037219E+0	3.85664841E+3	7.79610868E-1
3.90953531E+3	9.21044502E-1	3.69546307E+3	4.76938201E+0	3.90961307E+3	8.99468304E-1
3.95234804E+3	1.07341956E+0	3.69491389E+3	-7.21846376E+0	3.96655157E+3	1.04899867E+0
4.01615573E+3	1.23119791E+0	3.69995000E+3	8.79436940E+0	4.04097604E+3	1.23120662E+0

Calibrate-Test-Calibrate Phantom 2 Test 3:

I. Calibration		Phantom Test		F. Calibration	
E. Driving	E. Cal	E. Driving	E. Cal	E. Driving	E. Cal
3.66117292E+3	1.74070009E-1	3.69616112E+3	4.09621902E+0	3.64907565E+3	1.50317552E-1
3.69740212E+3	3.18479063E-1	3.69520595E+3	7.20512072E+0	3.68688050E+3	3.00430799E-1
3.74144667E+3	4.74471016E-1	3.69037647E+3	-6.79522480E+0	3.72895222E+3	4.43789949E-1
3.79480053E+3	6.28865654E-1	3.69084124E+3	4.69103775E-1	3.76883670E+3	6.06521028E-1
3.84847118E+3	7.52175474E-1	3.69214233E+3	2.48191968E+0	3.80312139E+3	7.22014018E-1
3.91004011E+3	8.97273020E-1	3.69186517E+3	-1.57752160E-1	3.88742549E+3	9.16695301E-1
3.97235903E+3	1.06769909E+0	3.69221782E+3	7.23513971E+0	3.94091594E+3	1.08628484E+0
4.02352673E+3	1.21784870E+0	3.69372491E+3	2.59819274E+0	4.03455010E+3	1.25593115E+0I.

Calibrate-Test-Calibrate Phantom 3 Test 1:

I. Calibration		Phantom Test		F. Calibration	
E. Driving	E. Cal	E. Driving	E. Cal	E. Driving	E. Cal
3.60763089E+3	1.63962621E-1	3.70257594E+3	8.73266904E+0	3.59702748E+3	1.66393546E-1
3.64004305E+3	3.08288359E-1	3.70073508E+3	1.11782766E+1	3.63011850E+3	3.00156369E-1
3.68896145E+3	4.65150697E-1	3.70068918E+3	7.71349037E+0	3.68074667E+3	4.49967467E-1
3.74684313E+3	6.15679749E-1	3.70391161E+3	-2.29414736E+0	3.73192957E+3	5.97827037E-1
3.80742891E+3	7.80456706E-1	3.70408785E+3	-8.10058831E+0	3.79330288E+3	7.30845329E-1
3.86664916E+3	9.30535443E-1	3.70261600E+3	7.44257727E+0	3.84437253E+3	9.02982557E-1
3.92422186E+3	1.07851662E+0	3.70032950E+3	1.04452628E+1	3.90702727E+3	1.08496149E+0
3.98917272E+3	1.26339575E+0	3.70115944E+3	-1.99508568E+1	4.00000200E+3	1.22600309E+0

Calibrate-Test-Calibrate Phantom 3 Test 2:

I. Calibration		Phantom Test		F. Calibration	
E. Driving	E. Cal	E. Driving	E. Cal	E. Driving	E. Cal
3.62068014E+3	1.56469807E-1	3.71651734E+3	-3.73629369E+0	3.61220858E+3	1.52672208E-1
3.65367050E+3	2.96741826E-1	3.71117567E+3	9.55984235E+0	3.65617340E+3	3.17978044E-1
3.70179535E+3	4.50137982E-1	3.71474482E+3	-3.13934161E+0	3.71041300E+3	5.08462156E-1
3.75712696E+3	6.08164128E-1	3.71048486E+3	-5.09825961E+0	3.75667062E+3	6.30930839E-1
3.82078967E+3	7.48168796E-1	3.71602517E+3	-3.01884930E+1	3.81106780E+3	7.51644474E-1
3.86627004E+3	8.88320049E-1	3.71624545E+3	2.47251828E+1	3.88545434E+3	9.49560062E-1
3.92056440E+3	1.05045595E+0	3.71145288E+3	1.29044020E+1	3.92691213E+3	1.05992872E+0
3.98611890E+3	1.23847716E+0	3.71659886E+3	-4.76353212E+0	4.00577100E+3	1.24910237E+0

Calibrate-Test-Calibrate Phantom 3 Test 3:

I. Calibration		Phantom Test		F. Calibration	
E. Driving	E. Cal	E. Driving	E. Cal	E. Driving	E. Cal
3.61202453E+3	1.90393374E-1	3.69945549E+3	-2.05870213E+1	3.60429945E+3	1.73892035E-1
3.64925795E+3	3.45796732E-1	3.69952970E+3	5.96302919E+0	3.64475324E+3	3.37022737E-1
3.69668231E+3	5.13651827E-1	3.69921111E+3	2.88578572E+1	3.69098812E+3	4.96981394E-1
3.74984206E+3	6.51286600E-1	3.69800755E+3	-7.70678208E+1	3.73909291E+3	6.38802926E-1
3.79515392E+3	7.65314610E-1	3.69483417E+3	-2.98024730E+1	3.74745204E+3	6.41849326E-1
3.86077963E+3	9.12959661E-1	3.69932953E+3	-2.01963857E+1	3.82652087E+3	9.03418919E-1
3.92767306E+3	1.07829887E+0	3.69958989E+3	8.85378159E+0	3.88049951E+3	1.05578052E+0
3.98993462E+3	1.24656494E+0	3.69791632E+3	4.47291212E+0	3.95775851E+3	1.26938118E+0

Calibrate-Test-Calibrate Phantom 4 Test 1:

I. Calibration		Phantom Test		F. Calibration	
E. Driving	E. Cal	E. Driving	E. Cal	E. Driving	E. Cal
3.82432150E+3	1.53953613E-1	3.92559869E+3	1.35102089E+0	3.80639159E+3	1.46672026E-1
3.85452051E+3	2.85724819E-1	3.92901753E+3	9.25557273E+0	3.84468011E+3	2.99722839E-1
3.88170912E+3	4.33961877E-1	3.92722480E+3	6.63376001E+0	3.88586861E+3	4.75244949E-1
3.92407798E+3	6.05701832E-1	3.92752784E+3	7.46366105E-1	3.94722407E+3	6.59429860E-1
3.95946929E+3	7.56611569E-1	3.92933632E+3	3.30749279E+0	3.97321912E+3	7.91382276E-1
4.01468033E+3	8.98192618E-1	3.92650900E+3	1.03916470E+0	4.01599298E+3	9.06162178E-1
4.09717426E+3	1.06440518E+0	3.92957362E+3	-2.64169815E+0	4.09731293E+3	1.03377312E+0
4.17691808E+3	1.23541001E+0	3.92807059E+3	-4.30948709E+0	4.16249461E+3	1.21087160E+0

Calibrate-Test-Calibrate Phantom 4 Test 2:

I. Calibration		Phantom Test		F. Calibration	
E. Driving	E. Cal	E. Driving	E. Cal	E. Driving	E. Cal
3.78514730E+3	1.56701156E-1	3.89706590E+3	7.70593781E+0	3.79077806E+3	1.73436199E-1
3.82489040E+3	2.99223245E-1	3.89541624E+3	-4.66130776E+0	3.82586762E+3	3.36768866E-1
3.86413664E+3	4.64887455E-1	3.89480185E+3	9.22807493E+0	3.85845857E+3	4.64555751E-1
3.90427557E+3	6.48002754E-1	3.89870535E+3	3.74805659E+0	3.90548107E+3	6.15258866E-1
3.92175579E+3	7.53311938E-1	3.89873089E+3	-3.74574638E+1	3.93433568E+3	7.68132530E-1
3.97991938E+3	8.87707188E-1	3.89688676E+3	-1.45783205E+0	3.93536690E+3	8.90392727E-1
4.06378349E+3	9.98261068E-1	3.89796193E+3	1.04750835E+1	4.01515103E+3	1.06591082E+0
4.12188871E+3	1.20917122E+0	3.90283015E+3	1.40588972E+1	4.12509336E+3	1.20052597E+0

Calibrate-Test-Calibrate Phantom 4 Test 3:

I. Calibration		Phantom Test		F. Calibration	
E. Driving	E. Cal	E. Driving	E. Cal	E. Driving	E. Cal
3.78084415E+3	1.26471057E-1	3.87463865E+3	-2.89544559E+0	3.78578997E+3	1.60213075E-1
3.82285940E+3	3.33478788E-1	3.87876739E+3	5.09696841E+0	3.81550977E+3	3.09593372E-1
3.79864687E+3	4.88542484E-1	3.87694387E+3	2.34893223E+1	3.86479974E+3	4.93684963E-1
3.90537747E+3	6.26233569E-1	3.87782801E+3	-2.22141558E+0	3.91595037E+3	6.34416377E-1
3.94099152E+3	7.63682564E-1	3.88062477E+3	1.00792014E+0	3.93717828E+3	7.06189981E-1
3.99416446E+3	9.57999152E-1	3.88178114E+3	-7.00528320E+0	3.96902196E+3	8.23313132E-1
4.03224509E+3	1.09526479E+0	3.88342986E+3	-4.52475499E-1	4.02855133E+3	1.00673052E+0
4.11384181E+3	1.20492310E+0	3.88080781E+3	-4.45453485E+0	4.10304460E+3	1.20036155E+0

Calibrate-Test-Calibrate Phantom 5 Test 1:

I. Calibration		Phantom Test		F. Calibration	
E. Driving	E. Cal	E. Driving	E. Cal	E. Driving	E. Cal
3.66800467E+3	1.55279830E-1	3.97593177E+3	2.63403216E+1	3.67086921E+3	1.78451174E-1
3.69914946E+3	2.95204764E-1	3.97485633E+3	1.25641460E+1	3.70560280E+3	3.33161854E-1
3.74623497E+3	4.58510126E-1	3.96781987E+3	-3.09780838E+0	3.75074626E+3	4.87427160E-1
3.79093607E+3	5.96188842E-1	3.96747759E+3	1.39175615E+0	3.79636178E+3	6.27648609E-1
3.86048559E+3	7.44266204E-1	3.96215088E+3	-1.80295508E-1	3.85121077E+3	7.36081263E-1
3.90576774E+3	8.61255040E-1	3.95598063E+3	3.63457751E+0	3.89904113E+3	8.67148055E-1
3.97753498E+3	1.03859244E+0	3.95558975E+3	-1.15709464E+1	3.94279372E+3	1.03524104E+0
4.05470376E+3	1.22887517E+0	3.94753768E+3	-7.38465944E-1	4.02009529E+3	1.25086753E+0

Calibrate-Test-Calibrate Phantom 5 Test 2:

I. Calibration		Phantom Test		F. Calibration	
E. Driving	E. Cal	E. Driving	E. Cal	E. Driving	E. Cal
4.04881971E+3	1.31121268E-1	4.30636315E+3	-2.84085721E+0	4.05156910E+3	1.61805748E-1
4.07295430E+3	2.78160660E-1	4.32022908E+3	-6.33206375E+0	4.07375325E+3	3.04457552E-1
4.10910792E+3	4.48269417E-1	4.31549620E+3	4.36175082E+0	4.10438684E+3	4.54936298E-1
4.13104566E+3	5.68576130E-1	4.32092665E+3	-1.64082901E+0	4.14146055E+3	6.06261398E-1
4.18099739E+3	7.07124703E-1	4.33046548E+3	3.58934616E+0	4.18985360E+3	7.49404480E-1
4.23081618E+3	8.42615899E-1	4.32312340E+3	-8.57921524E+0	4.23782418E+3	8.70701044E-1
4.28150031E+3	9.78584983E-1	4.33040262E+3	9.67600888E+0	4.28790549E+3	1.02856026E+0
4.33399655E+3	1.14273660E+0	4.32292240E+3	-8.61568714E+0	4.31223051E+3	1.17962176E+0

Calibrate-Test-Calibrate Phantom 5 Test 3:

I. Calibration		Phantom Test		F. Calibration	
E. Driving	E. Cal	E. Driving	E. Cal	E. Driving	E. Cal
4.00734817E+3	1.45024566E-1	4.25323332E+3	-8.91529277E+0	4.00759617E+3	1.54532724E-1
4.02846711E+3	2.90303967E-1	4.25646316E+3	7.65581566E+0	4.02669303E+3	3.00908236E-1
4.05997827E+3	4.30964837E-1	4.25073769E+3	7.79027277E-1	4.05999239E+3	4.53109564E-1
4.09570156E+3	5.74818181E-1	4.25256045E+3	6.15886399E+0	4.09630590E+3	6.02757573E-1
4.14570155E+3	7.10550187E-1	4.25074708E+3	6.32217683E-1	4.14848946E+3	7.45997046E-1
4.20751103E+3	8.96515813E-1	4.25015371E+3	2.10445782E+0	4.19755550E+3	8.82531342E-1
4.24950550E+3	1.01750479E+0	4.25150127E+3	8.44931845E-1	4.23934062E+3	1.05982948E+0
4.29371280E+3	1.15499355E+0	4.25440736E+3	-6.49596586E+0	4.29117643E+3	1.20246959E+0